IRON COORDINATION AND PROTEIN–PROTEIN INTERACTIONS OF THE PROTEIN FRATAXIN

by

LESLIE GENTRY–DYE

LAURA BUSENLEHNER, COMMITTEE CHAIR
PATRICK FRANTOM
STEVAN MARCUS
SHANE STREET
STEPHEN WOSKI

A DISSERTATION

Submitted in partial fulfillment of the requirements
for the degree of Doctor of Philosophy
in the Department of Chemistry
in the Graduate School of
The University of Alabama

TUSCALOOSA, ALABAMA

2014

ABSTRACT

Frataxin is a mitochondrial iron metallochaperone that transports ferrous iron to proteins that require it for function. This dissertation research explores the iron binding properties of human frataxin and how frataxin interacts with the mitochondrial [Fe–S] cluster scaffold Isu2 to assemble [Fe–S] clusters.

Friedreich's ataxia (FA) is a neurodegenerative progressive limb and gait ataxia that is caused by an exaggerated GAA triplet codon repeat that results in depleted levels of the iron metallochaperone frataxin. Depleted levels of frataxin have a two-fold consequence. The first is that the mitochondria do not have a way to bind and transport iron to proteins that require iron for function. The second is that the cell interprets this as an iron shortage and imports more iron into the mitochondria. As a result, there is both iron overload (caused by having excess non-bioavailable iron in ferric aggregates in the mitochondria) and iron deficiency (since this iron cannot be mobilized for [Fe–S] cluster assembly). Frataxin coordinates ferrous iron and transports it to Isu2 for the assembly of [Fe–S] clusters. In this dissertation, human frataxin Fe^{2+} coordination was characterized and applied to further study how frataxin interacts with Isu2 for iron transfer and [Fe–S] cluster assembly. This research supports that mature human frataxin coordinates 3 ferrous iron ions and interacts with Isu2 in the same vicinity of Fe^{2+} coordination for the stimulation of [Fe–S] cluster assembly and provides insight into the cause of FA.

LIST OF ABBREVIATIONS AND SYMBOLS

% v/v	percent volume to volume ratio
% w/v	percent weight to volume ratio
(D)	disordered form of Isu2
(S)	structured form of Isu2
[2Fe–2S] cluster	two iron–two sulfur cluster
[4Fe–4S] cluster	four iron—four sulfur cluster
[Fe–S] cluster	iron sulfur cluster
°C	degree celsius
His_6	hexahistidine tag
A	alanine
Å	angstrom
A_{280}	absorbance at 280 nm
A_{562}	absorbance at 562 nm
Ala	alanine
Arg	arginine

Asn	asparagine
Asp	aspartic acid
Atx1	*S. cerevisiae* copper metallochaperone protein
BCIP	5-bromo-4-chloro-3-indolyl phosphate
Bis-Tris	2-[bis(2-hydroxyethyl)amino]-2-(hydroxymethly)-1,3-propanediol
BSA	bovine serum albumin
C	cysteine
Ccc2	*S. cerevisiae* copper P-type ATPase
cm^{-1}	inverse centimeter
Co^{2+}	cobaltous ion
$CoCl_2$	cobaltous chloride
C-terminus	protein carboxyl terminus
Cu^{+}	cuprous ion
Cu^{2+}	cupric ion
$CuSO_4$	cupric sulfate
CyaY	*E. coli* frataxin homolog
Cys	cysteine
D	aspartic acid
D_2O	deuterium oxide
DEAE	diethylaminoethyl
DHB	dihydroxybenzoic acid
DMF	dimethylfuran
DNA	deoxyribonucleic acid

DTT	dithiothreitol
E	glutamic acid
EDC	1-ethyl-3-[3-dimethylaminopropyl]carbodiimide
EDTA	ethylenediaminetetraacetic acid
EPR	electron paramagnetic resonance
ER	endoplasmic reticulum
EXAFS	extended X-ray absorption fine structure
F	phenylalanine
FA	Friedreich's ataxia
Fdx	ferredoxin
FdxR	ferredoxin reductase
Fe^{2+}	ferrous iron
Fe^{3+}	ferric iron
FeCH	ferrocheletase
$FeCl_3$	ferric chloride
$FeSO_4(NH_4)_2SO_4$	ferrous ammonium sulfate
FXN	human frataxin gene
Fxn	human frataxin protein
Fz	ferrozine
G	glycine
GAA	guanine-adenine-adenine
Gln	glutamine
Glu	glutamic acid

Gly	glycine
h	hour
H	histidine
Hah1	Atx1 human homolog protein
HCl	hydrochloric acid
HDX MS	hydrogen/deuterium exchange mass spectrometry
HEPES	4-(2-hydroxyethyl)-1-piperazineethanesulfonic free acid
His	histidine
HPLC	high-performance liquid chromatography
HSAB	hard-soft-acid-base theory
Hsc20	heat shock protein 20 kDa
HSP	heat shock proteins
HSQC	heteronuclear single quantum coherence
I	isoleucine
IAA	iodoacetamide
IPTG	isopropyl-β-D-thiogalactopyranoside
Isa1	[4Fe–4S] chaperone
ISC	Iron–sulfur cluster system
Isd11	protein Isd11
Isu2	iron–sulfur cluster assembly protein
ITC	isothermal titration calorimetry
K	lysine
K_D	dissociation constant

kDa	kilodalton
K_f	formation constant
KH_2PO_4	potassium phosphate, monobasic
L	Liter
LB	Luria Bertani
LMCT	ligand to metal charge transfer
Lys	lysine
M	molar
M	methionine
m_0	natural isotope abundance
M^{-1}	inverse molar
m_{100}	theoretical number of exchangeable amide hydrogens
MALDI-ToF MS	matrix-assisted laser desorption/ionization-time of flight mass spectrometry
MES	2-(N-morpholino)ethanesulfonic acid
Met	methionine
Mg^{2+}	magnesium ion
$MgSO_4$	magnesium sulfate
min	minute
mL	milliliter
mM	millimolar
mm	millimeter
MOPS	3-(N-morpholino)propanesulfonic acid
MPP	mitochondrial processing peptidase

MS	mass spectrometry
mtHsp70	mitochondrial heat shock protein 70 kDa protein
N	nitrogen
Na_2S	sodium sulfide
NBT	nitro blue tetrazolium chloride
Nfs1	human cysteine desulfurase protein
NIF	nitrogen fixation system
NLS	nuclear localization sequence
nM	nanomolar
nm	nanometer
NMR	nuclear magnetic resonance
N-terminus	protein amino terminus
O_2^-	superoxide ion
OD_{600}	optical density at 600 nm
$OH\cdot$	hydroxyl radical
PAGE	polyacrylamide gel electrophoresis
PBS buffer	phosphate buffered saline
PEI	polyethyleneimine
Phe	phenylalanine
PLP	pyridoxal 5'-phosphate
PMSF	phenylmethylsulfonyl fluoride
ppm	parts per million
Pro	proline

PVDF	polyvinylidene fluoride
ROS	reactive oxygen species
rpm	revolutions per minute
s	second
S	serine
S. cerevisiae	*Saccharomyces cerevisiae*
S^{2-}	sulfide ion
SDS	sodium dodecyl sulfate
Ser	serine
SP	sulfopropyl
SUF	sulfur mobilization system
Sulfo-NHS	N-hydroxysulfosuccinimide
Sulfo-SBED	sulfo-N-hydroxysuccinimidyl-2-(6-[biotinamido]-2-(p-azido benzamido)-hexanoamido)ethyl-1,3'-dithioproprionate
t	time
TAE	tris base, acetic acid and EDTA
TBS	tris buffered saline
TBSTT	tris buffered saline + tween-20 and triton X-100
TCA cycle	citric acid cycle
TCEP	tris (2-carboxyethyl)-phosphine hydrochloride
Thr	threonine
Tris	2-amino-2-hydroxymethyl-propane-1,3-diol
tRNA	transfer ribonucleic acid

Trp	tryptophan
UV	ultra violet
UV–Vis	ultra violet–visible spectroscopy
V	volts
Val	valine
W	tryptophan
X	unspecified amino acid
Y	tyrosine
Yfh1	*S. cerevisiae* frataxin homolog protein
ZIP	zinc transporter
α1	alpha 1 helix
β1	beta 1 strand
β-ME	β-mercaptoethanol
δ_{NH}	change in amide proton chemical shift
λ_{max}	maximum absorbance at given wavelength
μg	microgram
μL	microliter
μM	micromolar

ACKNOWLEDGMENTS

I would like to begin by acknowledging my research advisor Dr. Laura Busenlehner for mentoring me through my years in graduate school. She is a wonderful teacher and mentor. Without her, I would never have been able to achieve the goal of a PhD. She has taught me how to be a scientist and also a great speaker and leader.

I would like to thank my committee Dr. Patrick Frantom, Dr. Stevan Marcus, Dr. Shane Street and Dr. Stephen Woski for their guidance and patience throughout my graduate career.

I would like to thank Dr. Qiaoli Liang and Dr. Carolyn Cassady for their help and guidance with mass spectrometry.

I would like to thank the wonderful staff in the chemistry office, Janice Voss, Carolyn Walker, Evelyn Jackson and Jackie McPherson for always putting out fires and giving me answers to questions I wasn't even sure how to ask. You always made the small things that seemed like big things easier to handle. You are incredibly valuable to all of us, and without you, our lives would be so much harder.

I would like to thank my lab mates, past and present. Dr. Harry Singh and Dr. Mier An who led the way for the Busenlehner lab and with whom I share so many memories. Dr. Yu Wang who is my lab sister and one of the best friends and scientists anyone could have. I wish you so much success in the future. To the younger lab members, Dokyong Kim and Yasmeen Shamseddin, you are becoming scientists right before my eyes, and I wish you luck and please don't destroy the lab when I'm gone.

I would like to thank and honor my parents for their support and encouragement during the many years of graduate school. They have stood behind me my entire life, drying my tears, encouraging me and always giving me the honesty I need. There is no way I could have survived anything without you.

Finally, I want to thank my husband, Gregory Dye. Chemistry and football brought us together, roll tide! You have definitely made life better and I cannot wait for the things to come. Thank you for being there to help me trouble shoot, encourage me and celebrate. Most of all thank you for never giving up on me and believing in me when I didn't believe in myself. I love you.

CONTENTS

LIST OF TABLES

LIST OF FIGURES

CHAPTER 1

INTRODUCTION

1.1 Molecular Chaperones

Molecular chaperones, proteins that assist in the proper folding of proteins and other cellular macromolecules, are ubiquitous evolutionarily conserved proteins. Organisms from archae and eubacteria to the highest order mammals have molecular chaperones. Molecular chaperones are most often found in the endoplasmic reticulum (ER) of the cell, as this is where proteins are synthesized and sent to the cytoplasm or to their specific organelles to perform their ultimate functions. The most common molecular chaperones are from the family known as heat shock proteins (HSP). HSPs are expressed to prevent damage and aggregation of newly synthesized proteins [1].

1.2 Metallochaperones

Metallochaperones differ from molecular chaperones in many ways. The most important difference between molecular chaperones and metallochaperones is their ability to bind and transport metals. Unlike molecular chaperones, metallochaperones are not concerned with the proper folding of proteins, but with binding metals and metallocofactors, protecting them from redox chemistry, and transporting them to specific apo-metalloproteins. Transition metals, such as iron and copper, are considered toxic to the cell in their free forms and require metallochaperones for insertion target protein.

Table 1.1 Metallochaperones

Metallochaperone	Metal	Organism	Reference
Fxn1	Fe^{2+}	*H. sapiens*, *E. coli*, *S. cerevisiae*	Pastore, Puccio 2013
SufA/IscA	Fe^{2+}	*E. coli*	Tan *et al.* 2009
SCO1/2	Cu^{+}	*H. sapiens*	Bourens *et al.* 2014
Atx1	Cu^{+}	*S. cerevisiae*	Huffman *et al.* 2001
ZnuA	Zn^{2+}	*E. coli*	Falconi *et al.* 2011
HypA	Ni^{2+}, Zn^{2+}	*E. coli*	Watanbe *et al.* 2009
UreE	Ni^{2+}	*E. coli*	Grossoehme *et al.* 2007
SlyD	Ni^{2+}, Zn^{2+}, Cu^{+}, Mn^{2+}	*E. coli*	Kaluarachchi *et al.* 2011

Prior to 1997, the term and the field of metallochaperones were non-existent. Tom O'Halloran coined the term "metallochaperone" based on his seminal studies with copper binding chaperones [2] **(Table 1)**. Copper is a redox active metal and if free in the cellular mileau, it can participate in Fenton chemistry and create toxic hydroxyl and superoxide radicals [3]. In fact, copper is so protected that free copper concentrations in a yeast cell were determined to be less than 10^{-17} M, or less than one free copper atom per cell [4]. Atx1, one of the most well-studied copper chaperones, was originally isolated from *S. cerevisiae* [5, 6]. The metallochaperone Atx1 has an essential function in protecting copper and delivering it to Ccc2, a P-type ATPase required for copper trafficking in yeast. It was determined that Ccc2 actually possesses an Atx1-like structural domain that docks with Atx1 and induces copper transfer [6-8]. This system is analogous to human Hah1 copper chaperone that interacts with the N-terminal metal binding domains of human P-type Cu^+ ATPase [9] **(Figure 1.1)**. Experiments using nuclear magnetic resonance (NMR) and extended x-ray absorption fine structure (EXAFS) spectroscopy determined that copper was coordinated by two cysteine sulfurs in a surface accessible loop near the N-terminus by a MXCXXC motif, where M is methionine, X is any amino acid and C is cysteine. The MXCXXC motif is conserved among copper chaperones, as well as in the Cu^+ ATPases [5]. The two cysteine residues in the MXCXXC motif are involved in Cu^+ coordination and the loop containing these residues undergoes a conformational change upon release of Cu^+ to the Cu^+ ATPase (**Figure 1.2**). Mutations in human Hah1 and the P-type ATPase are involved in Menke's and Wilson's diseases, which are the prototypical copper overload syndromes [10-12]. While there has been extensive study on copper metallochaperones, there is very little known about the trafficking of iron for iron homeostatic pathways.

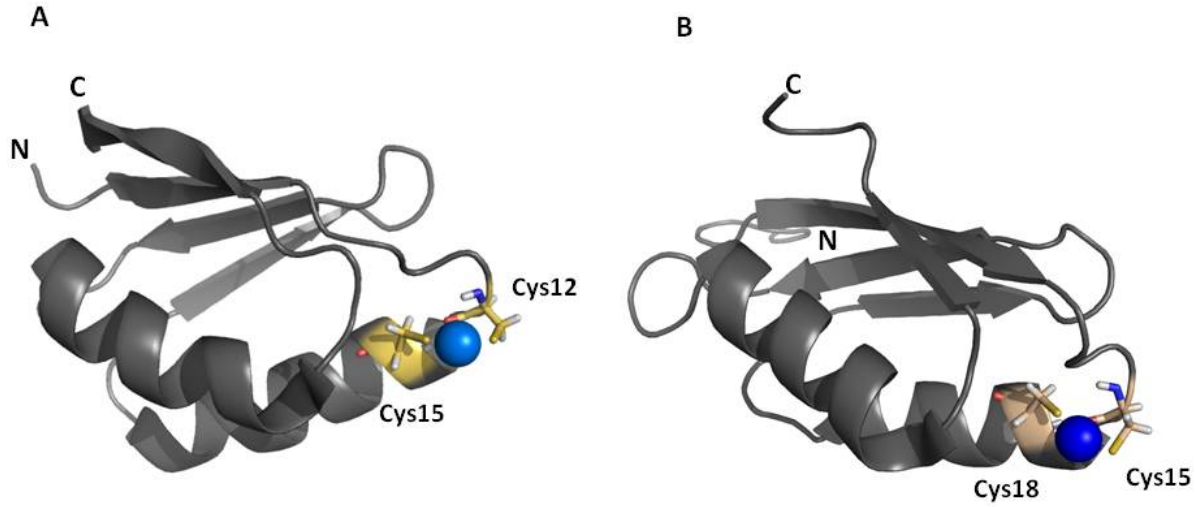

Figure 1.1 NMR structures of (A) Hah1 Cu^{+} chaperone (PDB: 1TL4) and (B) Cu^{+} ATPase Mnk1 (PDB:1KJV). The Cu^{+} atom (blue) is coordinated by Cys12 and Cys15 of Hah1 (A) and Cys15 and Cys18 of Mnk1 (B).

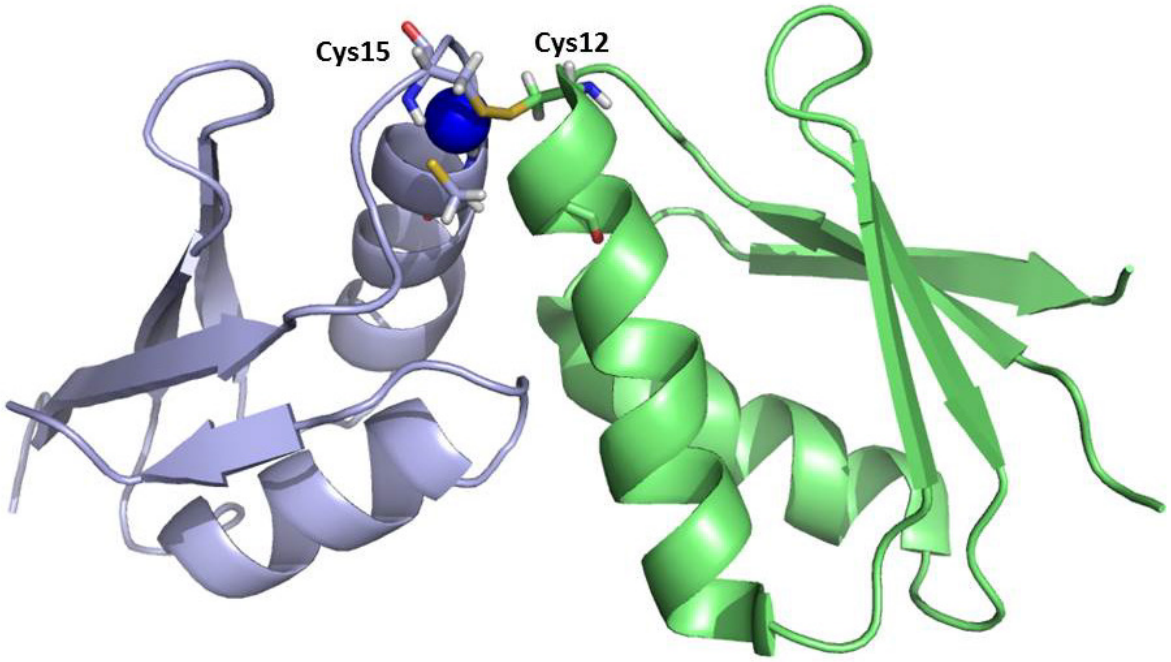

Figure 1.2 Model structure of Hah1 docked with Mnk1 for the disulfide bridge and copper transfer (PDB:2K1R)[13]. Hah1 (green) is docked with Mnk1(blue) through a disulfide bridge involving Cys12 of Hah1 and Cys15 of Mnk1 in order to complete the copper transfer from the chaperone, Hah1 to the Cu^{+} ATPase, Mnk1.

1.3 Iron Chemistry

Iron is an essential metal which is required for most living organisms. For humans, iron is acquired by the diet, is reduced by the low pH in the stomach, and is either trafficked to the endoplasmic reticulum or transported into the mitochondria for metallocofactor synthesis such as heme and iron–sulfur clusters [Fe–S]. Iron is ubiquitous because of the versatility of functions it can perform [14]. Iron can participate in vital biochemical processes including electron transport, cellular respiration and oxidative metabolism. These processes require bioavailable iron, which is not the same as solvated "free" iron. Iron is typically bound to proteins or other small molecule "chelates". This is because free iron in the cell can participate in damaging Fenton chemistry, which exploits the redox chemistry of iron. Fenton chemistry produces hydroxyl and superoxide radicals that are toxic to cells because they damage DNA, proteins, and lipids [15] **(Figure 1.3)**. Maintenance of iron homeostasis is extremely important since both iron deficiency and iron overload are destructive to cells. But, given the low concentration of free iron in the cell, is iron transported by metallochaperones to apo-proteins that require it for function? Does this mean that iron chaperones exist for each iron protein in the cell or are there a few "master" iron chaperones that can fulfill this role? There is an abundance of information on copper trafficking and chaperones, but is iron obtained and transported in the same fashion? The answers to these questions, over 15 years since the discovery of the first copper chaperones, are still unclear.

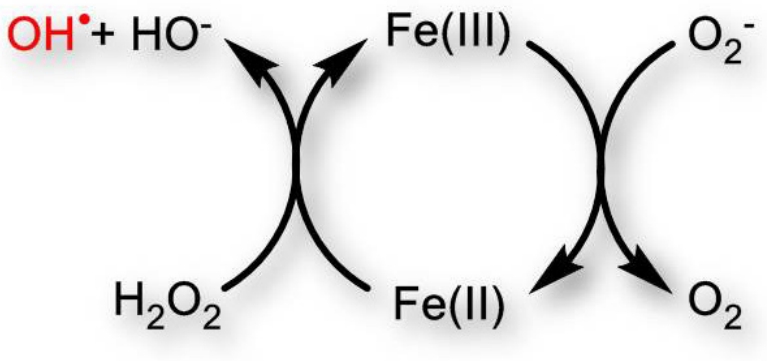

Figure 1.3 Fenton and Haber–Weiss chemical reaction. Free iron can participate with free oxygen and create toxic ions that damage DNA, proteins and lipids.

1.4 [Fe–S] Clusters

Iron that is imported into the mitochondria is used for [Fe–S] cluster cofactor assembly. [Fe–S] clusters are small cofactors that perform a wide variety of intracellular functions such as electron transport, iron uptake, iron and sulfur storage, regulation of gene expression, and regulation of enzyme activities [16]. The efficiency of [Fe–S] cluster biogenesis in the mitochondria is intimately linked to cellular iron homeostasis. Failure to properly assemble [Fe–S] clusters results in increased uptake of cellular iron and, eventually, mitochondrial iron overload. The decrease of [Fe–S] cluster proteins disturbs many cellular processes and puts the cell under stress and affects overall cellular function. The rate at which mitochondrial [Fe–S] clusters are assembled is known to regulate iron acquisition and intracellular iron distribution. This unique regulatory function is conserved from yeast to humans [17].

There are two types of basic iron–sulfur clusters, the [2Fe–2S] cluster and the [4Fe–4S] cluster **(Figure 1.4)**. There are other types of clusters that are required for very specific functions such as the FeMoCo cluster, which is found in nitrogenase enzymes of nitrogen-fixing bacteria and is synthesized by the NIF [Fe–S] pathway [18]. The [2Fe–2S] and the [4Fe–4S] clusters can be synthesized by either the SUF pathway or the ISC pathway [17]. The SUF pathway is only found in gammaproteobacteria and assembles [Fe–S] clusters under oxidative stress or iron limiting conditions [19]. The ISC pathway is found in prokaryotic and eukaryotic organisms and is expressed under normal cellular conditions [20, 21].

The human ISC system is composed of eight proteins: Isu2, Isa1 Nfs1, Isd11, Fdx1, FdxR, Hsc20 and mtHsp70 [22]. Isu2 is the scaffold protein that provides a surface for the cluster to be assembled [17]. The Isu2 scaffold has a unique structural fold that will be discussed in more detail in **Section 1.8** [1].

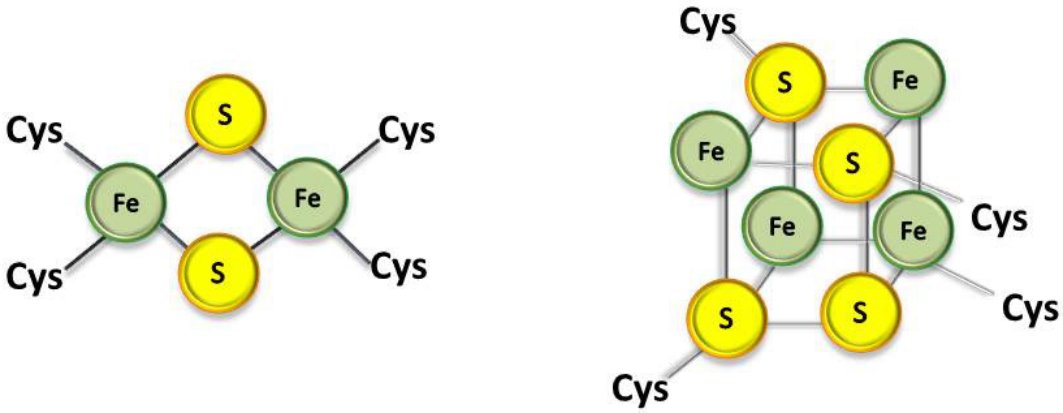

Figure 1.4 [2Fe–2S] cluster and [4Fe–4S] cluster. Coordinating cysteine residues can sometimes be replaced with histidine residues.

Isa1 is thought to be involved in the maturation and transport of [4Fe–4S] clusters [23]. Nfs1 is a pyridoxal 5'-phosphate (PLP) – dependent cysteine desulfurase that liberates sulfur from L-cysteine and donates sulfane sulfur to Isu2 for the assembly of the [Fe–S] cluster [24]. Isd11 is an accessory protein that aids in proper folding of Nfs1and enhances the cysteine desulfurase activity, but its exact function beyond this is unknown [25]. The other four proteins (Fdx, FdxR, Hsc20 and mtHsp70) are involved in the maturation and transport of the mature cluster to apo-target proteins [26, 27]. The main [Fe–S] cluster assembly complex is comprised of Isu2, Nfs1–Isd11 and an iron donor **(Figure 1.5)**. In the ISC operon, all components necessary for cluster formation and transport are present, with the exception of the iron donor. The identity of the iron donor has been debated, but is the proposed iron chaperone frataxin [28, 29].

1.5 Friedreich's Ataxia And Frataxin

The study of frataxin function stems from its relationship to the disease Friedreich's ataxia (FA). FA is an autosomal recessive, neurodegenerative progressive limb and gait ataxia that primarily afflicts children [30]. Friedreich's ataxia affects the peripheral nervous system, the spinal cord and muscle tissue, including the heart muscle [31]. Most often, FA patients are confined to a wheelchair the most common cause of death is cardiac arrest from cardiomyopathy (thickening of the heart muscle). FA is caused by decreased expression the mitochondrial protein frataxin in neural, muscle and pancreatic cells [32]. The decrease in frataxin levels comes from an exaggerated GAA codon repeat in the first intron of the gene [33] (**Figure 1.6**). In a normal gene, there can be 5–50 repeats, but when this repeat is exaggerated, it is increased to 100–2,000 GAA repeats.

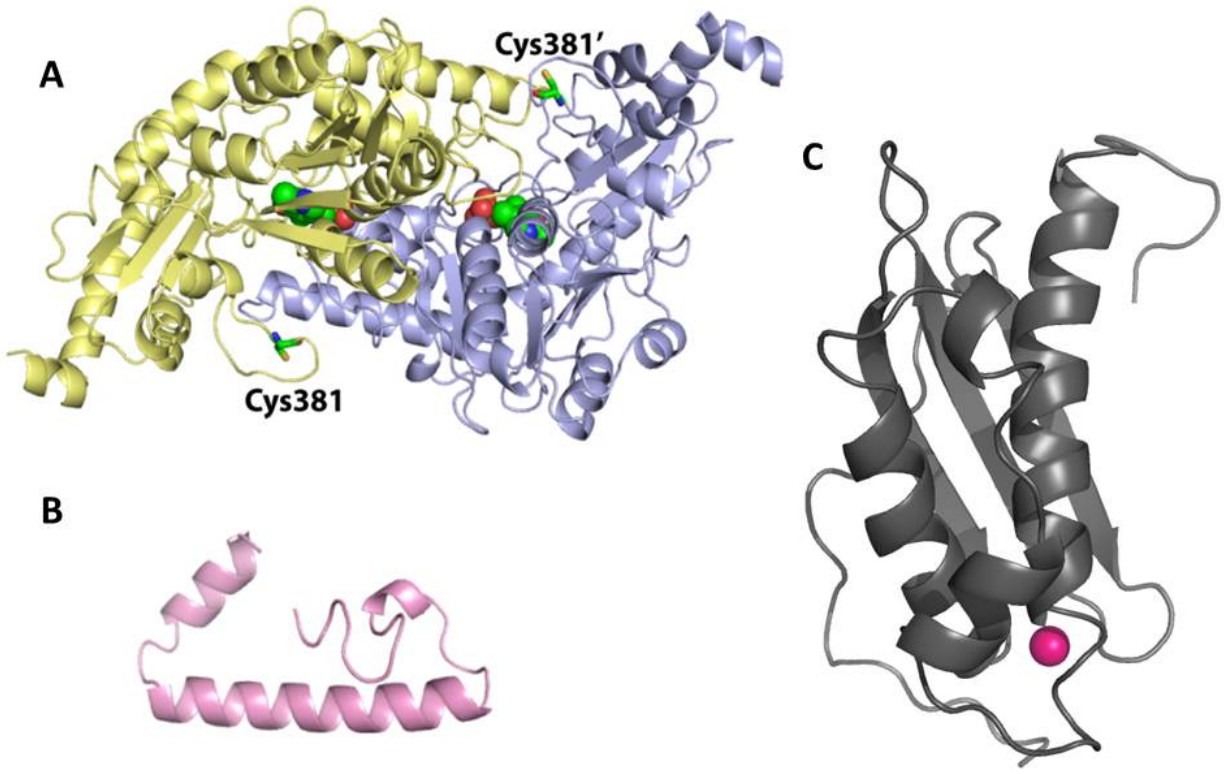

Figure 1.5 Members of the [Fe–S] cluster assembly complex as expressed in the ISC operon. (A) Model structure of homodimeric Nfs1, which requires PLP (green spheres) for function. (B) Model structure of Isd11, accessory protein co-expressed with Nfs1. (C) NMR structure of mouse Isu2. The structure was crystallized with zinc bound at the proposed [Fe–S] cluster assembly site (pink). This structure represents the structured form of Isu2 (PDB:1WFZ).

The exaggerated repeat impairs transcription and translation resulting in a decrease in frataxin protein in mitochondria [34]. Another cause of FA is from point mutations in the frataxin gene causing the replacement of an essential amino acid in addition to the GAA repeat. The point mutation can increase the severity of the disease, as well as the age of onset [35].

Depleted levels of frataxin have a two-fold consequence. The first is that the mitochondria do not have a way to bind and transport iron to proteins that require iron for function. The second is that the cell interprets this as an iron shortage and imports more iron into the mitochondria. As a result, there is both iron overload (caused by having excess non-bioavailable iron in ferric aggregates in the mitochondria) and iron deficiency (since this iron cannot be mobilized for [Fe–S] cluster assembly)[36, 37]. The increase in free iron increases oxidative stress in the mitochondria, which further damages [Fe–S] cluster proteins causing them to release toxic iron and sulfide ions. If the mitochondria cannot overcome the oxidative stress, the cell will die.

Frataxin has been proposed to have a myriad of functions including (1) an iron metallochaperone, (2) an iron storage protein, (3) a participant in electron transport and oxidative phosphorylation pathways, and (4) an activator of the ISC [Fe–S] cluster assembly complex [14]. While all of these functions have iron in common, some of them may be less physiologically relevant than others [38, 39]. For example, the research that frataxin can function as an oligomeric iron storage protein analogous to ferritin [40] has been refuted recently [38, 41-43]. The Stemmler group and the Cowan group have indicated that heme biosynthesis enzyme ferrocheletase receives iron from frataxin as a metallochaperone[14, 44, 45].

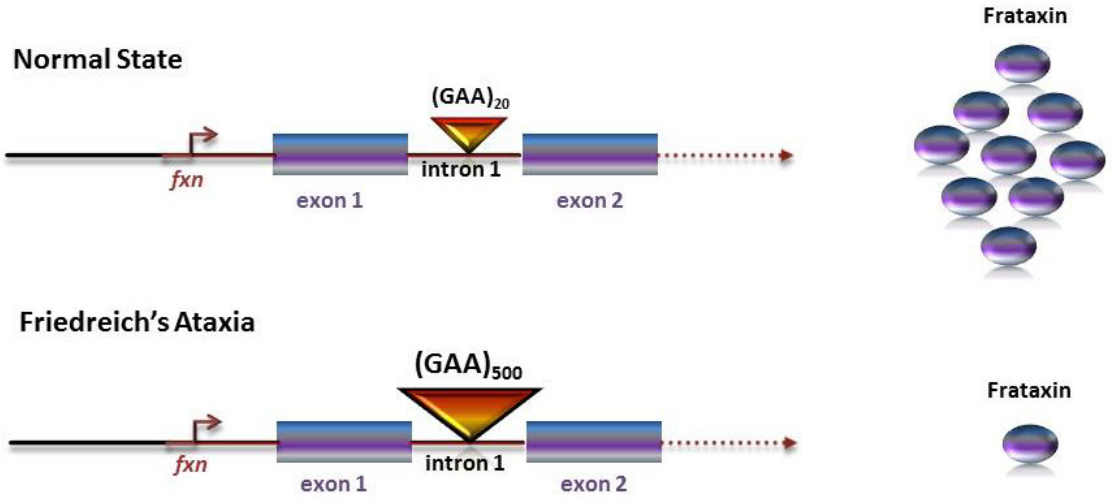

Figure 1.6 Cartoon representation of the normal *fxn1* gene vs. the FA *fxn1* gene. The exaggerated GAA repeat impacts the transcription and translation resulting in decreased expression of frataxin. Decreased levels of frataxin are detrimental to the mitochondria.

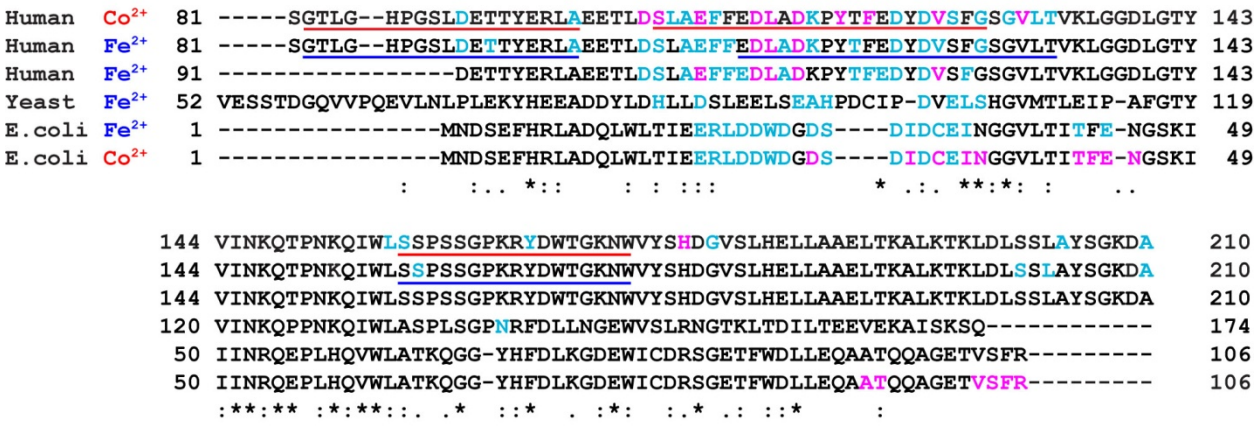

Figure 1.7 Sequence alignment of mature *H. sapiens* frataxin, *S. cerevisiae*Yfh1 and *E. coli* CyaY created with ClustalW [46]. The sequence alignment is a summary of Fe^{2+} and Co^{2+} NMR studies. Residues shown to broaden beyond detection (magenta) or have large chemical shifts in Fe^{2+} or Co^{2+} (cyan) NMR titrations. The first and second entries represent data that will be presented in this dissertation, the third entry (91–210 human frataxin) is from Nair *et al.* [14], the fourth (52 – 174 *S. cerevisiae* Yfh1) is from He *et al.* [48] and the fifth and sixth entries (1–106 *E. coli* CyaY) are from Pastore *et al.* [50-52]. The lines under the amino acid sequence represent peptides that had decreased deuterium incorporation in HDX –MS experiments with Fe^{2+} (blue) or Co^{2+} (red).

However, support for that hypothesis has diminished over the years with support from the Dailey group that ferrocheletase acquires iron from mitoferrin [47] and also unpublished data from the Busenlehner laboratory. Regardless, frataxin is an iron binding protein that is involved in mitochondrial iron metabolism [28, 35, 38, 48, 49]. The most recent research has demonstrated that frataxin had a direct role in [Fe–S] cluster synthesis, but the details of this function are unclear [48].

1.6 Frataxin Structure

Frataxin is a small nuclear-encoded protein of 210 amino acids. Frataxin contains an N–terminal mitochondrial targeting sequence that is cleaved once it enters the mitochondria by mitochondrial processing peptidase (MPP) in two sequential steps to the mature form (residues 81–210) [50]. Frataxin is a highly conserved protein (**Figure 1.7**) [14, 49, 51-53]. The most highly studied frataxin proteins are human frataxin (Fxn), the frataxin homologue from *S. cerevisiae* (Yfh1), and the bacterial homologue from *E. coli* (CyaY) (**Figure 1.8**). While the overall sequence identity between homologues is not very high, the conservation of residues in certain regions of the protein is striking **(Figure 1.9)**. The first highly conserved region of frataxin is the α1 helix. In human frataxin, there are 10 acidic residues (*e.g.*, Asp and Glu) in the first α-helix, with three additional residues heading into the first β-strand. The carboxylate side chains of these residues are all solvent exposed. Glu100, Glu108, Glu111, Asp112 and Asp124 are strictly conserved across all organisms, while the others are conserved in charge, meaning they may be exchanged for a glutamate in place of an aspartate [54].

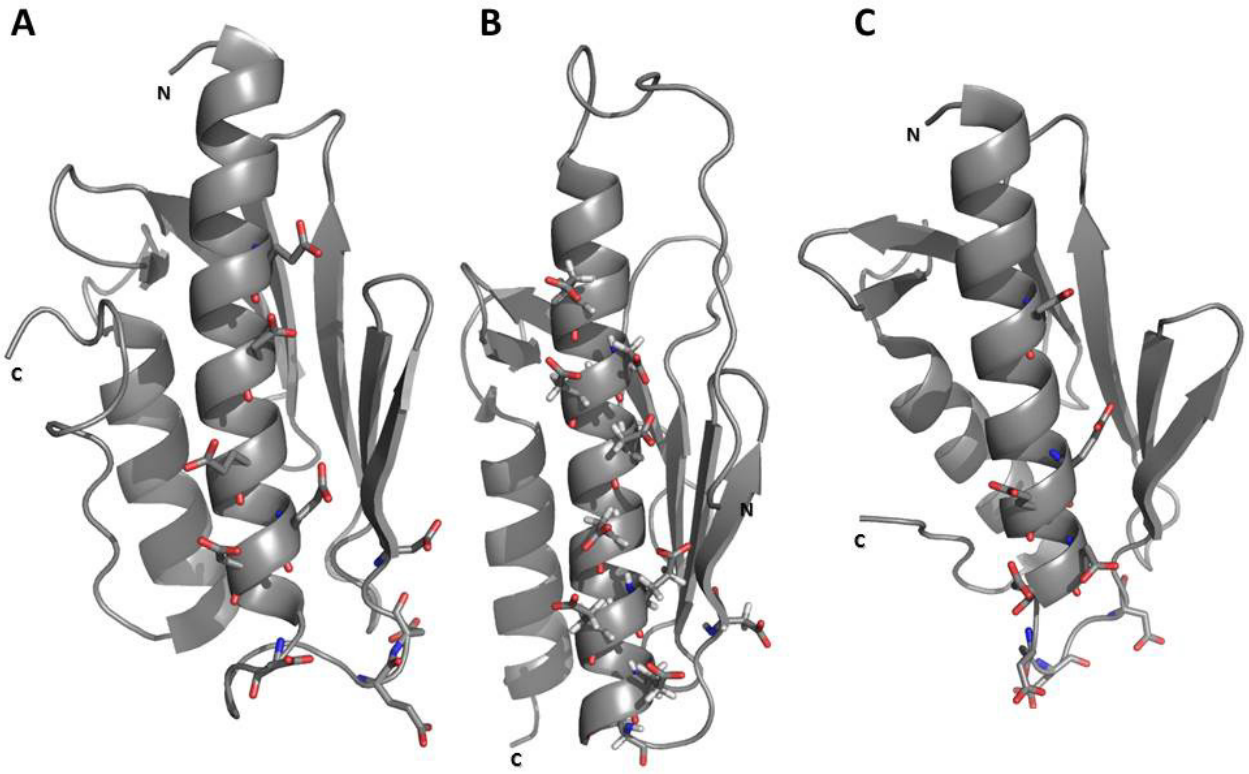

Figure 1.8 Crystal structures of frataxin homologues. (A) Human frataxin, frataxin (PDB:1EKG); (B) Yeast frataxin homologue, Yfh1 (PDB: 2GA5); (C) *E. coli* frataxin homologue, CyaY (PDB: 1EW4). The "acidic ridge" carboxylates (stick format) are well conserved among all frataxin homologs, implicating an important and conserved function.

The α1 helix region has been deemed the "acidic ridge", and has been proposed as the main site for iron binding, given the abundance of potential carboxylate ligands [55-57].

In 2007, the Pastore group examined the Fe^{2+} (and other metal) binding properties of bacterial frataxin CyaY using $^{1}H–^{15}N$ Heteronuclear Single Quantum Coherence (HSQC) NMR spectroscopy [55]. Pastore concluded that CyaY coordinates metal(s) at the end of the α1 helix and in the β1 strand based on the major shifting and broadening of the amide resonances by the paramagnetic metal. In 2009, the Pastore group examined the iron binding properties of 81–210 and 91–210 human frataxin to determine if the N–terminal tail (residues 81–90) impacted iron coordination [58]. HSQC NMR titration experiments with Fe^{2+} showed broadening and shifting of residues that were localized to the α1 helix–loop–β1 strand, including broadening of Asp112 and Asp115 and shifting of Asp124 resonances. Like CyaY, it was concluded that Fe^{2+} is coordinated by residues the α1 helix and β1 strand in human frataxin and that residues in the N-terminus from 81–90 were not involved in Fe^{2+} coordination because they saw no changes in the metal coordinating characteristics between the two constructs. In addition, there was no binding isotherm reported indicating a saturating Fe^{2+} stoichiometry. Since residues 81–90 at the N-terminal tail are disordered, those resonances are not observed in $^{1}H–^{15}N$ NMR experiments and no direct evidence of this conclusion was obtained. In 2010, the Stemmler group published the $^{1}H–^{15}N$ NMR chemical shift assignments for an unprocessed human frataxin intermediate containing residues 45–210 [59]. It was noted that residues 81–90 were also unstructured in this intermediate. Because there are no three-dimensional structures of any frataxin homologue with iron bound, the conservation of the α1 helix, and combined NMR results, the α1 helix and β1 strand were proposed to be the native, functional iron binding site(s) for frataxin.

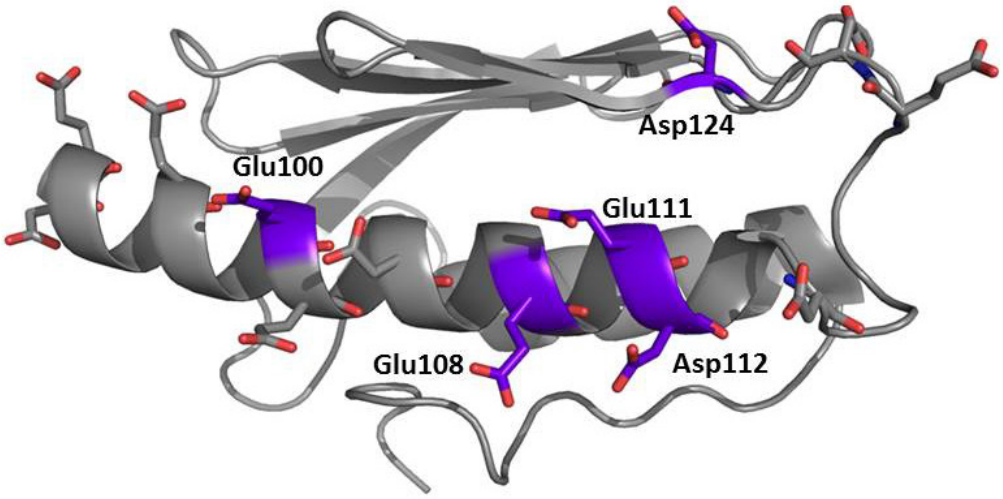

Figure 1.9 Conserved residues in the acidic ridge. Five of the 13 acidic residues in the "acidic ridge" are strictly conserved amongst all frataxin homologs (PDB: 1EKG). Shown in purple are the 5 conserved strictly conserved residues, Glu100, Glu108, Glu111, Asp112 and Asp124.

The second region of frataxin that has great evolutionary conservation is the hydrophobic region. The degree of identity/homology in this region is high, which may indicate that it has a conserved function. Val133, Val144, Pro150, Trp155, Pro159, Pro163 are strictly conserved in eukaryotes and eubacteria, and they comprise a large portion of the hydrophobic region (**Figure 1.10)**. Several point mutations of residues in this region such as I154F and W155R have also been shown to increase the symptoms of Friedreich's ataxia [35, 60].

The regions that are not well-conserved across different frataxin homologues include the N- and C- termini (**Figure 1.7**). The N-terminus of mature frataxin is probably the most highly differentiated region in frataxin, which is not surprising given that mitochondrial localization sequences are species–specific and that bacterial homologues do not need these sequences since they lack mitochondria. In humans, the N-terminus is cleaved by MPP peptidase after residues 51 and 80 [61]. In yeast, the partially-processed N-terminal tail is proposed to fold over the α1 helix to block iron binding [56]. The Cowan group also demonstrated that with this tail present, there is one iron binding site with nanomolar binding affinity. Only when the N-terminus is processed to the mature form does additional iron binding occur at the α1 helix, with much lower affinity [55]. The C-terminus of the different frataxin homologues is also quite divergent. In human frataxin, the C-terminal tail may stabilize the structure and protect the hydrophobic region. The C-terminal tail is absent in both Yfh1 and CyaY lending to their decreased chemical and thermal stability when compared to human frataxin [35]. While there is divergence amongst the structures of the frataxin homologs at their termini, this does not mean that there cannot be species-specific functions in these regions [49].

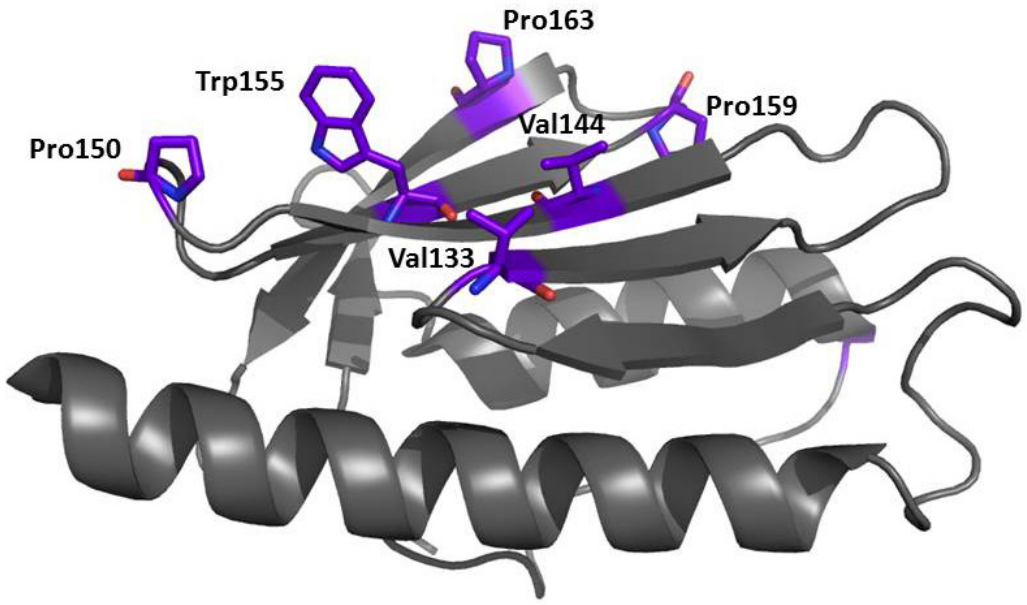

Figure 1.10 Conserved residues in the hydrophobic surface. Six residues in the hydrophobic region of frataxin are strictly conserved (PDB:1EKG). The residues in purple are Val133, Val144, Pro150, Trp155, Pro159 and Pro163.

1.7 Frataxin Protein–Protein Interactions

Iron–sulfur cluster assembly is a delicate process through which several proteins form a complex and all of the players must be present, not only for the formation, but for the release and transfer of the cluster to an apo-protein [27]. The [Fe–S] cluster assembly complex in humans is comprised of Isu2, Nfs1 and Isd11, as described in **Section 1.4**. The identity of the iron donor for this process is thought to be frataxin, but that role is still under scrutiny. Isothermal titration calorimetry and fluorescence binding experiments from the Cowan group [28], HSQC NMR titration experiments from the Markley group [22], and co-immunoprecipitation experiments from the Puccio group [62] support an interaction between frataxin and Isu2 *in vitro* and *in vivo*. While Isu2 on its own can assemble [Fe–S] clusters with exogenous free iron (and free sulfide) *in vitro* at an inefficient rate, this self-assembly of [Fe–S] clusters is not physiologically relevant [16, 63]. Some metallochaperone, metallated protein or small-molecule metal complex is the more likely to donate iron for this process. It is known that frataxin stimulates the rate of [Fe–S] cluster formation by Isu2 *in vitro* and thus the interaction between frataxin and Isu2 is specific and functional [28, 64]. However, whether frataxin transfers iron to Isu2 *in vivo* for the assembly of the cluster remains unknown.

1.8 The [Fe–S] Cluster Scaffold Isu2

Isu2 is referred to as the scaffold protein in the [Fe–S] cluster assembly complex. A scaffold is simply a surface on which something is assembled. Isu2 is very well conserved among all organisms that express the ISC operon and has a high degree of homology to the other forms of Isu from prokaryotes through higher eukaryotes [65, 66]. Isu2 contains four cysteine residues, three of which are strictly conserved (Cys69, Cys91, Cys138) and thought to ligate iron for [Fe–S] cluster assembly along with a highly conserved histidine residue (His137) [67]

(Figure 1.11). Without the conserved cysteine residues, an [Fe–S] cluster is not assembled, indicating the importance of the cysteine residues in cluster coordination [68].

Isu2 is an intrinsically disordered protein that exists in equilibrium between two states, the dynamically disordered (D) and structured (S) states [22]. Markley demonstrated that while bacterial IscU was 70% structured, human Isu2 is less than 30% structured. The only NMR structure of eukaryotic Isu2 (**Figure 1.5B**) is from mouse, which is 98% identical to human Isu2, but it was crystallized with zinc [65]. The Zn^{2+} ion was coordinated in the region proposed as the assembly site for [Fe–S] clusters (Cys69, Cys91, His137 and Cys138) and thus forces Isu2 into the structured (S) state. Human Isu2 shifts between the D state when bound to and accepting sulfur from Nfs1 versus the S state when bound to and transferring an assembled [Fe–S] cluster to the chaperone Hsc20. [69]. Currently it is not known which conformation of Isu2 (S or D) interacts with frataxin and if binding of frataxin and Nfs1 to Isu2 are mutually exclusive. More structural studies are needed to identify where and under what conditions frataxin and Isu2 interact for iron transfer and [Fe–S] cluster assembly, as well as how the structure of Isu2 is influenced by the interaction with the entire assembly complex.

1.9 Scope Of Dissertation Research

The goal of this dissertation research is to first characterize the metal binding properties of frataxin. We employed several spectroscopic techniques to gain a complete understanding of frataxin and its iron binding properties. Once a comprehensive understanding of how, where and how well frataxin binds iron is obtained, more in depth studies of frataxin interactions with protein partners can be undertaken. The second goal of this research is to determine the interface of the interaction between frataxin and Isu2 during Fe^{2+} transfer and [Fe–S] cluster assembly and

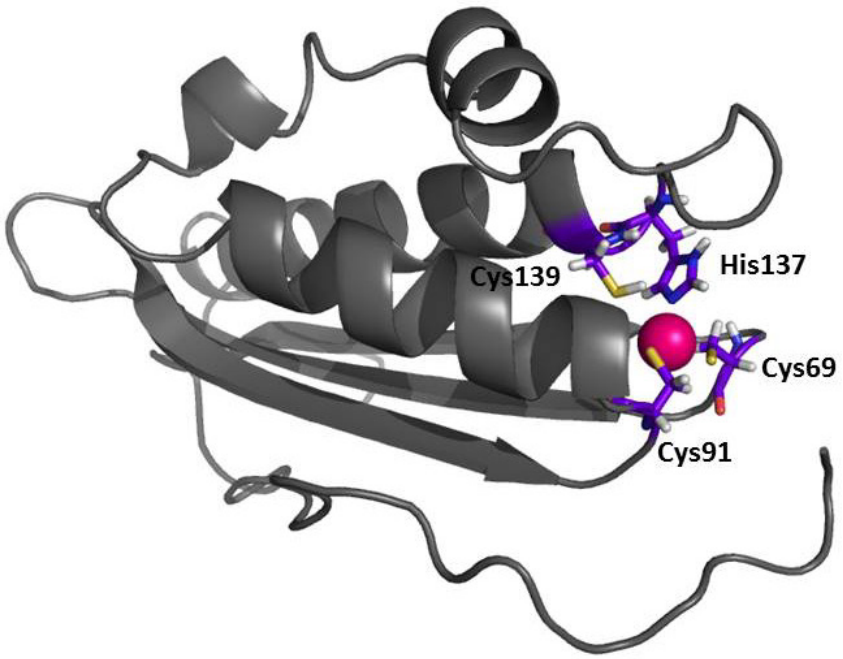

Figure 1.11 NMR structure of mouse Isu2 with zinc. Isu2 has 3 strictly conserved cysteine residues and 1 strictly conserved histidine residue that comprise the [Fe–S] cluster assembly site. The conserved residues in purple that ligate [Fe–S] clusters are Cys69, Cys91, His137 and Cys138. The structure was determined with Zn^{2+} in the assembly site and depicts Isu2 in the more structured (S) state (PDB:1WFZ).

also to determine how Isu2 structure is affected by frataxin, iron binding and [Fe–S] cluster assembly.

In Chapter 2, studies will be presented that address the Fe^{2+} coordination stoichiometry of human frataxin, the Fe^{2+} coordination sites of frataxin and what amino acid residues are involved in the coordination. Intrinsic tryptophan fluorescence will indicate the number of metal ions coordinated by frataxin. $^{1}H–^{15}N$HSQC NMR experiments will identify the regions of metal coordination for frataxin. UV–Visible and EPR spectroscopies will identify the types of amino acids involved in metal coordination as well as the metal coordination geometry for frataxin. A competition assay with Fe^{2+} chelator ferrozine will indicate if any of the frataxin coordination sites coordinate Fe^{2+} with a greater affinity than ferrozine.

In Chapter 3, the utility of the three histidine residues of frataxin will be evaluated for their metal coordinating characteristics in the same manner as that for wild type frataxin. UV–Visible spectroscopy and EPR spectroscopy will determine if the elimination of the histidine changes the coordination environment of frataxin.

In Chapter 4, studies will be presented that address the interaction between frataxin and Isu2 including the affinity with which frataxin binds Isu2, as well as the regions of frataxin and Isu2 that are involved in the interaction. Intrinsic tryptophan fluorescence experiments will demonstrate the affinity with which frataxin binds Isu2, and how Fe^{3+} influences the interaction. [Fe–S] cluster assembly assays will support the idea that frataxin stimulates the assembly of [Fe–S] clusters on Isu2. Crosslinking experiments will identify amino acid residues that are involved in the interface of the interaction as well as on the outer surface of the interaction. Hydrogen–deuterium exchange mass spectrometry deuterium trapping experiments will identify peptides on frataxin that are protected by Isu2 during the Fe^{3+} mediated interaction. $^{1}H–^{15}N$ HSQC NMR

experiments will identify the structural state of Isu2 during the interaction with frataxin as well as when an [Fe–S] cluster is bound.

REFERENCES

1. Hartl, F.U., R. Hlodan, and T. Langer, *Molecular chaperones in protein folding: the art of avoiding sticky situations.* Trends Biochem. Sci., 1994. **19**(1): p. 20-5.

2. Lin, S.J., et al., *A role for the Saccharomyces cerevisiae ATX1 gene in copper trafficking and iron transport.* J. Biol. Chem., 1997. **272**(14): p. 9215-20.

3. Thomas, C., et al., *Hydroxyl radical is produced via the Fenton reaction in submitochondrial particles under oxidative stress: implications for diseases associated with iron accumulation.* Redox. Rep., 2009. **14**(3): p. 102-8.

4. Rae, T.D., et al., *Undetectable intracellular free copper: the requirement of a copper chaperone for superoxide dismutase.* Science, 1999. **284**(5415): p. 805-8.
5. Huffman, D.L. and T.V. O'Halloran, *Function, structure, and mechanism of intracellular copper trafficking proteins.* Annu. Rev. Biochem., 2001. **70**: p. 677-701.

6. Pufahl, R.A., et al., *Metal ion chaperone function of the soluble Cu(I) receptor Atx1.* Science, 1997. **278**(5339): p. 853-6.

7. Banci, L., et al., *Solution structure of the yeast copper transporter domain Ccc2a in the apo and Cu(I)-loaded states.* J. Biol. Chem., 2001. **276**(11): p. 8415-26.

8. Arnesano, F., et al., *Characterization of the binding interface between the copper chaperone Atx1 and the first cytosolic domain of Ccc2 ATPase.* J. Biol. Chem., 2001. **276**(44): p. 41365-76.

9. Huffman, D.L. and T.V. O'Halloran, *Energetics of copper trafficking between the Atx1 metallochaperone and the intracellular copper transporter, Ccc2.* J. Biol. Chem., 2000. **275**(25): p. 18611-4.

10. Vulpe, C., et al., *Isolation of a candidate gene for Menkes disease and evidence that it encodes a copper-transporting ATPase.* Nat. Genet., 1993. **3**(1): p. 7-13.

11. Bull, P.C., et al., *The Wilson disease gene is a putative copper transporting P-type ATPase similar to the Menkes gene.* Nat. Genet., 1993. **5**(4): p. 327-37.

12. Tanzi, R.E., et al., *The Wilson disease gene is a copper transporting ATPase with homology to the Menkes disease gene.* Nat. Genet., 1993. **5**(4): p. 344-50.

13. Arumugam, K. and S. Crouzy, *Dynamics and stability of the metal binding domains of the Menkes ATPase and their interaction with metallochaperone HAH1.* Biochemistry. **51**(44): p. 8885-906.

14. Bencze, K.Z., et al., *The structure and function of frataxin.* Crit Rev Biochem Mol Biol, 2006. **41**(5): p. 269-91.

15. Cadet, J., et al., *Hydroxyl radicals and DNA base damage.* Mutat. Res., 1999. **424**(1-2): p. 9-21.

16. Gerber, J. and R. Lill, *Biogenesis of iron-sulfur proteins in eukaryotes: components, mechanism and pathology.* Mitochondrion, 2002. **2**(1-2): p. 71-86.

17. Lill, R., et al., *The role of mitochondria in cellular iron-sulfur protein biogenesis and iron metabolism.* Biochim. Biophys. Acta., **1823**(9): p. 1491-508.

18. Zheng, L. and D.R. Dean, *Catalytic formation of a nitrogenase iron-sulfur cluster.* J. Biol. Chem., 1994. **269**(29): p. 18723-6.

19. Nakamura, M., K. Saeki, and Y. Takahashi, *Hyperproduction of recombinant ferredoxins in escherichia coli by coexpression of the ORF1-ORF2-iscS-iscU-iscA-hscB-hs cA-fdx-ORF3 gene cluster.* J. Biochem., 1999. **126**(1): p. 10-8.

20. Zheng, L., et al., *Assembly of iron-sulfur clusters. Identification of an iscSUA-hscBA-fdx gene cluster from Azotobacter vinelandii.* J. Biol. Chem., 1998. **273**(21): p. 13264-72.

21. Garland, S.A., et al., *Saccharomyces cerevisiae ISU1 and ISU2: members of a well-conserved gene family for iron-sulfur cluster assembly.* J. Mol. Biol., 1999. **294**(4): p. 897-907.

22. Markley, J.L., et al., *Metamorphic protein IscU alternates conformations in the course of its role as the scaffold protein for iron-sulfur cluster biosynthesis and delivery.* FEBS Lett., **587**(8): p. 1172-9.

23. Sheftel, A.D., et al., *The human mitochondrial ISCA1, ISCA2, and IBA57 proteins are required for [4Fe-4S] protein maturation.* Mol. Biol. Cell., **23**(7): p. 1157-66.

24. Schwartz, C.J., et al., *The cysteine desulfurase, IscS, has a major role in in vivo Fe-S cluster formation in Escherichia coli.* Proc. Natl. Acad. Sci. U S A, 2000. **97**(16): p. 9009-14.

25. Wiedemann, N., et al., *Essential role of Isd11 in mitochondrial iron-sulfur cluster synthesis on Isu scaffold proteins.* EMBO J., 2006. **25**(1): p. 184-95.

26. Chandramouli, K. and M.K. Johnson, *HscA and HscB stimulate [2Fe-2S] cluster transfer from IscU to apoferredoxin in an ATP-dependent reaction.* Biochemistry, 2006. **45**(37): p. 11087-95.

27. Vickery, L.E. and J.R. Cupp-Vickery, *Molecular chaperones HscA/Ssq1 and HscB/Jac1 and their roles in iron-sulfur protein maturation.* Crit. Rev. Biochem. Mol. Biol., 2007. **42**(2): p. 95-111.

28. Yoon, T. and J.A. Cowan, *Iron-sulfur cluster biosynthesis. Characterization of frataxin as an iron donor for assembly of [2Fe-2S] clusters in ISU-type proteins.* J. Am. Chem. Soc., 2003. **125**(20): p. 6078-84.

29. Qi, W. and J.A. Cowan, *Structural, Mechanistic and Coordination Chemistry of Relevance to the Biosynthesis of Iron-Sulfur and Related Iron Cofactors.* Coord. Chem. Rev., **255**(7-8): p. 688-699.

30. Durr, A., et al., *Clinical and genetic abnormalities in patients with Friedreich's ataxia.* N. Engl. J. Med., 1996. **335**(16): p. 1169-75.

31. Montermini, L., et al., *Phenotypic variability in Friedreich ataxia: role of the associated GAA triplet repeat expansion.* Ann. Neurol., 1997. **41**(5): p. 675-82.

32. Monros, E., et al., *Phenotype correlation and intergenerational dynamics of the Friedreich ataxia GAA trinucleotide repeat.* Am. J. Hum. Genet., 1997. **61**(1): p. 101-10.

33. Campuzano, V., et al., *Frataxin is reduced in Friedreich ataxia patients and is associated with mitochondrial membranes.* Hum. Mol. Genet., 1997. **6**(11): p. 1771-80.

34. Filla, A., et al., *The relationship between trinucleotide (GAA) repeat length and clinical features in Friedreich ataxia.* Am. J. Hum. Genet., 1996. **59**(3): p. 554-60.

35. Correia, A.R., et al., *Conformational stability of human frataxin and effect of Friedreich's ataxia-related mutations on protein folding.* Biochem. J., 2006. **398**(3): p. 605-11.

36. Kim, J.H., et al., *Three-dimensional structure and determinants of stability of the iron-sulfur cluster scaffold protein IscU from Escherichia coli.* Biochemistry, **51**(28): p. 5557-63.

37. Koutnikova, H., et al., *Studies of human, mouse and yeast homologues indicate a mitochondrial function for frataxin.* Nat. Genet., 1997. **16**(4): p. 345-51.

38. Seguin, A., et al., *Evidence that yeast frataxin is not an iron storage protein in vivo.* Biochim. Biophys. Acta., **1802**(6): p. 531-8.

39. Gerber, J., U. Muhlenhoff, and R. Lill, *An interaction between frataxin and Isu1/Nfs1 that is crucial for Fe/S cluster synthesis on Isu1.* EMBO Rep., 2003. **4**(9): p. 906-11.

40. Gakh, O., et al., *Normal and Friedreich ataxia cells express different isoforms of frataxin with complementary roles in iron-sulfur cluster assembly.* J. Biol. Chem.. **285**(49): p. 38486-501.

41. Adinolfi, S., et al., *A structural approach to understanding the iron-binding properties of phylogenetically different frataxins.* Hum. Mol. Genet., 2002. **11**(16): p. 1865-77.

42. Layer, G., et al., *Iron-sulfur cluster biosynthesis: characterization of Escherichia coli CYaY as an iron donor for the assembly of [2Fe-2S] clusters in the scaffold IscU.* J. Biol. Chem., 2006. **281**(24): p. 16256-63.

43. Schmucker, S., et al., *The in vivo mitochondrial two-step maturation of human frataxin.* Hum. Mol. Genet., 2008. **17**(22): p. 3521-31.

44. Bencze, K.Z., et al., *Human frataxin: iron and ferrochelatase binding surface.* Chem. Commun. (Camb), 2007(18): p. 1798-800.

45. Yoon, T. and J.A. Cowan, *Frataxin-mediated iron delivery to ferrochelatase in the final step of heme biosynthesis.* J. Biol. Chem., 2004. **279**(25): p. 25943-6.

46. Larkin, M.A., et al., *Clustal W and Clustal X version 2.0.* Bioinformatics, 2007. **23**(21): p. 2947-8.

47. Jiang, F., et al., *Electron spin echo envelope modulation studies of the Cu(II)-substituted derivative of isopenicillin N synthase: a structural and spectroscopic model.* Biochemistry, 1991. **30**(48): p. 11437-45.

48. Martelli, A., et al., *Frataxin is essential for extramitochondrial Fe-S cluster proteins in mammalian tissues.* Hum. Mol. Genet., 2007. **16**(22): p. 2651-8.

49. Prischi, F., et al., *The N-terminus of mature human frataxin is intrinsically unfolded.* FEBS J., 2009. **276**(22): p. 6669-76.

50. Branda, S.S., et al., *Yeast and human frataxin are processed to mature form in two sequential steps by the mitochondrial processing peptidase.* J. Biol. Chem., 1999. **274**(32): p. 22763-9.

51. Condo, I., et al., *In vivo maturation of human frataxin.* Hum. Mol. Genet., 2007. **16**(13): p. 1534-40.

52. Bridwell-Rabb, J., et al., *Effector role reversal during evolution: the case of frataxin in Fe-S cluster biosynthesis.* Biochemistry, **51**(12): p. 2506-14.

53. Adinolfi, S., et al., *The factors governing the thermal stability of frataxin orthologues: how to increase a protein's stability.* Biochemistry, 2004. **43**(21): p. 6511-8.

54. Dhe-Paganon, S., et al., *Crystal structure of human frataxin.* J. Biol. Chem., 2000. **275**(40): p. 30753-6.

55. Prischi, F., et al., *Structural bases for the interaction of frataxin with the central components of iron-sulphur cluster assembly.* Nat. Commun., **1**: p. 95.

56. Yoon, T., E. Dizin, and J.A. Cowan, *N-terminal iron-mediated self-cleavage of human frataxin: regulation of iron binding and complex formation with target proteins.* J. Biol. Inorg. Chem., 2007. **12**(4): p. 535-42.

57. Pastore, A. and H. Puccio, *Frataxin: a protein in search for a function.* J. Neurochem. **126 Suppl 1**: p. 43-52.

58. Prischi Filippo, G.C., Adinolfi Salvatore, Pastore Annalisa, *The N-terminus of mature human frataxin is intrinsically unfolded.* FEBS J., 2009. **276**: p. 6669-6676.

59. Kondapalli, K.C., et al., *NMR assignments of a stable processing intermediate of human frataxin.* Biomol. NMR Assign., **4**(1): p. 61-4.

60. Tsai, C.L., J. Bridwell-Rabb, and D.P. Barondeau, *Friedreich's ataxia variants I154F and W155R diminish frataxin-based activation of the iron-sulfur cluster assembly complex.* Biochemistry, **50**(29): p. 6478-87.

61. Adinolfi, S., et al., *Bacterial frataxin CyaY is the gatekeeper of iron-sulfur cluster formation catalyzed by IscS.* Nat. Struct. Mol. Biol., 2009. **16**(4): p. 390-6.

62. Schmucker, S., et al., *Mammalian frataxin: an essential function for cellular viability through an interaction with a preformed ISCU/NFS1/ISD11 iron-sulfur assembly complex.* PLoS One. **6**(1): p. e16199.

63. Raulfs, E.C., et al., *In vivo iron-sulfur cluster formation.* Proc. Natl. Acad. Sci. U S A, 2008. **105**(25): p. 8591-6.

64. Huang, J., E. Dizin, and J.A. Cowan, *Mapping iron binding sites on human frataxin: implications for cluster assembly on the ISU Fe-S cluster scaffold protein.* J. Biol. Inorg. Chem., 2008. **13**(5): p. 825-36.

65. Ramelot, T.A., et al., *Solution NMR structure of the iron-sulfur cluster assembly protein U (IscU) with zinc bound at the active site.* J. Mol. Biol., 2004. **344**(2): p. 567-83.

66. Qi, W. and J.A. Cowan, *A structural and functional homolog supports a general role for frataxin in cellular iron chemistry.* Chem. Commun. (Camb). **46**(5): p. 719-21.

67. Wu, S.P., et al., *Iron-sulfur cluster biosynthesis. Kinetic analysis of [2Fe-2S] cluster transfer from holo ISU to apo Fd: role of redox chemistry and a conserved aspartate.* Biochemistry, 2002. **41**(28): p. 8876-85.

68. Wu, G., et al., *Characterization of an iron-sulfur cluster assembly protein (ISU1) from Schizosaccharomyces pombe.* Biochemistry, 2002. **41**(15): p. 5024-32.

69. Cai, K., et al., *Human Mitochondrial Chaperone (mtHSP70) and Cysteine Desulfurase (NFS1) Bind Preferentially to the Disordered Conformation whereas Co-chaperone (HSC20) Binds to the Structured Conformation of the Iron-Sulfur Cluster Scaffold Protein (ISCU)*. J. Biol. Chem. 2013 **288**(40): p.28755-70.

CHAPTER 2

CHARACTERIZATION OF IRON COORDINATION BY HUMAN FRATAXIN

2.1 INTRODUCTION

2.1.1 Frataxin Iron Coordination

Frataxin has many proposed functions. The involvement of iron in all of these functions is not questioned, but the precise role with which frataxin uses iron has been debated [1]. In the absence of frataxin, enzymes requiring [Fe–S] clusters have decreased activities, impairing mitochondrial and cellular functions [2]. There is indirect evidence that frataxin delivers the iron for [Fe–S] cluster biogenesis because of the correlation with [Fe–S] enzyme activities [3-6]. However, it remains unclear how frataxin coordinates Fe^{2+} and how it is transferred to protein acceptors. It has been thought that frataxin binds Fe^{2+} at the first α-helix and first β-strand using carboxylate side chains [7-9]. The only support for iron coordination at the α1 helix stems from the high conservation seen in this region (**Figure 1.7**, **Section 1.6**) and NMR titrations, as discussed in Chapter 1. Unlike copper metallochaperones, human frataxin contains no cysteine residues, which are the preferred metal binding amino acid residues for metals like Cu^{+} and Fe^{2+}. So frataxin ferrous iron coordination using solely carboxylate residues is unusual.

The debate surrounding the iron coordination by frataxin is not only in the location of the iron binding, but also in the stoichiometry and affinity with which frataxin coordinates Fe^{2+}. The iron binding stoichiometry of frataxin has been reported from as few as 1 iron ion to as many as 7 iron ions per frataxin monomer by NMR, ITC, and fluorescence titrations [7, 9-11]. Previously published NMR iron coordination studies are inconclusive because of the conditions under which the experiments were run [12-14]. Incompatible buffers such as phosphates and high concentrations of reducing agents such as DTT can interfere with metal coordination. The use of

Mg^{2+} has also been used in an attempt to reduce non-specific binding [15]. However, Mg^{2+} can compete with metal coordinating amino sites and can also interfere with the coordination stoichiometry. The controversy over this quantity is important because knowing the number of iron ions that frataxin coordinates is a first step towards understanding the mechanism by which frataxin coordinates iron for transfer to proteins such as Isu2 for [Fe–S] cluster assembly.

The Cowan group has reported that human frataxin can coordinate up to 7 Fe^{2+} ions with an average affinity of 55 μM using isothermal titration calorimetry [4]. Copper and other chaperones are known to bind their metals with high affinity (K_D < nM) [16], so the weak iron binding by frataxin is disconcerting if it is indeed a chaperone [1]. If frataxin is a an Fe^{2+} chaperone, whose interaction with Isu2 stimulates the rate of *in vivo* [Fe–S] cluster assembly, there must be a site (or sites) that coordinate Fe^{2+} with a greater affinity than 55 μM. For example, bacterial frataxin, CyaY and yeast frataxin, Yfh1 are reported to bind two Fe^{2+} ions with binding affinities of 3.8 μM and 0.1 μM, respectively [10, 17].

2.1.2 Role of the Frataxin N-Terminus

The mature form of frataxin that coordinates iron is a multiply processed form. Frataxin contains a mitochondrial localization sequence that is cleaved in two sequential steps by mitochondrial processing peptidase (MPP) to the mature form of 81–210 once it reaches the inner mitochondrial matrix [18]. While all frataxin homologs are processed to a mature form, there are unique differences in their N-terminal regions. Human frataxin contains a small N-terminal loop that is unstructured whereas the yeast frataxin homolog, Yfh1, has a much longer N-terminal loop that is also unstructured (**Figure 2.1**). The *E. coli* frataxin homolog CyaY does not contain an N-terminal extension. Thus, the divergence of the N-terminal amino acid sequence could indicate a unique function for human frataxin [14, 19]. There is currently no

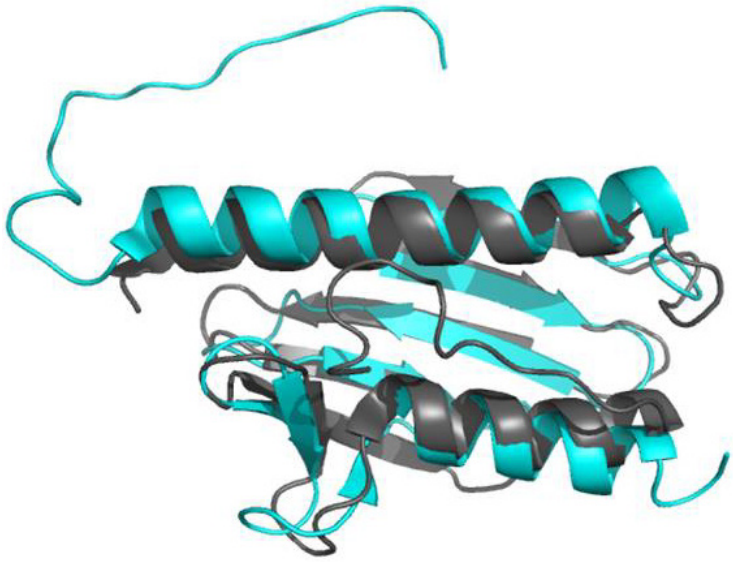

Figure 2.1 Overlay of human frataxin, gray (PDB:1EKG) and yeast frataxin, cyan (2GA5). The N-terminal tail of mature yeast frataxin is much longer than the N-terminal tail of human frataxin.

structure of human frataxin containing the 81–90 unstructured tail, nor are there NMR assignments for these residues. Having little structural information about the N-terminal loop makes defining its function difficult. To rule out the N-terminus as having no function in metal binding simply from the inability to observe it structurally is flawed. It is also possible that the N-terminus could play a role in binding partners like Isu2 or regulate iron transfer.

2.1.3 Surrogate Metals to Probe Frataxin Metal Coordination

In order to characterize the metal coordination chemistry of frataxin, we can employ the use of metal surrogates as spectroscopic probes in substitute of Fe^{2+}. The use of metal surrogates has been an acceptable way to study metalloproteins whose native metals are often difficult to work with or are spectroscopically silent in the UV–Visible region. Iron proteins fall into both categories. Ferrous iron can be rapidly oxidized to the 3+ state by oxygen in solution. In order to maintain iron in the reduced Fe^{2+} state in solution, the metal solution must be entirely anoxic or there must be reducing agents such as dithiothreitol (DTT) present to prevent oxidation; however, these reductants also coordinate metals to varying degrees so they should not be included in experiments to determine stoichiometry and binding affinity. In addition, the frataxin ferrous iron coordination cannot be determined by UV–Visible spectroscopy since it has no cysteine residues and thus no ligand-to-metal charge transfer transitions. Also, the *d–d* transitions of Fe^{2+} are usually in the near-IR range. Several transition metals have many similar properties to ferrous iron including ionic radii and ligand preference. From Hard-Soft Acid-Base (HSAB) theory, Fe^{2+} is an intermediate acid that typically prefers intermediate ligands such as imidazole nitrogen. Co^{2+} and Cu^{2+} are also intermediate acids according to HSAB theory and prefer similar ligands to that of Fe^{2+}. Co^{2+} and Cu^{2+} are also both air stable and do not require anaerobic conditions or harsh reducing agents in solution. Co^{2+} and Cu^{2+} have been widely used

as spectroscopic probes in substitute for iron in metalloproteins [20]. The *d–d* transitions of metals, while weak, are sensitive to the changes in the coordination environment. In addition, the intensity of the molar absorptivities also indicates the coordination geometry of the metal coordination site(s).

2.1.4 Approach to Defining Frataxin Iron Coordination

The iron coordination stoichiometry of human frataxin will be determined using Cu^{2+} and Co^{2+} metal surrogates in non-chelating buffers and in the absence of reducing agents by experiments such as intrinsic tryptophan fluorescence (ITF). ITF monitors saturable tryptophan fluorescence quenching as frataxin coordinates metal. $^{1}H–^{15}N$ HSQC NMR titrations with Cu^{2+}, Co^{2+} surrogates and with Fe^{2+} can be compared in order to properly discern the amino acid residues that are most likely involved in iron binding. Coordination of paramagnetic metals such as Co^{2+}, Cu^{2+} and Fe^{2+} to amino acid residues cause line broadening and shifting of the amide nitrogen and proton chemical shifts as a result of through–bond coupling of the free electrons and the protein nuclei. Although NMR can give structural information regarding iron coordination in the structured regions of frataxin, the involvement of the N-terminus in iron coordination to frataxin, which was previously implicated in iron binding by hydrogen/deuterium exchange mass spectrometry (HDX–MS), cannot be determined. In order to determine the overall frataxin metal coordination, other spectroscopic methods such as UV–Visible and electron paramagnetic resonance (EPR) spectroscopies can reveal the types of amino acid residues and coordination geometries involved. With the use of the metal surrogates, the *d–d* electronic transitions of the metal can be observed upon coordination to frataxin. EPR also has very characteristic signatures for different metal-amino acid coordination sites and can distinguish between metal–oxygen coordination and metal–nitrogen coordination. Hyperfine splitting and *g*-values give specific information as to the types of coordination that occur are

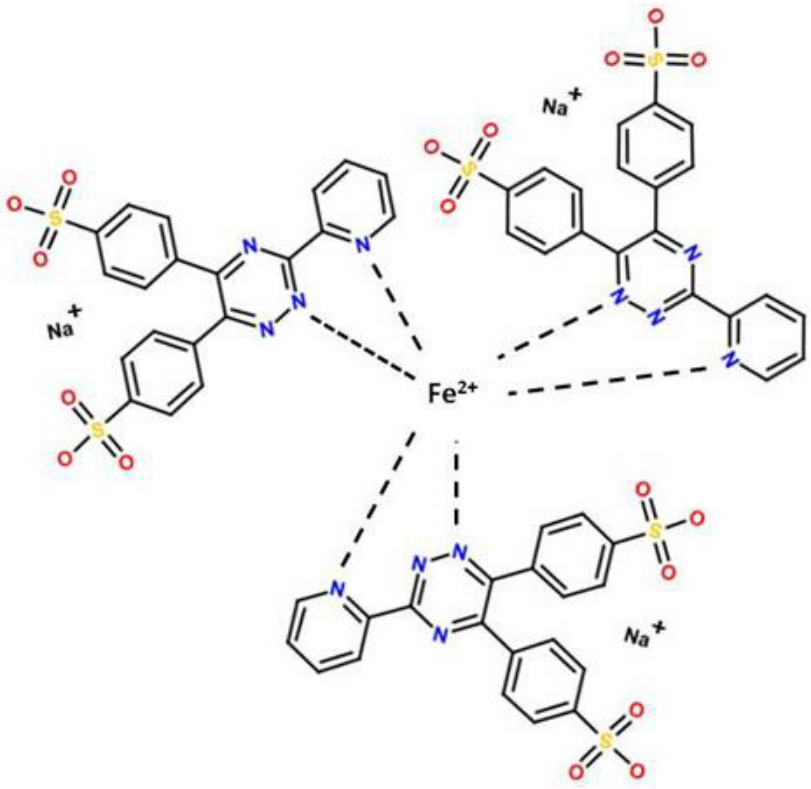

Figure 2.2 Ferrozine$_3$/Fe^{2+} cartoon schematic. One Fe^{2+} ion is coordinated by three ferrozine molecules, resulting in a purple color and an increase in absorbance at 562 nm.

occurring at separate coordination sites. In order to determine the affinity of frataxin for iron, competition assays with the Fe^{2+} chelator ferrozine were performed. Ferrozine has a known formation constant for iron ($K_f = 10^{15}$ M^{-3}) and has a large increase in absorbance at 562 nm upon Fe^{2+} binding [21]. The ferrozine competition assay will determine if frataxin contains any iron binding sites that bind with a higher affinity than ferrozine (**Figure 2.2**).

2.2 METHODS AND MATERIALS

2.2.1 General Chemicals

Competent cells and 2-mercaptoethanol were purchased from Novagen. Polyethyleneimine (PEI), 2-[bis(2-hydroxyethyl)amino]-2-(hydroxymethly)-1,3-propanediol (Bis-Tris), and ferrozine were purchased from Acros Organics. Ampicillin, carbenicillin, chloramphenicol, isopropyl β-D-1-thiogalactopyranoside (IPTG), 2-(N-morpholino)ethanesulfonic acid (MES), 4-(2-hydroxyethyl)-1-piperazineethanesulfonic acid (HEPES), ethylenediaminetetraacetic acid (EDTA), sodium chloride (NaCl), and ammonium sulfate were purchased from VWR. Copper sulfate, ferric chloride, magnesium chloride, and ammonium acetate were purchased from Fisher Scientific. Diethylaminoethyl (DEAE) sepharose resin andsulfopropyl (SP) sepharose resin were purchased from GE Life Sciences. Circlegrow media and ferrous ammonium sulfate were purchased from MP Biochemical. Glycerol was purchased from EMD Chemical. Phenylmethanesulfonyl fluoride (PMSF) protease inhibitor was purchased from Biosynth. Cobalt chloride was purchased from Mallinckrodt.

2.2.2 Frataxin Expression and Purification

Mature human frataxin was expressed in *E. coli* BL21(DE3)*pLysS* cells from the plasmid *pET81–210Fxn*. The cells were plated on LB-agar plates containing 100 μg/μL ampicillin and

34 μg/μL chloramphenicol. The cells were grown overnight at 37 °C and then inoculated into Circlegrow medium containing 50 μg/L of carbenicillin and 34 μg/L chloramphenicol. The cells were grown at 37 °C with 250 rpm shaking and induced at an OD_{600} of 0.8–1.0 with a final concentration of 1 mM IPTG. The temperature was reduced to 25 °C and the cells continued to grow overnight. Cells were harvested via centrifugation at 6,000 rpm for 30 min at 4 °C. Cell pellets were resuspended in 150–300 mL of buffer M (25 mM MES, 50 mM NaCl, 1 mM EDTA, pH 5.8) with addition of 0.1 mM PMSF protease inhibitor and stirred on ice for up to 30 min. Cells were lysed by a Branson Sonifier at 40% duty cycle for a total of 10 min with cycles of 30 s on/off and centrifuged at 14,000 rpm for 30 min at 4 °C. The lysis supernatant was subjected to PEI precipitation at a final concentration of 0.03% *v*/*v* of 5% PEI solution and stirred on ice for 1–2 hr and centrifuged at 14,000 rpm for 30 min at 4 °C. The PEI supernatant was then subjected to a 60% ammonium sulfate precipitation and stirred on ice for 1–2 hr and centrifuged at 14,000 rpm for 30 min at 4 °C. The ammonium sulfate pellet contained frataxin and was resuspended in 100–150 mL of buffer M and dialyzed against buffer M to remove excess ammonium sulfate.

Following dialysis, the protein solution was loaded onto DEAE anionic exchange resin pre-equilibrated with buffer M. The resin was then washed with 50 mL of buffer M. A 150 mL linear gradient of 50–500 mM NaCl was used to elute frataxin from the resin. Fractions were analyzed by a 15% polyacrylamide gel to determine the purity. The fractions containing frataxin (~14 kDa) were combined for SP cation exchange chromatography. The fractions were diluted 3–4 fold with buffer M to reduce the NaCl concentration. The same purification procedure was used for the SP resin as for the DEAE resin. Fractions were combined and dialyzed into buffer

H (50 mM HEPES, 150 mM NaCl, 5% glycerol, pH 7.4). Frataxin was concentrated and stored at –20 °C. Concentration was determined with the ε_{280} of 26.93 mM^{-1} cm^{-1}.

2.2.3 Intrinsic Tryptophan Fluorescence Metal Titrations

Five micromolar frataxin was titrated with cuprous sulfate or cobaltous chloride in either 50 mM Bis-Tris (for Cu^{2+}) or 50 mM HEPES (for Co^{2+}) with 150 mM NaCl at pH 7.2. Metal stock concentrations were determined via atomic absorption analysis. Metal solutions were titrated in 7.5 µL increments up to 4 molar equivalents of the protein concentration. All experiments were corrected for non-specific binding of metal to buffer. Fluorescence experiments were performed on a SPEX Fluoromax-3 Fluorimeter (Edison, NJ) at 23 °C with a circulating water bath. Buffers were filtered immediately before use. The excitation and emission wavelengths were 295 nm and 343 nm, respectively. The fluorescence data was analyzed with KaleidaGraph. Each experiment was run in triplicate. Identical titrations were performed on an Agilent 8453 UV–Visible spectrophotometer to correct for inner filter effect as in equation 1.

$$F_{\text{corrected}} = F_1 \times 10^{\left(\frac{A_{290\text{nm}} + A_{343\text{nm}}}{2}\right)} \qquad (1)$$

2.2.4 ^{1}H–^{15}N HSQC NMR Spectroscopy

Mature human frataxin was expressed in *E. coli* BL21(DE3)*pLysS* cells from the plasmid *pET81–210Fxn*. The cells were grown in M9 minimal media supplemented with 1 g/L 86% ^{15}N-enriched ammonium sulfate. Cultures were inoculated from fresh transformation plates into the M9 minimal media with 50 µg/µL carbenicillin and 34 µg/L chloramphenicol and grown at 37 °C with 250 rpm shaking. Cells were induced at an OD_{600} of 0.6–1.0 with 1 mM IPTG. Cells were grown for 3–4 hours at 37 °C to an OD_{600} not exceeding 2.0. Cells were harvested via

centrifugation at 6,000 rpm for 30 min at 4 °C. ^{15}N-frataxin was purified as described in **Section 2.7.2**, except the final buffer was chelex-treated 25 mM d_{18}-HEPES, 100 mM NaCl, pH 7.0. Frataxin was confirmed to contain ~85% ^{15}N via MALDI–ToF mass spectrometry.

Samples for NMR were prepared by adding 400 μL of 0.56 mM ^{15}N-Fxn and 100 μL of 25 mM d_{18}-HEPES with 5% *v*/*v* D_2O to an acid-washed NMR tube. ^{1}H–^{15}N spectra were collected at 298 K on a Brüker Avance 600 MHz spectrometer (Fremont, CA) with a triple resonance ^{1}H/^{13}C/^{15}N probe equipped with z-axis pulsed field gradients. The fingerprint main chain amide region was recorded by two-dimensional ^{1}H–^{15}N HSQC experiment using the standard Brüker pulse program [22]. Cu^{2+}, Co^{2+}, Mg^{2+} and Fe^{2+} titrant stocks were made in d_{18}-HEPES and their concentrations determined by atomic absorption analysis. For the magnesium and cobalt titrations, 0.2–6.0 molar equivalents were aerobically titrated into frataxin. For the copper titration, 0.3–4.0 molar equivalents were aerobically titrated into frataxin. For the Fe^{2+} titration, however, individual samples containing 1.0–4.0 molar equivalents of Fe^{2+} were prepared under strict anaerobic conditions in a Vacuum Atmosphere anaerobic glovebox. NMR spectra were collected and formatted by Dr. Russell Timkovich. Resonances were assigned according to Musco *et al.* [23]. Spectra were analyzed with SPARKY (T.D. Goddard and D. G. Kneller, University of California, San Francisco).

2.2.5 UV–Visible Metal Titrations

Four hundred micromolar frataxin was titrated with cuprous sulfate or cobaltous chloride in 50 mM Bis-Tris buffer (Cu^{2+}) or 50 mM HEPES buffer (Co^{2+}) with 400 mM NaCl at pH 7.2. Metal stock concentrations were determined via atomic absorption analysis. Metal solutions were titrated in 2 μL increments up to 4 molar equivalents of the frataxin concentration. Spectra were collected from 200–1100 nm and the data was plotted as absorbance as a function of metal

equivalents. All experiments were corrected for non-specific binding of metal to buffer. UV–Visible titration experiments were performed on an Agilent 8453 UV–Visible spectrophotometer. Data was analyzed with Kaleidagraph.

2.2.6 Ferrozine Iron Competition Assay

To better characterize the Fe^{2+} binding affinity of frataxin, a colorimetric assay was employed with the Fe^{2+} specific chelator, ferrozine. All solutions were degassed prior to the experiment and prepared in a Vacuum Atmosphere anaerobic glovebox. A 6.5 mM ferrozine stock was prepared with 2.5 M ammonium acetate in 25 mM HEPES, 150 mM NaCl, pH 7.4. A 530 mM ferrous ammonium sulfate stock was prepared in the same buffer and the concentration of iron was determined by atomic absorption analysis. Samples containing 12 μM frataxin were prepared with increasing concentrations of ferrous ammonium sulfate. Spectra were collected from 240–800 nm on an Agilent 8453 UV–Visible spectrophotometer. A control experiment using final dialysis buffer (chelex-treated 50 mM HEPES, 150 mM NaCl, pH 7.4) was also performed in the same manner. The Fe^{2+}–ferrozine$_3$ complex has an extinction coefficient of 27.9 mM^{-1} cm^{-1} at 562 nm and a formation constant (K_f) of 3.65×10^{15} M^{-3} [21].

2.2.7 Copper EPR Spectroscopy

All frataxin samples contained a final concentration of 30% (*v*/*v*) glycerol and a total volume of 200 μL. One hundred twenty five microliters of 1 mM frataxin was combined with 75 μL of 80% glycerol and either 0.9 or 1.9 molar equivalents of cuprous sulfate. As a control, a sample containing final dialysis buffer (50 mM HEPES, 150 mM NaCl, pH 7.4) and 0.9 or 1.9 equivalents of cuprous sulfate was prepared. The cuprous sulfate was prepared in 50 mM Bis-Tris, pH 7 and its concentration was determined by atomic absorption analysis. EPR samples for each frataxin mutant were prepared in the same manner at that for wild-type frataxin. The EPR

spectra were measured at 60–77 K with an X-band Brüker E-580 spectrometer equipped with a CW resonator (1 mW microwave power and 100 kHz field modulation with 0.3 mT amplitude), an Oxford instruments CF935 helium cryostat and electrically controlled Oxford helium transfer line. The spectrometer is controlled through a Linux workstation with Xepr, the data acquisition and manipulation Brüker software.

2.3 RESULTS

2.3.1 Co^{2+} and Fe^{3+} Intrinsic Tryptophan Fluorescence

Previous HDX–MS results from Dr. Busenlehner indicated that frataxin has three Fe^{2+} coordination sites. To confirm these findings, intrinsic tryptophan fluorescence was employed to determine a stoichiometry for metal coordination to frataxin. Co^{2+} and Fe^{3+} were used as substitutes for oxidation-sensitive Fe^{2+} since titrations could not be performed anaerobically. The addition of metal affects the environment of tryptophan residues and quenched the tryptophan emission signal (343 nm) until 3 equivalents Co^{2+} or Fe^{3+} had been added **(Figure 2. 3).** This result indicates that frataxin coordinated three Fe^{3+} or Co^{2+} ions, which was consistent with the results seen from HDX–MS.

2.3.2 Ferrozine Iron Competition Assay

To determine if frataxin contained any high-affinity Fe^{2+} coordination sites, a metal competition assay was performed using the Fe^{2+} chelator ferrozine. Ferrozine has a known formation constant (K_f of 10^{15} M^{-3}) in a Fe^{2+}:ferrozine ratio of 1:3 and a λ_{max} at 562 nm (ε_{562} = 27.9 mM^{-1} cm^{-1}) [21]. Samples containing ferrozine with and without frataxin were titrated with increasing amounts of Fe^{2+} and the absorbance monitored at 562 nm. The sample containing apo-frataxin binds one equivalent of Fe^{2+} before any purple color of the Fe^{2+}–ferrozine$_3$ complex forms (**Figure 2.4**). The lack of purple color at the first equivalent of Fe^{2+} indicates that frataxin

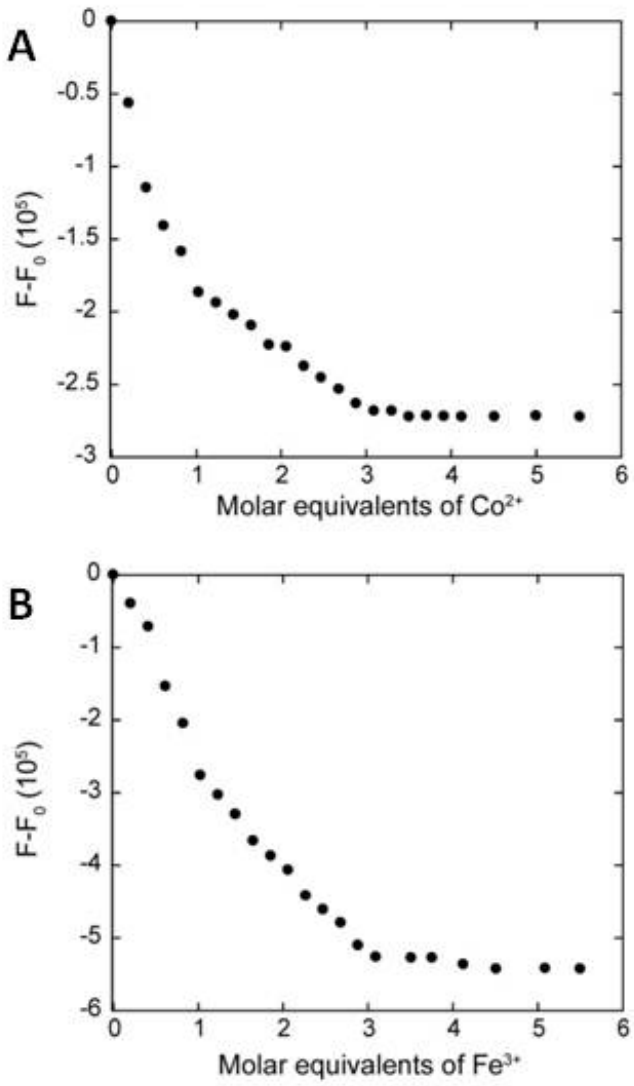

Figure 2.3 Intrinsic Tryptophan Fluorescence Co^{2+} and Fe^{3+} titrations. Fluorescence emission spectra were recorded for Fe^{3+} or Co^{2+} titrations of fiveμM wild-type frataxin with an excitation at 295 nm. The corrected fluorescence intensity was plotted against molar equivalents of Co^{2+} (A) and Fe^{3+} (B) For both Co^{2+} and Fe^{3+}, stoichiometric binding was observed with saturation at ~3 equivalents of metal. Titrations were performed in 50 mM HEPES, 150 mM NaCl, pH 7.2, 23 °C.

has one Fe^{2+} coordination site with a greater affinity than ferrozine, along with two weaker binding sites.

2.3.3 Co^{2+} Metal Coordination Environment

Co^{2+} was chosen as a spectroscopic surrogate because of its electronic similarities to Fe^{2+} and its common use as a substitute for Fe^{2+} [20]. The Co^{2+} titration revealed a broad transition of overlapping peaks centered at 532 and 485 nm after the first equivalent of Co^{2+} was added **(Figure 2.5)**. The wavelengths for these transitions were consistent with nitrogen and/or oxygen metal coordination. As additional equivalents of Co^{2+} were added, the λ_{max} shifted to 511 and 466 nm, which is indicative of more oxygen-based coordination. Low molar absorptivities for the Co^{2+} *d–d* transition ($\varepsilon_{max} < 15\ M^{-1}\ cm^{-1}$) consistent with octahedral coordination geometry were also observed [24]. Binding isotherms for Co^{2+} gave a more linear shaped curve rather than hyperbolic which is characteristic with stoichiometric binding (*i.e.*, no free metal). A stoichiometry of 3 metal ions per frataxin monomer was confirmed.

2.3.4 HSQC NMR Co^{2+} Titrations

To determine the localization of the three coordination sites on frataxin, HSQC NMR spectra were collected from uniformly ^{15}N-labeled apo–frataxin that was aerobically titrated with Co^{2+}. Note that the N-terminus of frataxin is at residue 81; however, resonances for residues 81–90 are not observed in the NMR spectra [7, 14]. Because Co^{2+} is also a paramagnetic metal, through–bond coupling of the free electrons of the metal and protein nuclei results in line broadening and large chemical shifts for amide protons in close proximity to the free electrons of a metal ion [25]. Magnesium chloride was used in the frataxin titration with Co^{2+} as it has been accepted that diamagnetic metals do not affect chemical shifts and reduce non-specific metal binding [15]. The $^{1}H–^{15}N$ HSQC NMR Co^{2+} titrations were performed with and without 10 mM

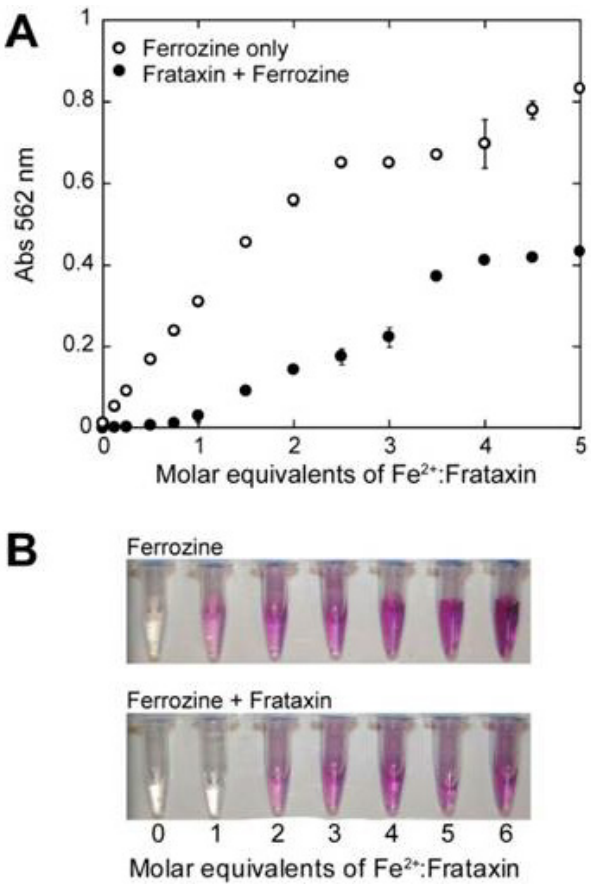

Figure 2.4 Ferrozine iron competition titration. (A) The binding isotherms at 562 nm for the ferrozine titration without frataxin (open circles) and with 13 μM frataxin (black circles). (B) Representative samples from a Fe^{2+} titration of 108 μM ferrozine (bottom). The $ferrozine_3/Fe^{2+}$ complex is purple in color. Up to 1.0 molar equivalent of Fe^{2+}, the Fe^{2+} preferentially binds to frataxin as shown by the lack of purple color and absorbance at 562 nm. Ferrozine stock was prepared with 2.5 M ammonium acetate and 25 mM HEPES, 150 mM NaCl at pH 7.4. The titration was performed in 25 mM HEPES, 150 mM NaCl, pH 7.4 and 25 °C.

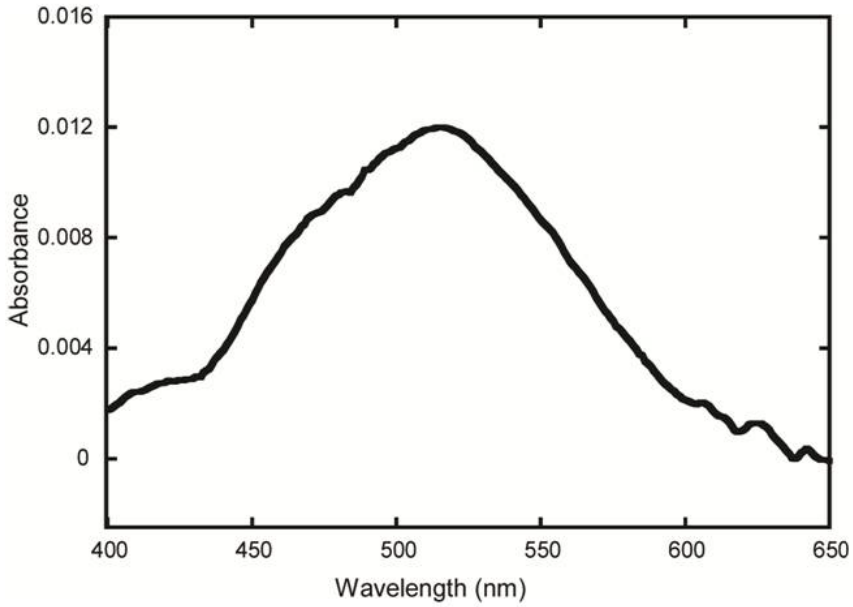

Figure 2.5 UV–Visible spectrum of cobalt titration of wild-type frataxin. The broad *d–d* transition of 300 μM wild-type frataxin with 2 equivalents of Co^{2+} is observed. The transitions from 450–550 nm are observed with a λ_{max} of 535 nm. Titrations were performed in 50 mM HEPES, 400 mM NaCl, pH 7.2, and 25 °C.

Mg^{2+} to determine if Mg^{2+} could reduce non-specific metal binding without affecting the metal coordination of frataxin. We observed differences between the Co^{2+} spectra with and without Mg^{2+}. When the Co^{2+} binding isotherms were compared, it was clear that Mg^{2+} was competing with Co^{2+} for frataxin coordination, especially at the α1 helix and β1 sheet (**Figure 2.6**). Thus, an NMR titration with Mg^{2+} was performed to determine the effects on chemical shifts. We observed that resonances in α1/β1 (Ala114, Lys116, Tyr123 Asp124 Phe127 and Gly138) had line broadening and shifting from the addition of Mg^{2+} (**Figure 2.7**) After discovering that Mg^{2+} affected binding stoichiometries of Co^{2+} titrations, all subsequent HSQC NMR metal titrations were performed *without* Mg^{2+}.

For the titration of Co^{2+} in the absence of Mg^{2+} we observed significant line broadening for resonances in the α1 helix and β1 sheet. After the 3rd equivalent of Co^{2+} was added, resonances from the α1 helix (Asp104, Ser105, Glu108, Asp112, Leu113, Ala114, Asp115 and those in close proximity, Tyr118, Val125, Phe127, Val131) had broadened beyond detection (**Figure 2.8**). The severe line broadening for these resonances indicated they are most likely within 8–15 Å of a Co^{2+} ion [25]. A plot of normalized chemical shifts for each residue also showed that the majority of the residues affected by Co^{2+} occurred in clusters between residues 103–117 and 122–133, which are in the α1–loop–β1 region. Some amide proton shifting was also observed at the beginning of the α1 helix, specifically at resonances for Asp91 and Ala99. No additional changes in chemical shifts were detected beyond 3 equivalents of Co^{2+}.

2.3.5 Cu^{2+} Metal Coordination Environment

To confirm the coordination geometry and types of ligands used by frataxin for metal coordination, the spectroscopic surrogate Cu^{2+} was also used. The *d–d* transition was monitored to confirm the coordination geometry and ligand type determined for Co^{2+} coordination by

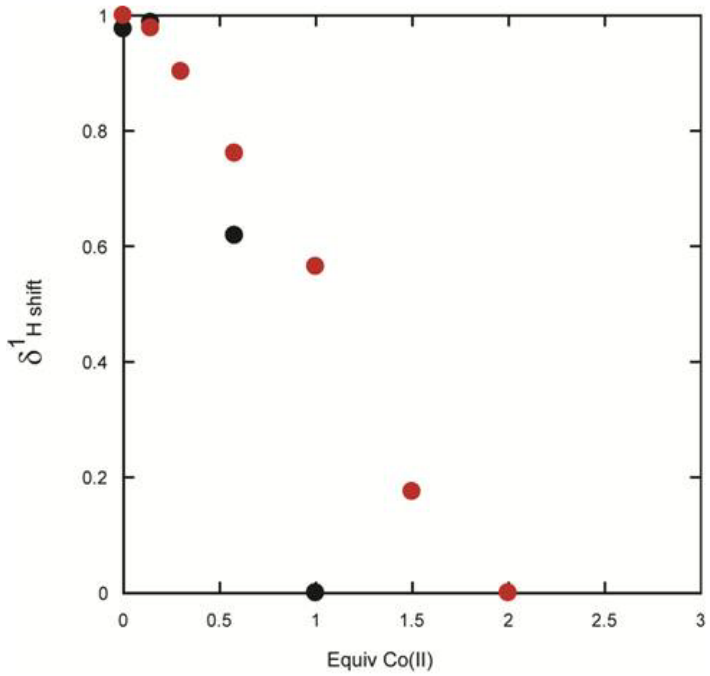

Figure 2.6 Comparison binding isotherm of wild-type frataxin residue Asp112 Co^{2+} with (red) and without Mg^{2+} (black) NMR titrations. NMR samples were prepared in 25 mM d_{18}-HEPES with 5% *v*/*v* D_2O.

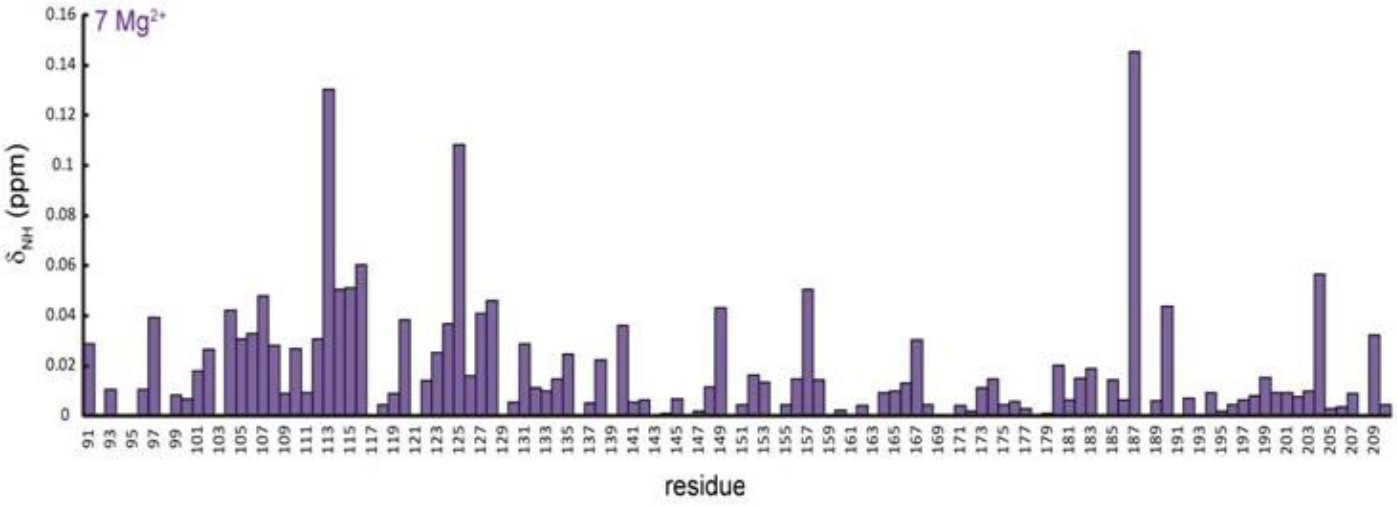

Figure 2.7 NMR titration of frataxin with magnesium. The changes in normalized chemical shift (δ_{NH}) of 560 μM ^{15}N-frataxin with a total of 7 molar equivalents of Mg^{2+}. NMR samples were prepared in 25 mM d_{18}-HEPES with 5% *v*/*v* D_2O at pH 7.2.

frataxin. Apo–frataxin had overlapping Cu^{2+} *d–d* transitions with λ_{max} at 605 and 645 nm (**Figure 2.9**). Typically, *d–d* transitions for Cu^{2+} with oxygen and/or nitrogen ligands exist in the far UV region [20], from 600–800 nm; thus the transitions observed for Cu^{2+} were consistent with oxygen/nitrogen-based Cu^{2+} coordination.

2.3.6 HSQC NMR Cu^{2+} Titrations

HSQC NMR spectra were collected for uniformly ^{15}N-labeled apo–frataxin, to which Cu^{2+} was aerobically titrated. Like Co^{2+}, Cu^{2+} is also a paramagnetic metal and should cause large chemical shifts and significant line broadening of nuclei close to the metal center [24]. The broadening of the frataxin amide resonances indicates the presence of Cu^{2+} electrons within 8–15 Å of the ligating atom [25]. Upon addition 0.3 equivalents of Cu^{2+}, the resonances for His177 and Val125 broadened beyond detection. His177 is in a solvent accessible loop, whereas Val125 is at the beginning of the first β-sheet and neighbors Asp124, which has been implicated in the interaction with the iron-sulfur cluster scaffold protein Isu2 [26]. The His177 cross-peak was also shown to broaden beyond detection in the presence of Fe^{2+} [7]. It was noted, however, that His177 side chain being in a solvent accessible, flexible loop may be the only reason for its coordinating capability and may not be physiologically relevant.

Upon the addition of 1.0 equivalent of Cu^{2+} resonances in the α1 helix (Asp112, Asp115) and the β1 strand (Asp122, Asp124) exhibited line broadening, while Trp168 and Ser176 (near His177) were nearly broadened beyond detection. Residues displaying shifted amide resonance with 1.0 equivalent of Cu^{2+} included those in α1 (Arg97, Phe110, Leu113, Ala114, Lys116), β1 (Tyr123, Asp124), and the C-terminus (Lys195), indicating a change in the surrounding environment but not necessarily direct coordination to the nearby metal center.

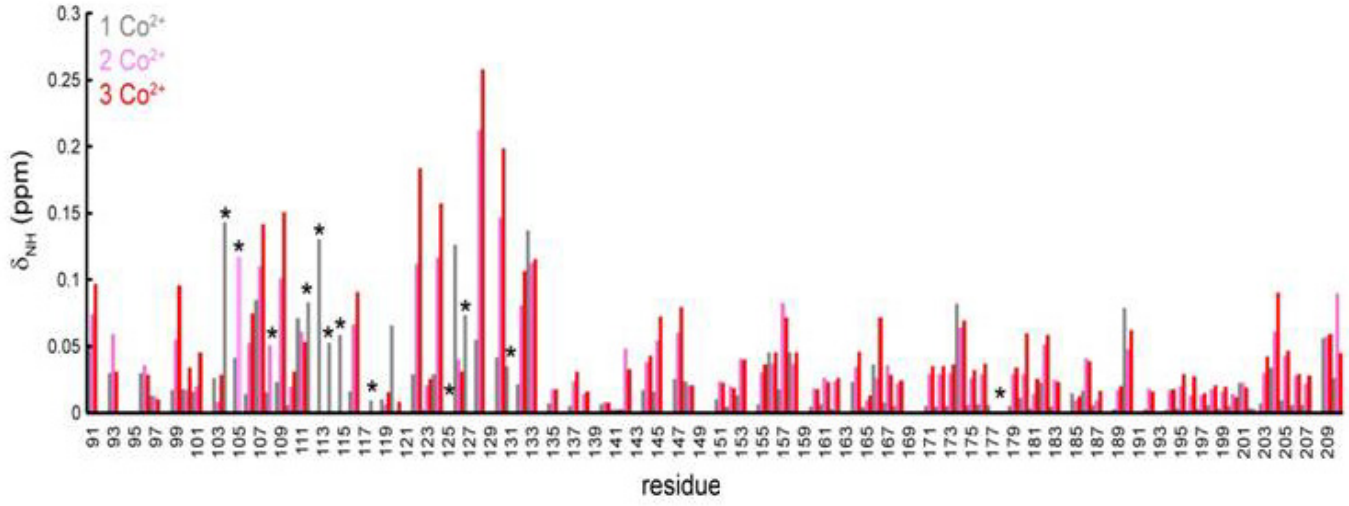

Figure 2.8 NMR titration of frataxin with cobalt. The changes in normalized chemical shift (δ_{NH}) of 560 μM ^{15}N-frataxin with 1, 2 and 3 molar equivalents of Co^{2+} in gray, pink and red, respectively. Asterisks denote the positions of the amino acids whose resonances broadened beyond detection during the titration. NMR samples were prepared in 25 mM d_{18}-HEPES with 5% *v*/*v* D_2O.

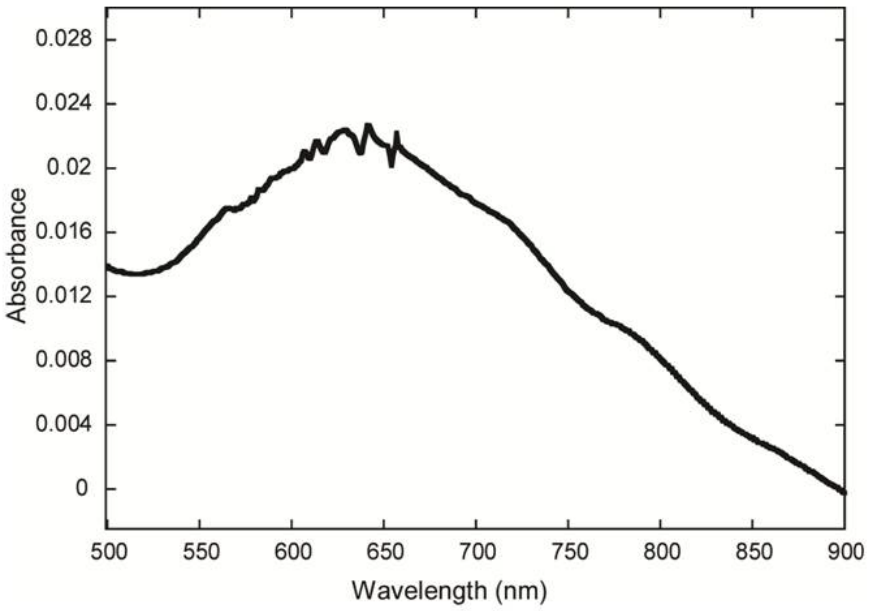

Figure 2.9 UV–Visible spectra of copper titration of wild-type frataxin. The broad *d–d* transition of 300 μM wild-type frataxin with 2 equivalents of Cu^{2+} is observed. The transitions from 600–800 nm are observed with a λ_{max} of 645 nm. Titrations were performed in 50 mM Bis-Tris, 400 mM NaCl, pH 7.2, and 25 °C.

At the addition of 2.0 equivalents of Cu^{2+}, several resonances in α1 (Glu101, Asp104, Ser105, Ala107, Glu108, Phe110, Asp112, Leu113, Ala114, Asp115) and β1 (Gly130 and Gly179) broadened beyond detection (data not shown). Several amide proton resonances were shifted upfield with 2 equivalents of Cu^{2+}, including Thr119, Asp122, Tyr123, Asp124, Gly138, Lys164, Lys195, and Thr196. Thr119, Asp122 and Asp124 are residues in the first loop and β1 strand. The plot of normalized amide proton chemical shifts shows a cluster at the end of the α1 helix and the first β-sheet, indicating that metal coordination is occurring primarily in this region. It is important to note that although metal coordination may be occurring in the N-terminal loop of frataxin, it is not observed by NMR due to the lack of resonances for these residues. It is also important to note that no further changes were observed between 2.0 and 4.0 equivalents of Cu^{2+}.

2.3.7 HSQC NMR Fe^{2+} Titrations

$^{1}H–^{15}N$ HSQC spectra were collected for uniformly ^{15}N-labeled apo–frataxin in which samples containing 1–4 equivalents of Fe^{2+} had been prepared anaerobically and sealed prior to removing from the anaerobic glovebox. High spin Fe^{2+} causes significant line broadening and shifting of amide proton resonances at a distance of 5–7 Å of bound iron [27]. After 2.0 equivalents of Fe^{2+} had been added the largest changes in shifting and line broadening were observed in the α1 helix (Asp104, Ser105, Asp112, Leu113, Ala114 and Asp115) and the β1 strand (Tyr119, Asp122, Asp124 and Val125). After 3.0 equivalents of Fe^{2+}, some additional shifting of amide proton resonances was observed including Asp91, Asp104 and Asp122, but in contrast to the Co^{2+} titration, the only resonances to broaden beyond detection were Asp112, Leu113 and Asp115 in the α1 helix (**Figure 2.11**). As with Co^{2+} and Cu^{2+}, no additional changes were observed after 3 equivalents of Fe^{2+}.

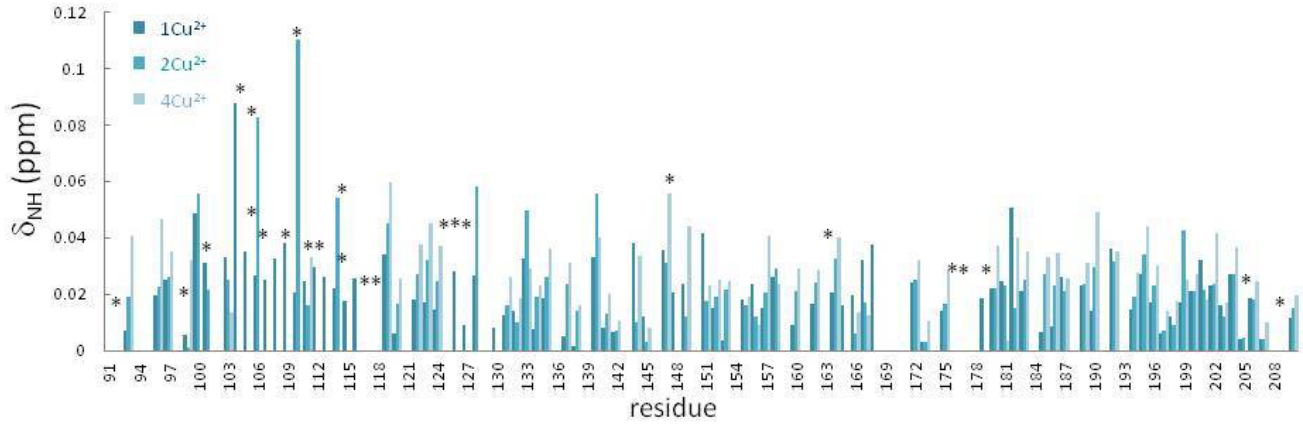

Figure 2.10 NMR titration of frataxin with copper. The changes in normalized chemical shift (δ_{NH}) of 560 μM ^{15}N-frataxin with 1, 2 and 4 molar equivalents of Cu^{2+} in teal, sky blue and grey, respectively. Asterisks denote the positions of the amino acids whose resonances broadened beyond detection during the titration. NMR samples were prepared in 25 mM d_{18}-HEPES at pH 7.2 with 5% *v*/*v* D_2O. The metal stock was prepared in 50 mM Bis-Tris at pH 7.2.

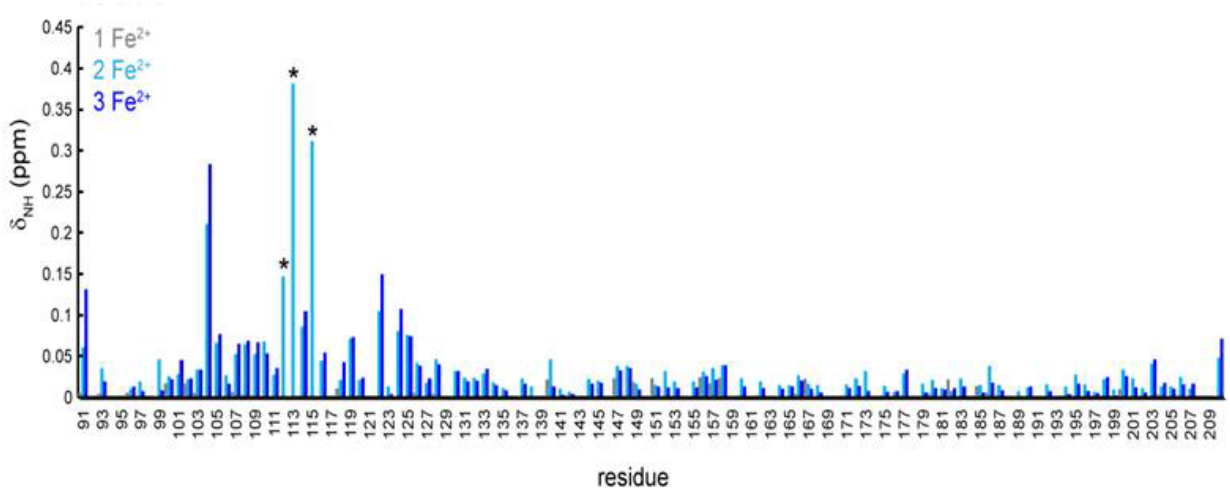

Figure 2.11 NMR titration of frataxin with iron. The changes in normalized chemical shift (δ_{NH}) of 560 μM ^{15}N-frataxin with 1, 2 and 4 molar equivalents of Fe^{2+} in gray, cyan and blue, respectively. Asterisks denote the positions of the amino acids whose resonances broadened beyond detection during the titration. NMR samples were prepared in 25 mM d_{18}-HEPES with 5% *v*/*v* D_2O at pH 7.2.

2.3.8 EPR Reveals Cu^{2+}–Imidazole Coordination

HDX–MS (L. Busenlehner) indicated that frataxin may coordinate metals using residues within the disordered N-terminal tail (residues 81–90); however, structural information for this region was not observed by NMR spectroscopy. Add to this the lack of an identifiable third metal binding site by NMR, EPR spectroscopy was used to shed light on additional coordination sites missed by NMR. EPR gives very specific *g*-tensor and hyperfine (A) splitting values that are characteristic for the metal, its particular oxidation state, and its coordinating ligands [28]. In contrast to UV–Visible spectroscopy, EPR can distinguish between nitrogen and oxygen ligands. Fe^{3+} and Co^{2+} EPR is less sensitive to coordination environment than other metals, so Cu^{2+} was then used as a surrogate metal for Fe^{2+} since we have demonstrated similar binding to frataxin with NMR titrations (**Figures 2.10** and **2.11**). Frataxin was incubated with 0.9 equivalents of Cu^{2+} and 1.9 equivalents of Cu^{2+} and EPR X–band continuous wave scans were collected. The EPR spectra indicated two distinct Cu^{2+} coordination environments (**Figure 2.12**). The spectrum of $0.9Cu^{2+}$–frataxin was subtracted from $1.9Cu^{2+}$–frataxin to obtain the pure EPR spectrum of the second binding site compared to the first site (**Figure 2.13**). The spectral subtraction gives two Cu^{2+} centers with different EPR parameters. The first Cu^{2+} site has $g_{II} = 2.345$ Hz and $A_{II} = 151$ G and the second Cu^{2+} center has $g_{II} = 2.29$ Hz and $A_{II} = 159$ G. According to the literature [28], a decrease in the parallel component of the Cu^{2+} *g* tensor (g_{II}) and an increase in the parallel component of the Cu^{2+} hyperfine tensor (A_{II}) indicates the presence of nitrogen atom(s) in the Cu^{2+} coordination. Thus, the second Cu^{2+} site most likely contains nitrogen atom(s). Control experiments of buffer with 0.9 and 1.9 equivalents of Cu^{2+} confirmed that the nitrogen-based signals were not an artifact of buffer–copper coordination. Pulsed EPR methods show that one of the Cu^{2+} species has a histidine imidazole nitrogen as a

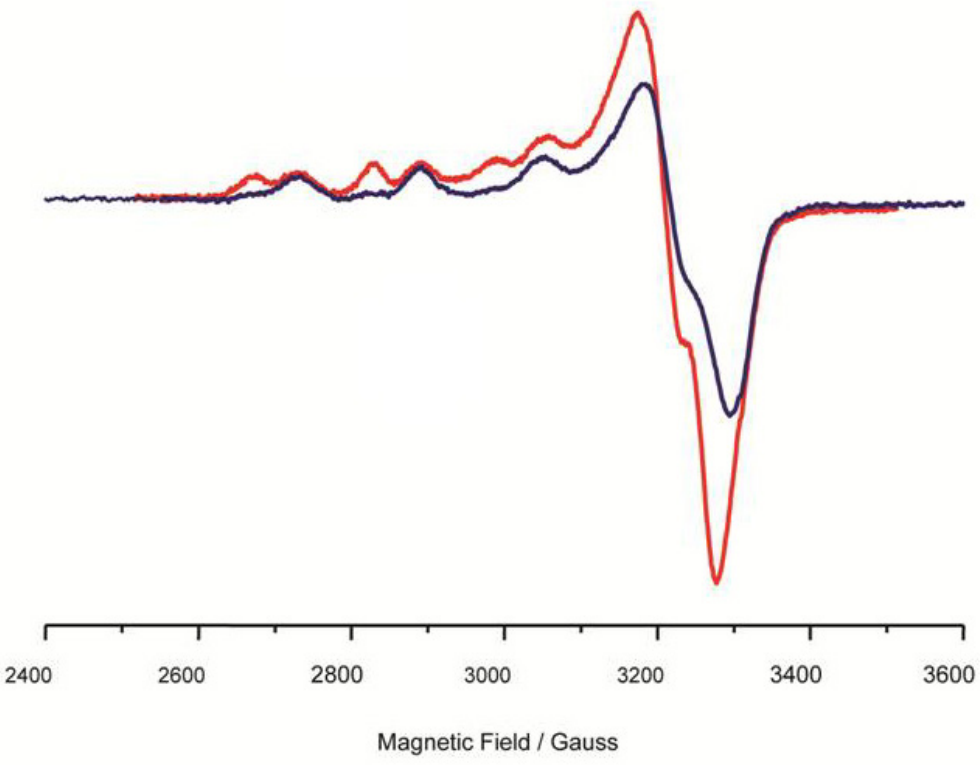

Figure 2.12 EPR X–band continuous wave spectra of wild type frataxin. The spectrum of 1 mM wild-type frataxin with 0.9 and 1.9 equivalents of Cu^{2+} are shown in blue and red, respectively. Samples were prepared in 50 mM HEPES, 150 mM NaCl at pH 7. Copper stocks were prepared in 50 mM Bis-Tris at pH 7.

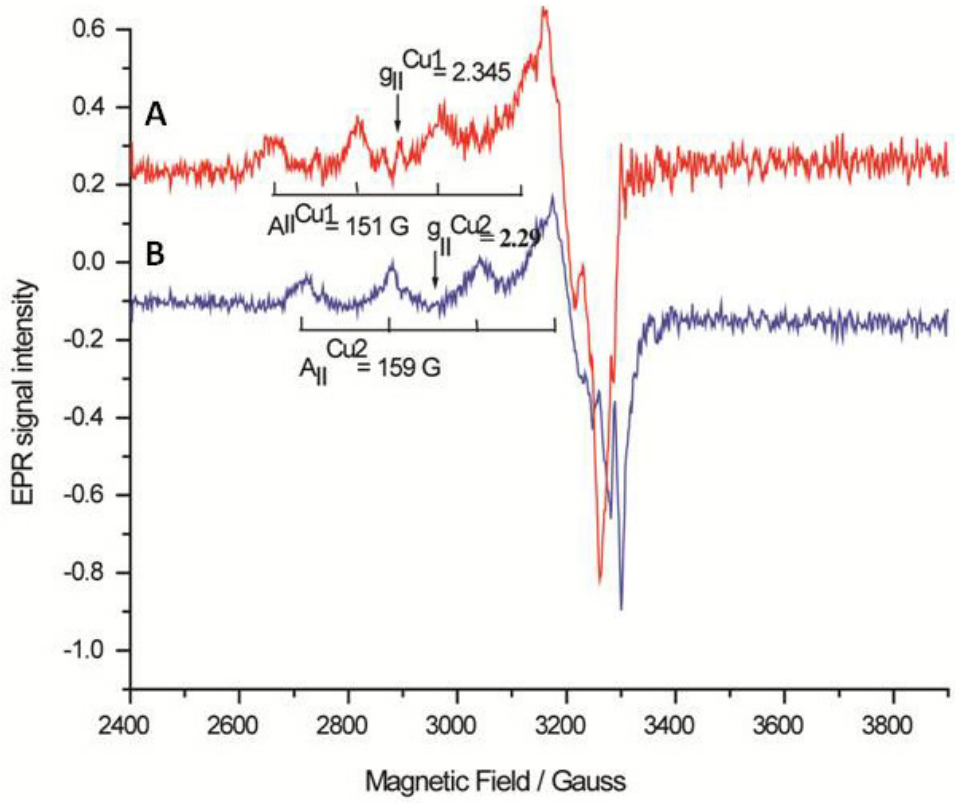

Figure 2.13 EPR X–band continuous wave spectra of wild type frataxin. (A) EPR spectrum of 1.0 mM frataxin indicating the g_{II} values for the first Cu^{2+} binding site. (B) The subtraction of 2.0 equivalents from 1.0 equivalent of Cu^{2+} to show the second Cu^{2+} binding site. Samples were prepared in 50 mM HEPES, 150 mM NaCl at pH 7. Copper stocks were prepared in 50 mM Bis-Tris at pH 7.

ligand. Pulsed ESEEM and HYSCORE spectra show the intense signals (absent for Cu^{2+} in the buffer) characteristic of the 'remote', non-coordinating imidazole nitrogen in a Cu^{2+}–histidine complex, while ENDOR shows a large hyperfine coupling from a directly coordinated nitrogen (data not shown, Dr. Michael Bowman).

2.4 DISCUSSION

Human frataxin is a mitochondrial protein proposed to coordinate and transport Fe^{2+} to [Fe–S] cluster containing proteins [4, 9, 29]. The iron coordination of frataxin is different from classical metallochaperone proteins because frataxin contains no cysteine residues. To coordinate Fe^{2+}, frataxin must make use of other metal coordinating residues such as aspartate, glutamate and histidine residues, which provide nitrogen or oxygen as metal ligands. The goal of this chapter was to investigate the number and nature of Fe^{2+} coordination sites in frataxin so that the mechanism by which frataxin transfers iron to proteins for [Fe–S] cluster assembly can be discerned in subsequent chapters.

2.4.1 Metal Coordination Environment

The iron binding stoichiometry of frataxin has been reported from as few as 1 iron ion to as many as 7 iron ions per frataxin monomer [7, 9-11]. Many of these reports used experimental conditions containing buffers and reducing agents that can coordinate metals and are not amenable for binding studies. The use of metal surrogates to study iron-binding sites has been employed for many years. Co^{2+} and Cu^{2+} are also intermediate acids according to HSAB theory and prefer similar ligands to that of Fe^{2+} [20]. Fe^{2+} is spectroscopically silent in the UV–Visible range because it does not have cysteine residues, which give characteristic ligand-to-metal transitions. It is assumed that because frataxin has no cysteine residues and has a large number of carboxylate residues on the surface of the α1 helix that metal binding occurs at only at this

site [13, 14, 30]. This has been demonstrated with published NMR metal binding experiments, but again, many of these had questionable buffer conditions. First, fluorescence titrations with Co^{2+}, Cu^{2+} and Fe^{3+} confirmed that 3 metal ions bind to one frataxin monomer, thus validating the use of surrogates for this system (Figure 2.3). In addition, the ferrozine competition assays clearly demonstrated that frataxin contains one high-affinity Fe^{2+} coordination site (Figure 2.6), but it is unclear which site this is.

To further investigate the metal coordination environment, we monitored the *d–d* electronic transitions of Co^{2+} and Cu^{2+} upon coordination by frataxin. Both Co^{2+} and Cu^{2+} exhibit broad *d–d* transitions in the visible region upon binding to frataxin that are characteristic of nitrogen/oxygen coordination (Figures 2.7 and 2.11). In addition, the low molar absorptivities indicate octahedral coordination geometry, which is also reported for other frataxin homologs [17]. Even though these transitions are broad and overlapping, it was possible to distinguish two different metal coordination environments, especially for Co^{2+}. EPR spectroscopy can distinguish between metal–oxygen coordination and metal–nitrogen coordination, especially when imidazole nitrogen is present. Hyperfine splitting and *g*-values give specific information as to the types of coordination that occur are occurring at separate coordination sites [28]. EPR revealed that frataxin has two distinct Cu^{2+} coordination environments (Figure 2.15). In addition to the carboxylate residues of the α1 helix, it appears that there is contribution from a nitrogen-containing ligand for Fe^{2+} coordination, as well. The most logical nitrogen ligand is histidine. Frataxin contains 3 His residues. Further localization of these binding sites was clarified with paramagnetic NMR spectroscopy.

2.4.2 Metal Coordination Sites for Frataxin Determined Using Paramagnetic NMR

Magnesium chloride has been an accepted addition for frataxin metal coordination studies as it presumably reduces the effects of non-specific binding without interfering with actual metal coordination [15]. However, the studies presented in this chapter demonstrated that Mg^{2+} was actually competing with frataxin Co^{2+} coordination sites, leading to shifts in the stoichiometries to higher molar ratios (**Figure 2.6**). The inclusion of Mg^{2+} in metal coordination studies may lend an explanation, in part, to Fe^{2+} stoichiometries of 6–7 reported in the literature [4]. Once Mg^{2+} was excluded from our NMR metal binding studies, changes in the two-dimensional NMR spectra up to 3 equivalents of metal, without significant changes at higher metal:frataxin ratios, were consistently observed. $^{1}H–^{15}N$ HSQC NMR experiments were performed with Cu^{2+}, Co^{2+} and Fe^{2+} and compared in order to properly discern the amino acid residues that are most likely involved in iron binding. The NMR titration experiments give information on the proximity of the paramagnetic metal to amino acid residue nuclei by causing line broadening and shifting of the amide nitrogen and proton cross-peak.

One clear metal binding site containing Asp112 and Asp115 was observed with Co^{2+}, Cu^{2+}, and Fe^{2+}. In the NMR titrations the amide resonances of Asp112 and Asp115 broadened beyond detection, which indicated direct involvement in metal binding (**Figure 2.13**). These residues are also highly conserved and indicated in Fe^{2+} coordination in frataxin homologues [14, 15, 31]. The results from the $^{1}H–^{15}N$ HSQC NMR experiments presented here are also consistent with HDX–MS [31] that reported decreased backbone deuterium incorporation for peptide 110–123 in the presence of Co^{2+} and Fe^{2+}. Thus, it is evident that Asp112 and Asp115 residues are involved in Fe^{2+} coordination. Although the α1 helix was also shown to coordinate

metals with residues like Asp112 and Asp115, the binding is most likely of more non-specific nature [1].

The Asp122 and Asp124 resonances also showed large chemical shifts with the addition of Cu^{2+}, Co^{2+} and Fe^{2+}, which strongly suggests that although they may not directly coordinate metal, their environments were influenced by the presence of metal (**Figure 2.13**). As reported by Schmucker *et al.*, Asp 122 and Asp124 are more likely to be involved in the interaction with [Fe–S] cluster biogenesis machinery rather than specific Fe^{2+} coordination [26]. The residues within peptide 122–127 were also implicated in Co^{2+} and Fe^{2+} binding by HDX–MS [31]. To determine if Asp122 and Asp124 are vital for the interaction between frataxin and Isu2, further studies are needed with Isu2 and the entire [Fe–S] assembly complex including Nfs1 and Isd11.

The metal binding site that contained nitrogen, most likely an imidazole, was also explored with NMR spectroscopy. The three histidines in frataxin are His86, H177, and His183. The His183 cross-peak was not affected by any metal, so we can eliminate this as a ligand. Interestingly, the His177 resonance immediately broadened beyond detection in the Cu^{2+} and Co^{2+} titrations, but not in the Fe^{2+} titration. His177 was first identified as a potential Fe^{2+} ligand in the crystal structure of human frataxin by Dhe-Paganon in 2000. In the structure, His177 was coordinated to the Fe^{2+} ion along with the carboxylate side chain from Asp115 of an adjacent frataxin molecule [7]. However, the location of His177 in a flexible, solvent accessible loop made it questionable as a true Fe^{2+} coordinating ligand and not an artifact. Further experiments are needed to determine if His1177 can coordinate or participate in Fe^{2+} coordination. Unfortunately, His86 is in the disordered in N-terminus and does not have a cross-peak in HSQC spectra so we cannot rule this in or out as a ligand without further experimentation. This will be explored further in **Chapter 3** of this dissertation.

REFERENCES

1. Pastore, A. and H. Puccio, *Frataxin: a protein in search for a function.* J. Neurochem., **126 Suppl 1**: 2013 p. 43-52.

2. Martelli, A., et al., *Frataxin is essential for extramitochondrial Fe-S cluster proteins in mammalian tissues.* Hum. Mol. Genet., 2007. **16**(22): p. 2651-8.

3. Gerber, J., U. Muhlenhoff, and R. Lill, *An interaction between frataxin and Isu1/Nfs1 that is crucial for Fe/S cluster synthesis on Isu1.* EMBO Rep., 2003. **4**(9): p. 906-11.

4. Yoon, T. and J.A. Cowan, *Iron-sulfur cluster biosynthesis. Characterization of frataxin as an iron donor for assembly of [2Fe-2S] clusters in ISU-type proteins.* J. Am. Chem. Soc., 2003. **125**(20): p. 6078-84.

5. Ramazzotti, A., V. Vanmansart, and F. Foury, *Mitochondrial functional interactions between frataxin and Isu1p, the iron-sulfur cluster scaffold protein, in Saccharomyces cerevisiae.* FEBS Lett., 2004. **557**(1-3): p. 215-20.

6. Tsai, C.L. and D.P. Barondeau, *Human frataxin is an allosteric switch that activates the Fe-S cluster biosynthetic complex.* Biochemistry, **49**(43): p. 9132-9.

7. Dhe-Paganon, S., et al., *Crystal structure of human frataxin.* J. Biol. Chem., 2000. **275**(40): p. 30753-6.

8. Bencze, K.Z., et al., *Human frataxin: iron and ferrochelatase binding surface.* Chem. Commun. (Camb), 2007(18): p. 1798-800.

9. Huang, J., E. Dizin, and J.A. Cowan, *Mapping iron binding sites on human frataxin: implications for cluster assembly on the ISU Fe-S cluster scaffold protein.* J. Biol. Inorg. Chem., 2008. **13**(5): p. 825-36.

10. Bou-Abdallah, F., et al., *Iron binding and oxidation kinetics in frataxin CyaY of Escherichia coli.* J. Mol. Biol., 2004. **341**(2): p. 605-15.

11. Bencze, K.Z., et al., *The structure and function of frataxin.* Crit. Rev. Biochem. Mol. Biol., 2006. **41**(5): p. 269-91.

12. Nair, M., et al., *NMR assignment of the 1H, 15N and 13C resonances of the E. coli frataxin orthologue, CyaY.* J. Biomol. NMR, 2003. **27**(4): p. 403-4.

13. He, Y., et al., *Yeast frataxin solution structure, iron binding, and ferrochelatase interaction.* Biochemistry, 2004. **43**(51): p. 16254-62.

14. Kondapalli, K.C., et al., *NMR assignments of a stable processing intermediate of human frataxin.* Biomol. NMR Assign., **4**(1): p. 61-4.
15. Pastore, C., et al., *Understanding the binding properties of an unusual metal-binding protein--a study of bacterial frataxin.* FEBS J., 2007. **274**(16): p. 4199-210.
16. Huffman, D.L. and T.V. O'Halloran, *Function, structure, and mechanism of intracellular copper trafficking proteins.* Annu. Rev. Biochem., 2001. **70**: p. 677-701.
17. Cook, J.D., et al., *Monomeric yeast frataxin is an iron-binding protein.* Biochemistry, 2006. **45**(25): p. 7767-77.
18. Branda, S.S., et al., *Yeast and human frataxin are processed to mature form in two sequential steps by the mitochondrial processing peptidase.* J. Biol. Chem., 1999. **274**(32): p. 22763-9.
19. Prischi, F., et al., *The N-terminus of mature human frataxin is intrinsically unfolded.* FEBS J., 2009. **276**(22): p. 6669-76.
20. Maret, W. and B.L. Vallee, *Cobalt as probe and label of proteins.* Methods Enzymol., 1993. **226**: p. 52-71.
21. Thompsen, J., *Kinetics of the Complexation of Iron(II) with Ferrozine.* Analalytical Chemistry, 1984. **56**: p. 755-757.
22. Kay L.E., K.P., Saarinen T., *Pure Absorption Gradient Enhanced Heteronuclear Single Quantum Correlation Spectroscopy with Improved Sensitivity* J. Am. Chem. Soc, 1992. **114**: p. 10663-10665.
23. Musco, G., et al., *Assignment of the 1H, 15N, and 13C resonances of the C-terminal domain of frataxin, the protein responsible for Friedreich ataxia.* J. Biomol. NMR, 1999. **15**(1): p. 87-8.
24. Bertini, I. and C. Luchinat, *High spin cobalt(II) as a probe for the investigation of metalloproteins.* Adv. Inorg. Biochem., 1984. **6**: p. 71-111.
25. Otting, G., *Protein NMR using paramagnetic ions.* Annu Rev Biophys. **39**: p. 387-405.
26. Schmucker, S., et al., *Mammalian frataxin: an essential function for cellular viability through an interaction with a preformed ISCU/NFS1/ISD11 iron-sulfur assembly complex.* PLoS One, **6**(1): p. e16199.
27. Bertini, I., et al., *NMR spectroscopy of paramagnetic metalloproteins.* Chembiochem, 2005. **6**(9): p. 1536-49.

28. Peisach, J. and W.E. Blumberg, *Structural implications derived from the analysis of electron paramagnetic resonance spectra of natural and artificial copper proteins.* Arch. Biochem. Biophys., 1974. **165**(2): p. 691-708.

29. Yoon, T., E. Dizin, and J.A. Cowan, *N-terminal iron-mediated self-cleavage of human frataxin: regulation of iron binding and complex formation with target proteins.* J. Biol. Inorg. Chem., 2007. **12**(4): p. 535-42.

30. Correia, A.R., et al., *Dynamics, stability and iron-binding activity of frataxin clinical mutants.* FEBS J., 2008. **275**(14): p. 3680-90.

31. Gentry, L.E., et al., *His86 from the N-terminus of frataxin coordinates iron and is required for Fe-S cluster synthesis.* Biochemistry. 2013 **52**(35): p. 6085-96.

CHAPTER 3

FRATAXIN MUTAGENESIS AND METAL COORDINATION

3.1 INTRODUCTION

3.1.1 Localization of Iron Coordination by Frataxin

Previous studies of frataxin metal binding capability performed indicated that frataxin contains three distinct Fe^{2+} coordination sites. Chelator competition assays in **Chapter 2** revealed that frataxin contained one high-affinity Fe^{2+} coordination site, with two weaker binding sites. The HSQC NMR experiments in **Chapter 2** implicated highly conserved residues Asp112 and Asp115 in the first α helix as metal ligands because the amide resonances for Asp112 and Asp115 broadened beyond detection with addition of Cu^{2+}, Co^{2+} and Fe^{2+}. Asp122 and Asp124, both conserved, were also impacted by the addition of metal, but in contrast to Asp112/115, they only experienced chemical shifts of their amide proton resonances. UV–Visible spectroscopy indicated octahedral coordination geometry for both Co^{2+} and Cu^{2+} and EPR spectroscopy indicated that a nitrogen-based ligand, most likely His, was involved in at least one Cu^{2+} metal coordination site. It is clear that two frataxin metal coordination sites are carboxylate-containing: one with Asp112/Asp115 and another with Asp122/Asp124. The location of the third site, which likely has nitrogen coordination, is unclear.

Frataxin contains 3 histidine residues, His86 in the unstructured N-terminal loop, His177, in a solvent accessible loop between the β6 and β7 strands, and His183 whose side chain has limited solvent exposure (**Figure 3.1**). Although none of the 3 histidine residues in human

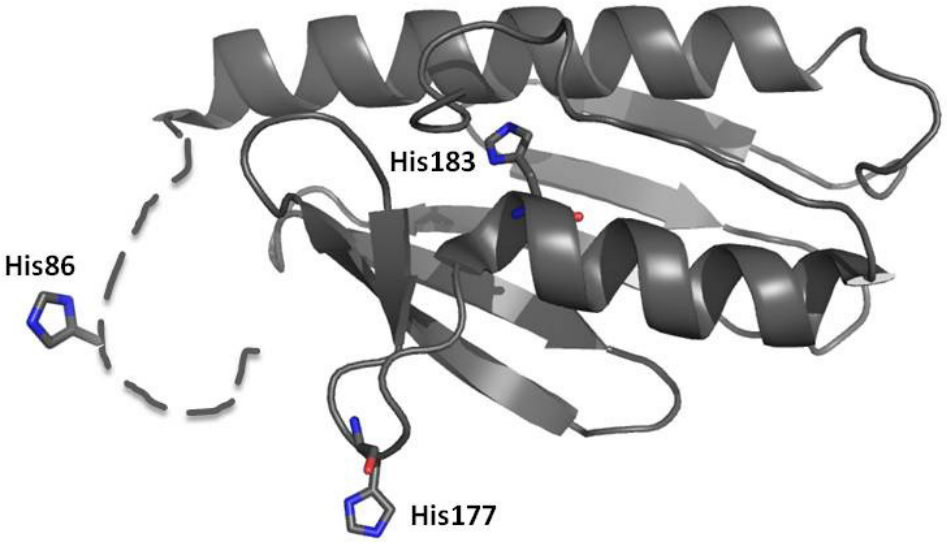

Figure 3.1 Histidine residues of mature human frataxin. Mature human frataxin has 3 histidine residues, His86, in the N-terminal tail (not in crystal structure), His177 in the solvent accessible loop between β6 and β7 and His183 that is buried in the α2 helix (PDB:1EKG).

frataxin are conserved in other frataxin homologs (**Figure 1.7**) a metal binding residue such as histidine, aspartate or glutamate exists at position 86 (or the equivalent) of the N-terminus of all eukaryotic frataxin homologs [1, 2]. Thus, the role of His86 as a potential Fe^{2+} coordinating residue has not previously been studied because of the lack of evolutionary conservation. His177 has also been implicated as an iron coordinating ligand for frataxin in a crystallographic structure by Dhe-Paganon in 2000. However, the validity of His177 as a true iron binding ligand was questioned because of its solvent accessibility [3]. Our NMR titrations in **Chapter 2** showed that with Cu^{2+} or Co^{2+}, the His177 resonance broadened beyond detection before the first full equivalent of metal. However, with Fe^{2+}, the His177 resonance showed no chemical shifts or line broadening, suggesting it is not a ligand to the native metal. His183 has not been implicated as a metal binding residue. The side chain is involved in the protein hydrophobic core, thus may not be available to act as a ligand. This is supported by the fact that the His183 resonance was unaffected in Co^{2+}, Cu^{2+} and Fe^{2+} NMR titrations.

3.1.2 Scope of the Research

To determine if His86, His177, or His183 are Fe^{2+} ligands, these residues were individually mutated to an alanine (H86A, H177A, and H183A). Alanine was chosen because the methyl side chain is not a metal coordinating residue and is a conservative mutation that should not disturb the surrounding residues or hydrogen bond networks. The metal coordination characteristics of each mutant will be studied as for wild-type frataxin to determine if a coordination site has been affected. The metal coordination of each mutant was characterized by UV–Visible spectroscopy and EPR spectroscopy using the metal surrogates discussed in **Chapter 2**. UV–Visible titrations and EPR spectroscopy determine if the metal coordination environment of each mutant has been altered from that of wild-type frataxin. The ferrozine assay

was performed for each mutant to determine if the eliminated coordination site was the high-affinity Fe^{2+} coordination site, if such change of metal coordination exists.

3.2 METHODS AND MATERIALS

3.2.1 Mutagenesis and Protein Purification

The codons for His86, His177, and His183 of frataxin in *pET81–210Fxn* were mutated to alanine codons with QuikChange Lightning Site-Directed Mutagenesis to create plasmids *pET81–210(H86A)Fxn, pET81–210(H177A)Fxn,* and *pET81–210(H183A)Fxn.* Successful mutagenesis was confirmed by DNA sequencing. The *pET81–210(H86A)Fxn, pET81–210(H177A)Fxn,* and *pET81–210(H183A)Fxn* plasmids were transformed into *E. coli* BL21(DE3)*pLysS* cells via heat shock and purified as for wild-type frataxin in **Chapter 2 Section 2.2.2**. The molecular weights of the mutant proteins were confirmed by MALDI–ToF mass spectrometry with dihydroxybenzoic acid (DHB) matrix at a 1:5 ratio of protein:matrix.

3.2.2 UV–Visible Metal Titrations

Cu^{2+} and Co^{2+} titrations with each frataxin mutant were performed and analyzed the same as for wild-type frataxin as described in **Chapter 2 Section 2.2.5**.

3.2.3 Ferrozine Iron Competition Assay

The ferrozine assay was performed and analyzed in the same manner at that for wild-type frataxin as described in **Chapter 2 Section 2.2.6**.

3.3 RESULTS

Two of the three Fe^{2+} coordination sites for frataxin appear to be in the α1 helix and the β1 strand, described in **Chapter 2**. HDX–MS indicated that N-terminal residues may also coordinate metal. Also in **Chapter 2**, Cu^{2+} EPR was consistent with potential imidazole coordination. In the N-terminal region (residues 81–90) the only common metal binding residue

is His86. To validate that His86 is a ligand, it and two other histidine residues were mutated to alanine, and similar metal coordination experiments were performed as described in **Chapter 2** for wild-type frataxin (*i.e.*, native frataxin without mutations).

3.3.1 Effects of Mutagenesis on Co^{2+} Coordination by Frataxin

The UV–Visible titrations demonstrated that wild-type frataxin coordinated Co^{2+} in an octahedral coordination geometry with oxygen and/or nitrogen ligands (**Figure 3.2**). There appear to be two distinct coordination environments that populate during the titration. The first site has *d–d* transitions centered at 532 nm and 485 nm, and the second centered at 511 nm and 466 nm. However, when H86A frataxin was titrated with Co^{2+}, the Co^{2+} coordination site with λ_{max} at 532 nm and 485 nm was lost and a 2-fold decrease molar absorptivity was observed (**Figure 3.2**). Saturation was reached after 2 molar equivalents of Co^{2+} for H86A frataxin, in contrast to the 3 equivalents of Co^{2+} needed to saturate wild-type frataxin. Because Co^{2+} absorption spectroscopy is sensitive enough to detect changes in the metal coordination environment [4], the shifts in the *d–d* transitions between wild-type frataxin and H86A frataxin indicate the importance of His86 in metal coordination. These data support that mutation of His86, leads to loss of a lower energy metal binding site, such as loss of a nitrogen-containing coordination sphere.

H177A frataxin was constructed because of the dramatic effects observed for the His177 resonance in the NMR titration experiments described in **Sections 2.8.2** and **2.8.3** of **Chapter 2**. When H177A frataxin was titrated with Co^{2+}, the Co^{2+} coordination site with λ_{max} at 532 nm and 485 nm was lost and also had a 2-fold decrease in the molar absorptivity, as was seen with H86A frataxin (**Figure 3.3**). The loss of transition indicates that the change in the environment caused by the elimination of His177 altered a Co^{2+} coordination sphere. The H183A frataxin mutant

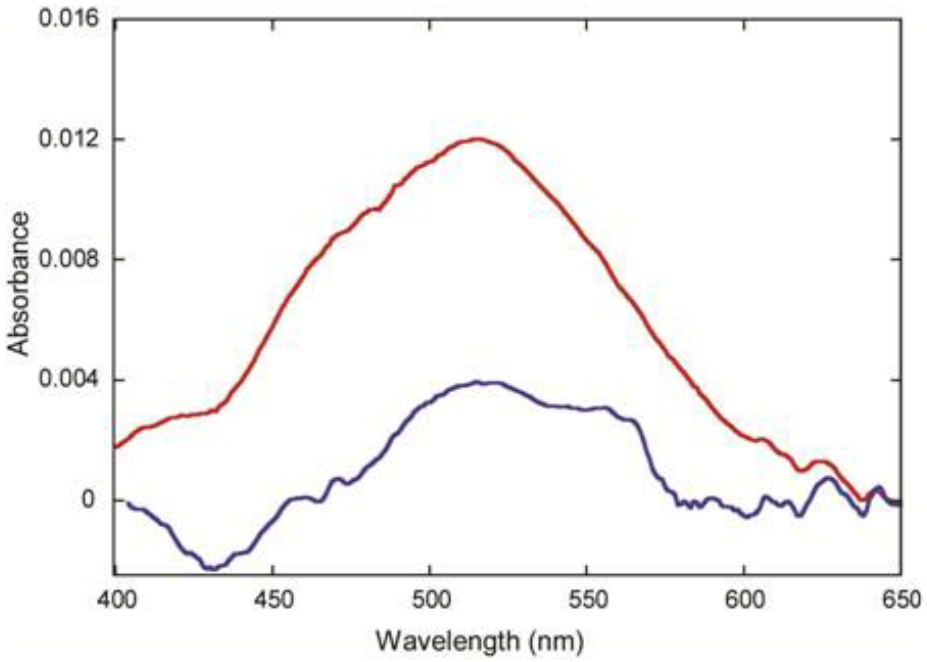

Figure 3.2 UV–Visible spectrum of cobalt titration of wild-type frataxin (red) and H86A frataxin (blue). The *d–d* transitions of 300 μM frataxin with 2 equivalents of Co^{2+} from 450–550 nm are observed. Titrations were performed in 50 mM HEPES, 400 mM NaCl, pH 7.2, and 25 °C.

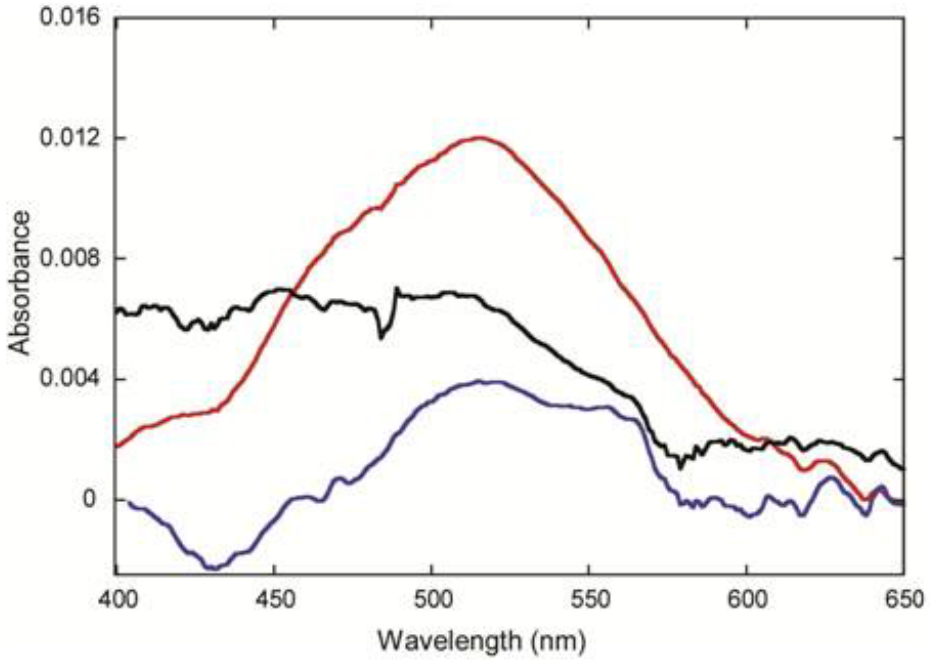

Figure 3.3 UV–Visible spectrum of cobalt titration of wild-type frataxin (red), H86A frataxin (blue) and H177A frataxin (black). The *d–d* transitions of 300 μM frataxin with 2 equivalents of Co^{2+} from 450–550 nm are observed. Titrations were performed in 50 mM HEPES, 400 mM NaCl, pH 7.2 and 25 °C.

showed no differences in *d–d* transitions from that of wild-type frataxin. As a result, the characterization of H183A was no longer pursued.

3.3.2 Effects of Mutagenesis on Cu^{2+} Coordination by Frataxin

For additional support, H86A frataxin was also titrated with Cu^{2+}. Wild-type frataxin had overlapping Cu^{2+} *d–d* transitions with λ_{max} at 605 and 645 nm. However, when H86A frataxin was titrated with Cu^{2+}, the Cu^{2+} transition at 645 nm was diminished (**Figure 3.4**). Additional features in the spectra of both wild-type frataxin and H86A frataxin were observed at ~715 nm and are attributed to contributions from weak Cu^{2+} binding of the Bis-Tris buffer at pH 7.2. As was observed for the Co^{2+} titration, a 2-fold decrease in the molar absorptivity from wild-type frataxin was also observed for Cu^{2+} coordination. When H177A was titrated with Cu^{2+}, the transition at 605 nm was lost (**Figure 3.5**). As observed with the Co^{2+} titrations, the loss of the transition is different than that of H86A frataxin and could indicate a unique coordination site, but its accessibility to solvent makes the validity of His177 as a true metal binding site questionable.

3.3.3 Cu^{2+} EPR Reveals Importance of His86 as Metal Binding Ligand

Cu^{2+} EPR spectroscopy shed light onto whether His86 and His177 are both ligands to metals. The CW EPR spectrum of H86A frataxin with 2 equivalents of Cu^{2+} was compared to the EPR spectrum from wild-type frataxin (**Figure 3.6A**). Deconvolution of the CW EPR spectrum of H86A frataxin with 2 equivalents of Cu^{2+} reveals that the first Cu^{2+} site (g_{II} = 2.29 Hz, A_{II} = 465 G) is the same as the first Cu^{2+} site in wild-type frataxin (**Figure 3.6B**). However, the EPR spectrum of frataxin with ~2 equivalents of Cu^{2+} shows a new sets of lines without corresponding hyperfine- and *g*-tensors than in wild-type frataxin (**Figure 3.6C**). Thus the

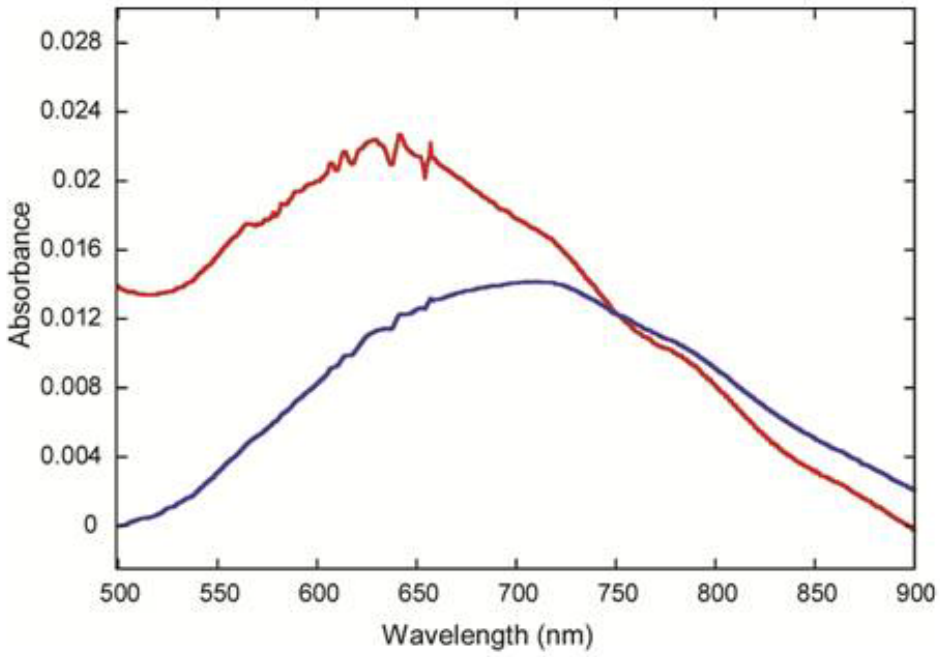

Figure 3.4 UV–Visible spectra of copper titration of wild-type frataxin (red) and H86A frataxin (pink). The *d–d* transition of 300 μM H86A frataxin with 2 equivalents of Cu^{2+} from 600–800 nm is observed. Titrations were performed in 50 mM Bis-Tris, 400 mM NaCl, pH 7.2, and 25 °C.

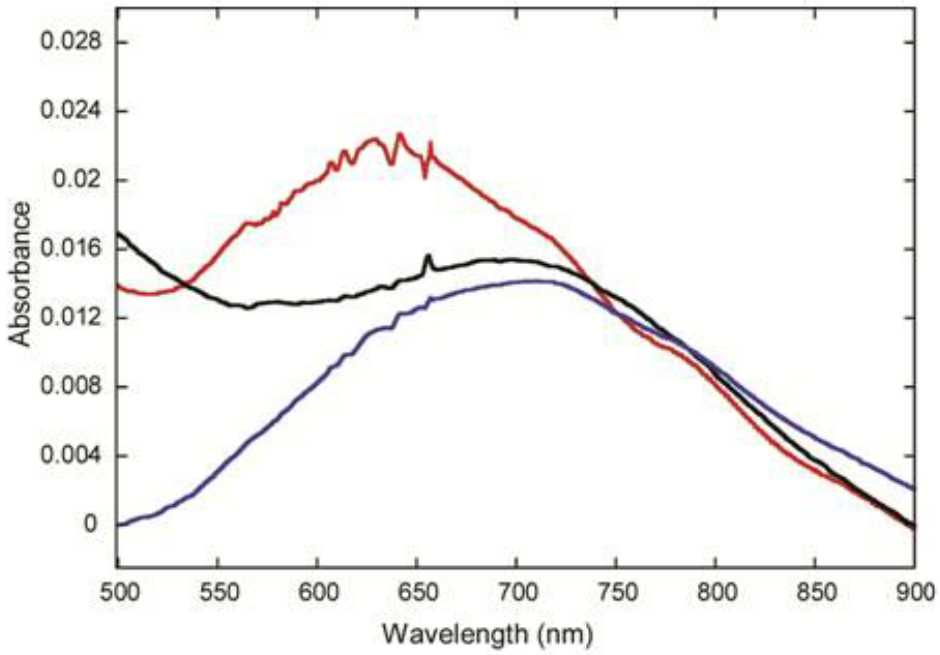

Figure 3.5 UV–Visible spectra of copper titration of wild-type frataxin (red), H86A frataxin (blue) and H177A frataxin (black). The *d–d* transition of 300 μM frataxin with 2 equivalents of Cu^{2+} from 600–800 nm is observed. The titration was performed in 50 mM Bis-Tris, 400 mM NaCl pH 7.2 and 23 °C.

second Cu^{2+} binding site has been altered for the H86A mutant (**Table 2**). The strong modulation from the imidazole nitrogen is absent in H86A frataxin, as is the ENDOR signal from the directly coordinating nitrogen ligand (Michael Bowman, data not shown). These EPR measurements confirm that wild-type frataxin binds Cu^{2+} at two distinct sites, one of which contains His86 as a coordinating ligand.

3.3.4 H86A Indicates a Loss of the High-Affinity Fe^{2+} Coordination Site

To test whether the coordination site eliminated in H86A frataxin was the high-affinity binding site, the ferrozine Fe^{2+} competition assay was performed with H86A frataxin as for wild-type frataxin. Unlike wild-type frataxin, the absorbance at 562 nm corresponding to the Fe^{2+}–$Ferrozine_3$ complex increased linearly up to upon addition of Fe^{2+} and was comparable to the control without frataxin (**Figure 3.7**). The fact that ferrozine was able to coordinate the first equivalent of Fe^{2+} without competition from frataxin indicated that the high-affinity Fe^{2+} coordination site in wild-type frataxin had been eliminated by the replacement of His86 with alanine. Thus, His86 participates in the high-affinity Fe^{2+} coordination.

3.4 DISCUSSION

Frataxin is an iron binding protein that may transport iron to proteins that require it for function, such as for [Fe–S] cluster biogenesis. It has been shown that frataxin coordinates ferrous iron at the α1 helix using the collection of carboxylate residues in a region referred to as the acidic ridge [1, 5-7]. It is also assumed that frataxin does not coordinate Fe^{2+} with high-affinity, but more non-specifically with a weak affinity [8]. Human frataxin coordinating Fe^{2+} with such weak affinity seems unlikely considering the bacterial and yeast frataxin homologs coordinate Fe^{2+} with much higher affinities [9, 10]. Although some residues on the surface of

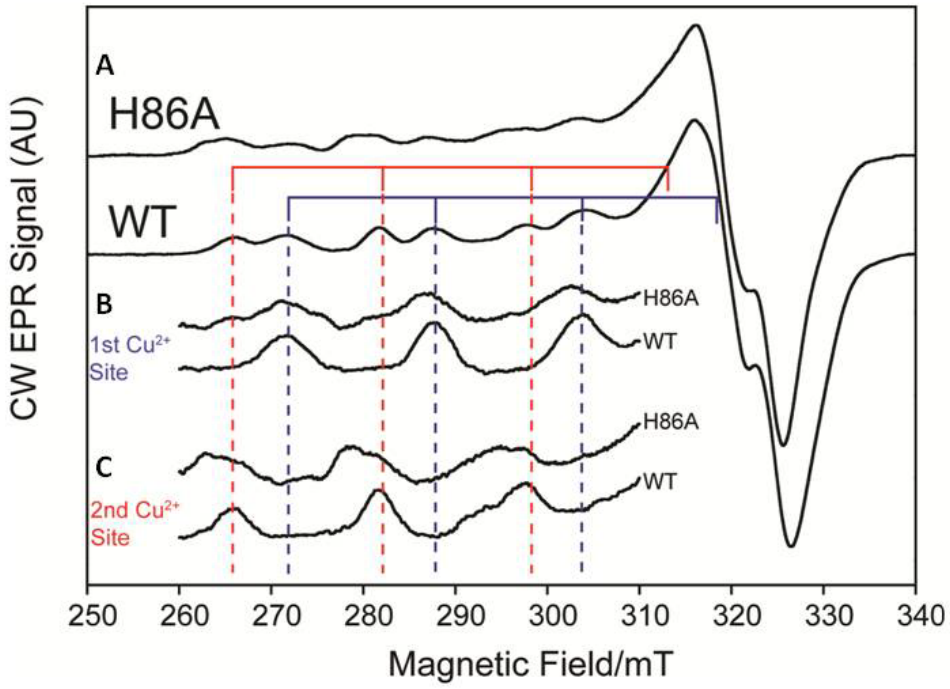

Figure 3.6 Copper EPR of wild-type versus H86A frataxin. (A) X–band continuous wave EPR spectra of 1 mM wild-type frataxin and 1 mM H86A frataxin with 2 equivalents of Cu^{2+}. (B) Comparison of the first Cu^{2+} binding site for H86A frataxin (top) and wild-type frataxin (bottom). (C) Comparison of the second Cu^{2+} binding site for H86A frataxin (top) and wild-type frataxin (bottom) . The sample was prepared in 50 mM HEPES, 150 mM NaCl at pH 7. The metal stock was prepared in 50 mM Bis-Tris, pH 7.

Table 2. EPR values for wild-type frataxin and H86A frataxin.

	g_{II} 0.9 equivalents Cu^{2+}	A_{II} 0.9 equivalents Cu^{2+}	g_{II} 1.9 equivalents Cu^{2+}	A_{II} 1.9 equivalents Cu^{2+}
Wild-type frataxin	2.345 Hz	151 G	2.29 Hz	159 G
H86A frataxin	2.337 Hz	446 G	2.29 Hz	465 G

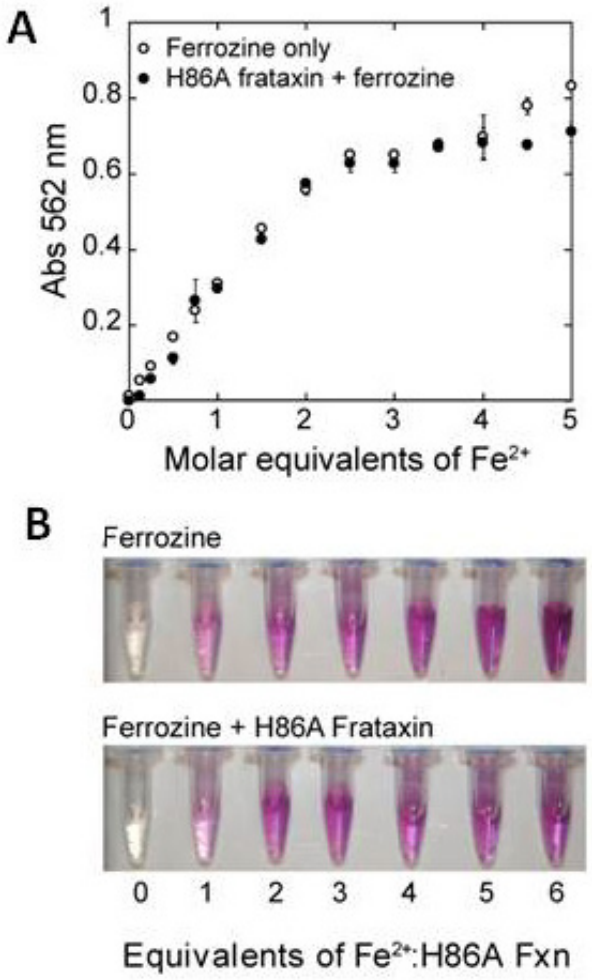

Figure 3.7 Ferrozine iron competition titration. (A) The binding isotherms at 562 nm for the ferrozine titration without frataxin (open circles) and with 13 μM H86Afrataxin (black circles). (B) Representative samples from a Fe^{2+} titration of 108 μM ferrozine (bottom). The $ferrozine_3/Fe^{2+}$ complex is purple in color. H86A frataxin no longer preferentially binds up to 1.0 equivalent of Fe^{2+} indicated by the purple color and absorbance at 562 nm comparable to ferrozine with no frataxin. The titration was performed in 25 mM HEPES, 150 mM NaCl, pH 7 and 25 °C.

frataxin may comprise one or two coordination sites, our studies presented in **Chapter 2** reveal there is a coordination site that is presumably less labile and binds Fe^{2+} with a greater affinity than previously reported for human frataxin [11]. Previous HDX–MS results [12] indicated three Fe^{2+} coordination sites by frataxin, two of which were also observed by NMR (Asp112/115, Asp122/124) in **Chapter 2**. The third site was postulated to include coordination from residues in the N-terminus. Because mature wild-type frataxin lacks cysteine residues commonly known to coordinate metals, Fe^{2+} is likely coordinated with aspartate, glutamate or histidine residues. Since EPR spectroscopy in **Chapter 2** indicated that an imidazole nitrogen is in the Cu^{2+} coordination sphere lead to the investigation of the histidine residues for metal coordination by frataxin. The goal of **Chapter 3** of this dissertation was to determine if any of the histidine residues of frataxin are involved in the high-affinity Fe^{2+} coordination sphere.

3.4.1 His86 is a Key Ligand in the High-Affinity Fe^{2+} Coordination Site

The first histidine mutant was H86A, which is in the N-terminus of mature frataxin and showed protection by Fe^{2+} in HDX–MS experiments. For wild-type frataxin, there were two sets of overlapping transitions (λ_{max} = 532/485 nm and 511/466 nm) corresponding to 2 different coordination environments. However, the *d–d* transitions for H86A frataxin with Co^{2+} showed that the 532/485 nm transition set was no longer observed, indicating a loss of nitrogen-based coordination (**Figure 3.2**). In addition, only 2 equivalents of Co^{2+} were required to saturate H86A frataxin in comparison to the 3 equivalents needed for wild-type. The 2-fold decrease in the molar absorptivity between wild-type frataxin and H86A frataxin also supported the loss of a metal coordination site. Similar effects were seen with Cu^{2+} where nitrogen-based coordination site and decreased molar absorptivity were observed for H86A frataxin when compared to wild-type frataxin (**Figure 3.3**). The Cu^{2+} EPR spectra of H86A frataxin compared to wild-type

frataxin had g_{II} and hyperfine values consistent with the loss of a nitrogen-containing site (**Figure 3.6**). It was determined in **Section 2.3.2** that wild-type frataxin contained a high-affinity Fe^{2+} binding site that out-competed the colorimetric chelator ferrozine until one equivalent of Fe^{2+}; however, H86A frataxin no longer out-competed ferrozine for Fe^{2+}(**Figure 3.7**). From all of these results, His86 is likely an Fe^{2+} coordinating ligand in a high-affinity binding site.

His86 has never before been identified as a key metal coordinating residue for frataxin because of its location in the N-terminus. Most dismiss the N-terminus and His86 of human frataxin from having any key functions due to the non-conservation; however, the N- and C-termini of proteins can be important for species specific functions, metal binding and stabilization of protein–protein interactions [13-15]. Although His86 is the key ligand in the high-affinity Fe^{2+} coordination site, it is not yet known if this site is important to the interaction with Isu2 or the assembly of [Fe–S] clusters and will be explored in **Chapter 4**.

The importance of His86 and the N-terminus as a high-affinity Fe^{2+} binding site has never been investigated for human frataxin. The importance of the N-terminus in functional Fe^{2+} coordination has not gone unnoticed, however. In 2007, the Stemmler group reported a high-affinity Fe^{2+} coordination site in the N-terminal tail of Yfh1[7]. The flexible N-terminal tail of Yfh1 covered the acidic ridge of the α1 helix, prohibiting the population of the weaker Fe^{2+} binding sites and giving access only to the high-affinity site. However, when Yfh1 was processed to the mature form and the N-terminus was cleaved, the high-affinity site was lost. This is significant because a high-affinity binding site is also found in other homologs of frataxin but remains unstudied because the N-terminus is not evolutionarily conserved.

3.4.2 Metal Coordination by His177 Still in Question

Characterization of His177 as a potential metal binding ligand has yielded conflicting results. UV–Visible spectroscopy showed that mutation of His177 to alanine did affect the coordination environment of Co^{2+} and Cu^{2+} based on changes in the *d–d* transitions (**Figures 3.3** and **3.5**). In addition, Co^{2+} and Cu^{2+} broadened the H177 amide cross-peak beyond detection by 0.3 equivalents of Cu^{2+} and Co^{2+} in NMR spectra, but Fe^{2+} neither broadened nor shifted the His177 resonance. Because of the solvent accessibility of His177 and the immediate broadening of the His177 amide proton cross-peak in the Cu^{2+} and Co^{2+} HSQC spectra, it is more likely that His177 is experiencing collisional non-specific binding. His177 was previously identified as an Fe^{2+} binding ligand in crystal structures, but it was located at the crystal packing interface and was loosely associated with backbone carbonyl oxygens and a carboxylate side chain from an adjacent monomer [3]. The validity of His177 as a true ligand was questioned due to its location in a solvent accessible loop between β6 and β7 strands and the lack of conservation. It could be possible that His177 aids in Fe^{2+} transfer to Isu2 for the assembly of [Fe–S] clusters and will be explored in **Chapter 4**.

3.4.3 Significance of His86 as High-Affinity Fe^{2+} Coordinating Ligand

The N-terminus of mature human frataxin has not been explored as a possible site of Fe^{2+} coordination. Although there were indications that the N-terminus could be important for Fe^{2+} coordination the lack of conservation has been assumed that it also has no function. For the first time, the N-terminus and His86 have been identified as the high-affinity Fe^{2+} coordination site for mature human frataxin.

REFERENCES

1. Pastore, C., et al., *Understanding the binding properties of an unusual metal-binding protein--a study of bacterial frataxin.* FEBS J., 2007. **274**(16): p. 4199-210.

2. He, Y., et al., *Yeast frataxin solution structure, iron binding, and ferrochelatase interaction.* Biochemistry, 2004. **43**(51): p. 16254-62.

3. Dhe-Paganon, S., et al., *Crystal structure of human frataxin.* J. Biol. Chem., 2000. **275**(40): p. 30753-6.

4. Bertini, I. and C. Luchinat, *High spin cobalt(II) as a probe for the investigation of metalloproteins.* Adv. Inorg. Biochem., 1984. **6**: p. 71-111.

5. Nair, M., et al., *Solution structure of the bacterial frataxin ortholog, CyaY: mapping the iron binding sites.* Structure, 2004. **12**(11): p. 2037-48.

6. Prischi, F., et al., *Structural bases for the interaction of frataxin with the central components of iron-sulphur cluster assembly.* Nat. Commun., 2009 **1**: p. 95.

7. Yoon, T., E. Dizin, and J.A. Cowan, *N-terminal iron-mediated self-cleavage of human frataxin: regulation of iron binding and complex formation with target proteins.* J. Biol. Inorg. Chem., 2007. **12**(4): p. 535-42.

8. Pastore, A. and H. Puccio, *Frataxin: a protein in search for a function.* J. Neurochem., **126 Suppl 1**: 2013 p. 43-52.

9. Bou-Abdallah, F., et al., *Iron binding and oxidation kinetics in frataxin CyaY of Escherichia coli.* J. Mol. Biol., 2004. **341**(2): p. 605-15.

10. Cook, J.D., et al., *Monomeric yeast frataxin is an iron-binding protein.* Biochemistry, 2006. **45**(25): p. 7767-77.

11. Yoon, T. and J.A. Cowan, *Iron-sulfur cluster biosynthesis. Characterization of frataxin as an iron donor for assembly of [2Fe-2S] clusters in ISU-type proteins.* J. Am. Chem. Soc., 2003. **125**(20): p. 6078-84.

12. Gentry, L.E., et al., *His86 from the N-terminus of frataxin coordinates iron and is required for FeS cluster synthesis.* Biochemistry. 2013 **52**(35): p. 6085-96.

13. Prischi, F., et al., *The N-terminus of mature human frataxin is intrinsically unfolded.* FEBS J., 2009. **276**(22): p. 6669-76.

14. Adinolfi, S., et al., *Bacterial frataxin CyaY is the gatekeeper of iron-sulfur cluster formation catalyzed by IscS.* Nat Struct Mol Biol, 2009. **16**(4): p. 390-6.

15. Uversky, V.N., *The most important thing is the tail: multitudinous functionalities of intrinsically disordered protein termini.* FEBS Lett., 2013 **587**(13): p. 1891-901.

CHAPTER 4

PROTEIN–PROTEIN INTERACTIONS

4.1 INTRODUCTION

4.1.1 Components of the [Fe–S] Cluster Assembly Complex

Iron-sulfur clusters are important cofactors having roles in electron transport, substrate binding and activation, and redox catalysis [1, 2]. [Fe–S] clusters do not assemble spontaneously *in vivo* as both free ferrous iron and sulfide are toxic to the cell [3, 4]. The biogenesis of [Fe–S] clusters in humans is controlled by proteins expressed in the ISC operon [5]. Isu2 is the scaffold protein on which [Fe–S] clusters are assembled (**Figure 1.12**) [6], and its molten globular structure makes Isu2 the perfect surface for cluster assembly. Nfs1 is a PLP-dependent cysteine desulfurase that donates sulfane sulfur for [Fe–S] cluster biogenesis [7]. Isd11 is an accessory protein that enhances the activity of Nfs1, although its exact function remains unclear [8]. Frataxin is proposed to interact with the ISC machinery to form a quaternary complex [9-16].

4.1.2 The Role ff Frataxin in [Fe–S] Cluster Biogenesis

There have been several roles proposed for frataxin, all involving iron. The one with the most supporting evidence is that frataxin delivers Fe^{2+} to the [Fe–S] cluster assembly complex [17]. There are two possible roles through which frataxin can participate in the [Fe–S] cluster assembly complex. The first proposed role is that frataxin delivers Fe^{2+} to Isu2 through protein–protein interactions [10, 11, 18, 19]. The second role is frataxin as an allosteric regulator of the [Fe–S] cluster assembly complex [14]. The Barondeau group reported an increase in Nfs1 cysteine desulfurase activity and [Fe–S] cluster assembly rate when frataxin was present in the cluster assembly complex [14, 20] . It is possible that frataxin participates in both roles, and the

different cellular conditions delineate the exact function of frataxin at that time [16]. To determine the role of frataxin in the [Fe–S] cluster assembly complex and the mechanism by which Fe^{2+} is transferred from frataxin to the assembly complex, the interaction between frataxin and Isu2 needs to be investigated. The knowledge of the defined frataxin–Isu2 interaction surface and Fe^{2+} transfer site will contribute greatly to the study of frataxin function.

4.1.3 Evidence that Frataxin and Isu2 Interact

The interaction between human frataxin and Isu2 has been demonstrated using pull-down assays [10], binding titrations [21], and kinetic assays [18]. In 2010, the Stemmler group reported a surface for yeast frataxin homolog Yfh1that is involved in the interaction with Isu2 based on NMR studies. The Puccio group reported amino acids of human frataxin that are possibly involved in the interaction with the [Fe–S] cluster assembly complex [13, 22]. However, the location of the human frataxin–Isu2 interaction has not been reported. Additionally, none of these studies provide information about the residues or surface on Isu2 that interacts with frataxin. If frataxin stimulates [Fe–S] cluster assembly by interacting with Isu2, how and where is the interaction occurring? Are the Fe^{2+} coordinating residues of frataxin involved in the interaction with Isu2? Is the high-affinity Fe^{2+} coordination site required for stimulation of [Fe–S] cluster assembly? Is a surface created during interaction and Fe^{2+} transfer?

While there is much focus on the mechanism by which frataxin transfers Fe^{2+} to Isu2, the dynamic nature of Isu2 and how it interacts with proteins in the [Fe–S] cluster assembly complex is also important. Isu2 exists in an equilibrium of two states, dynamically disordered (D) and structured (S) [2]. Cysteine desulfurase, Nfs1, interacts preferentially with the disordered (D) form of Isu2 [23], but the conformation of Isu2 with the interaction with frataxin is not known. Additionally, mapping an interaction surface on the three-dimensional structure of the dynamic

form of Isu2 is not currently possible as the only NMR structure is in the (S) state. If Isu2 is interacting with the proteins in the [Fe–S] cluster assembly complex in the (D) state, mapping the interaction surface on the (S) state would be misleading. To determine an interaction surface for Isu2, a structure in the (D) state is needed. Determining the state in which Isu2 interacts with frataxin and the amino acids involved in the interaction will lend information toward a more appropriate Isu2 structure.

4.1.4 Scope of the Research

$^{1}H–^{15}N$-HSQC NMR experiments will indicate if Isu2 changes conformation when it interacts with frataxin during Fe^{2+} transfer or after [Fe–S] cluster assembly. The stimulatory effects of frataxin on the rate of [Fe-S] cluster assembly will also be ascertained, including the histidine mutants characterized in **Chapter 3** to determine if any of the histidine residues impair [Fe–S] cluster assembly. The frataxin–Isu2 interaction will then be studied with chemical crosslinking and HDX–MS. Crosslinking will indicate potential residues involved in the frataxin–Isu2 interaction. Two different chemical crosslinkers will be used, sulfo-SBED and EDC/NHS. Sulfo-SBED is a trifunctional crosslinker with an N-hydroxysuccinimide ester group that will react with the lysine amines of frataxin ("bait"), a photoreactive phenyl azide group that will crosslink to Isu2 ("prey") and a biotin group which will aid in detection of the crosslinked complex (**Figure 4.1A**). EDC/NHS is a covalent zero-length crosslinker that will result in direct conjugation of the carboxylate side chains of frataxin to the primary amines of Isu2 without interference of the crosslinker (**Figure 4.1B**). In complement to the crosslinking reactions, HDX–MS deuterium trapping experiments will identify the peptides from frataxin that are protected during the interaction with Isu2. In the deuterium trapping experiments Isu2 and frataxin are individually pre-exchanged with deuterium prior to forming a complex. After back-

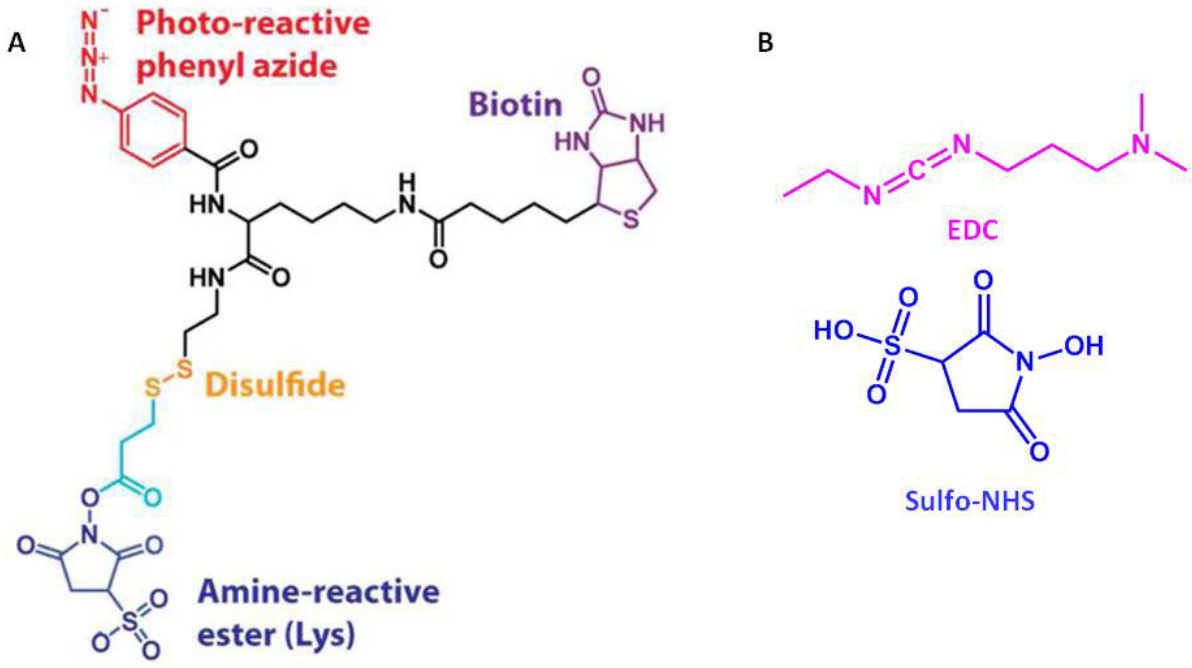

Figure 4.1 (A) Structure of sulfo–SBED photo-activated chemical crosslinker. The amine reactive ester group conjugates to lysine residues of the bait protein. The photo-reactive phenyl azide group reacts with the bait protein upon activation with UV light. The biotin label aids in detection of a crosslinked complex. (B) Structure of EDC/sulfo-NHS crosslinker. The zero-length crosslinker conjugates to free carboxylate residues of the bait protein. The sulfo–NHS stabilizes the EDC–protein conjugate for crosslinking with the free amines of the prey protein.

exchanging the complex with water the regions involved in the interaction will have an increase in deuterium retention, thus identifying the interface of the frataxin–Isu2 interaction. The results from crosslinking and HDX–MS will be used together to determine a surface for the frataxin–Isu2 interaction.

4.2 METHODS AND MATERIALS

4.2.1 General Chemicals

Dimethylfuran (DMF) and TWEEN-20 were purchased from Acros Organics. Kanamycin, dithiothreitol (DTT), sodium dodecylsulfate (SDS), Tris-HCl, iodoacetamide (IAA), ammonium bicarbonate, and deuterium oxide were purchased from VWR. 3-(N-morpholino)propanesulfonic acid (MOPS), Sodium phosphate (dibasic), methanol, glacial acetic acid were purchased from Fisher Scientific. Talon resin and N-hydroxysulfosuccinimide (Sulfo-NHS) were purchased from Thermo. Sulfo-N-hydroxysuccinimidyl-2-(6-[biotinamido]-2-(p-azido benzamido)-hexanoamido) ethyl-1,3'-dithioproprionate (sulfo-SBED) and 1-ethyl-3-[3-dimethylaminopropyl]carbodiimide (EDC) were purchased from Pierce. Streptavidin–alkaline phosphatase was purchased from Promega. Tris(2-carboxyethyl)phosphate, and nitro-blue tetrazolium chloride (NBT) were purchased from Amresco. Triton-X 100, bovine serum albumin fraction V (BSA) and acetonitrile were purchased from EMD chemical. 5-bromo-4-chloro-3'-indolyphosphate p-toluidine salt (BCIP) was purchased from Biosynth. Porcine pepsin and trypsin gold were purchased from Sigma Aldrich. Mouse anti–His antibody was purchased from ABGENT. Goat anti–mouse alkaline phosphatase conjugated antibody was purchased from Southern Biotech.

4.2.2 Isu2 Expression and Purification

The *pETisu2-stop* plasmid containing the gene for human Isu2 residues 35–167 was transformed into BL21(DE3)*pLysS* cells via heat shock and plated on LB agar plates containing 50 μg/μL kanamycin and 34 μg/μL chloramphenicol. Cells were grown overnight at 37 °C and then inoculated into LB growth medium containing 50 μg/L of kanamycin and 34 μg/μL chloramphenicol. The cells were grown at 37 °C with 250 rpm shaking and induced at an OD_{600} of 0.8–1.0 with a final concentration of 1 mM IPTG. The cells were grown at either 37 °C for 3–4 hr to an OD_{600} of ~2.0 or at 25 °C overnight to an OD_{600} of ~2. Cells were harvested via centrifugation at 6,000 rpm for 30 min at 4 °C. Cell pellets were resuspended in 150–200 mL of buffer O (50 mM MOPS, 50 mM NaCl, 1 mM EDTA, 2 mM DTT, 5% glycerol, pH 6.8) with a final concentration of 0.1 mM PMSF protease inhibitor. Cells were stirred on ice for up to 20 min before lysis via sonication. Cells were lysed by a Branson Sonifier at 40% duty cycle for a total of 4 min with cycles of 30 s on/off and centrifuged at 14,000 rpm for 30 min at 4 °C. The lysis supernatant was subjected to PEI precipitation at a final concentration of 0.03% *v*/*v* of 5% PEI solution and stirred on ice for 1–2 hr and centrifuged at 14,000 rpm for 30 min at 4 °C. The PEI supernatant was then subjected to a 60% ammonium sulfate precipitation and stirred on ice for 1–2 hr and centrifuged at 14,000 rpm for 30 min at 4 °C. The ammonium sulfate supernatant contained Isu2 and it was dialyzed against buffer O to remove ammonium sulfate prior to ion exchange chromatography.

The dialyzed protein solution was loaded onto diethylaminoethyl (DEAE) sepharose resin. The resin was subsequently washed with 50 mL of buffer O. Isu2 does not bind to the DEAE resin. The load flow-through and wash flow-through were combined and loaded on sulfopropyl (SP) sepharose resin. The SP resin was washed with 50 mL of buffer O. A 150 mL

linear gradient of 50–500 mM NaCl was used to elute Isu2 from the resin. The elution was collected in fractions and run on a 15% polyacrylamide gel to determine purity. Pure fractions with the correct molecular weight (~14 kDa) were combined and dialyzed into buffer H (50 mM HEPES, 150 mM NaCl, 2 mM DTT, 10% glycerol, pH 7.4). Protein was concentrated as needed and the concentration was determined using $\varepsilon_{280} = 9970\ M^{-1}\ cm^{-1}$. Reducing agent was removed from Isu2 through dialysis in a Vacuum Atmospheres anaerobic glovebox with 4–5 changes of buffer H without DTT every 2–3 hr. Isu2 samples were sealed with parafilm and placed in secondary containment, which was also sealed with parafilm before removing from the glovebox to be stored at –80 °C.

4.2.3 Isu2–His_6 HSQC NMR Spectroscopy

The *pETisu2-His$_6$* plasmid containing the gene for Isu2 with an C-terminal hexahistidine (His_6) affinity tag was transformed into BL21(DE3)*pLysS* cells via heat shock. Cultures were inoculated from fresh transformation plates into the M9 minimal media supplemented with 1.0 g/L 86% ^{15}N-enriched ammonium sulfate, 50 μg/L kanamycin and 34 μg/L chloramphenicol and grown at 37 °C with shaking at 250 rpm. Cells were induced at an OD_{600} of 0.6 –1.0 to a final concentration of 1 mM IPTG. Cells were grown for 3–4 hr at 37 °C to an OD_{600} not exceeding 2.0. Cells were harvested via centrifugation at 6,000 rpm for 30 min at 4 °C. Cells were resuspended in 50–100 mL of buffer N (50 mM Na_2HPO_4, 300 mM NaCl, 2 mM β-ME, 10% glycerol, pH 7) with a final concentration of 0.1 mM PMSF protease inhibitor and stirred on ice for approximately 20 min. Cells were then lysed by a Branson Sonifier at 40% duty cycle for a total of 4 min of sonication with cycles of 30 s on/off. The lysed cells were centrifuged at 14,000 rpm for 30 min at 4 °C and the lysis supernatant was loaded onto pre-equilibrated Talon resin for at least 4 hr with gentle oscillation at 4 °C. The resin was washed with 10 bed volumes

of buffer N, followed by 5 bed volumes of buffer N containing 5 mM imidazole, followed by 5 bed volumes of buffer N containing 10 mM imidazole. ^{15}N-Isu2–His$_6$ was eluted from the resin with 10 bed volumes of buffer N with 250 mM imidazole. The purification fractions were subjected to SDS–PAGE and a western blot was performed with mouse anti–His primary antibody and goat anti–mouse conjugated with alkaline phosphatase secondary antibody. Pure ^{15}N-Isu2–His$_6$ was dialyzed into buffer H (50 mM HEPES, 150 mM NaCl, 4 mM TCEP, pH 7.4) to remove imidazole. ^{15}N-Isu2–His$_6$ was concentrated as needed and was buffer exchanged into 50 mM d_{18}-HEPES, 100 mM NaCl, pH 7 for NMR experiments.

4.2.4 ^{1}H–^{15}N HSQC NMR Spectroscopy

Samples for NMR were prepared by adding 400 μL of 0.75 mM ^{15}N-Isu2–His$_6$ and 100 μL of d_{18}-HEPES to an acid-washed NMR tube. Samples containing frataxin were made with a 1:1 molar ratio of Isu2:frataxin at a total volume of 400 μL of protein. Samples with iron were made at a ratio of 1:2 Isu2 to metal. Samples with frataxin and an [Fe–S] cluster were made as that of the [Fe–S] cluster assembly assays (**Section 4.2.6**) and centrifuged to remove any sulfide precipitate before placing in NMR tubes. NMR data were collected at 298 K on a Brüker Avance 600 MHz spectrometer (Fremont, CA) with a triple resonance ^{1}H/^{13}C/^{15}N probe equipped with z-axis pulsed field gradients. The fingerprint main chain amide region was recorded by two-dimensional ^{1}H–^{15}N HSQC experiment using the standard Brüker pulse program [24]. NMR spectra were collected and formatted by Dr. Russell Timkovich. Spectra were analyzed using SPARKY (T.D. Goddard and D. G. Kneller, University of California, San Francisco).

4.2.5 N88A and D37A Isu2 Mutagenesis

The codons for Asp37 in *pETisu2–stop* and Asn88 in *pETisu2–His$_6$* were mutated to that of an alanine via site-directed mutagenesis using QuikChange Lightning. Successful mutagenesis was confirmed by DNA sequencing. The mutated plasmids *pETisu2(D37A)–stop* and *pETisu2(N88A)–His$_6$* were transformed into BL21(DE3)*pLysS* cells via heat shock and purified as for wild-type Isu2 and Isu2–His$_6$.

4.2.6 [Fe–S] Cluster Assembly Assays

All assays were performed under strict anaerobic conditions in a Vacuum Atmosphere anaerobic glovebox and sealed in an anaerobic cuvette fitted with a gas-tight syringe. The reaction was carried out in 25 mM HEPES, 100 mM NaCl pH 7.4. One hundred micromolar frataxin was incubated with 200 μM ferrous ammonium sulfate for 30 min at room temperature and was placed in the gas-tight syringe. The anaerobic cuvette contained 100 μM D37A Isu2 or N88A Isu2–His$_6$ and 2.4 mM Na_2S. The reaction was initiated by the immediate addition of the iron-loaded frataxin and the reaction was monitored at 426 nm using an Agilent 8453 spectrophotometer (Santa Clara, CA) in kinetics mode. Iron controls included 200 μM ferrous ammonium sulfate (no frataxin) and bovine serum albumin with200 μM ferrous ammonium sulfate. Each reaction was performed in triplicate. The data were fit to a first order rate equation to determine the rate of [Fe–S] cluster formation.

4.2.7 Frataxin–Isu2 Fluorescence Binding Assay

Intrinsic tryptophan fluorescence experiments were performed at 23 °C using a Spex Fluoromax-3 fluorimeter (Edison, NJ) with excitation at 295 nm. Samples contained 0.5 μM wild-type or H86A frataxin in 50 mM HEPES, 150 mM NaCl at pH 7.4. Frataxin with and

without 1 μM ferric chloride (2 molar equivalents) was titrated with 4 molar equivalents of D37A Isu2 in the same buffer. Buffer was also titrated with Isu2 as a control. Experiments comparing wild-type frataxin and H86A frataxin were corrected and fit to determine the dissociation constant for the Isu2–frataxin interaction.

4.2.8 Heterotrifunctional Photo-Activated Chemical Crosslinking

All samples were prepared under strict anaerobic conditions in a Vacuum Atmosphere anaerobic glovebox with muted lighting. Sulfo-SBED was rehydrated from powder with 25 μL of dimethylformamide and protected from light. Frataxin was diluted to 10 mg/mL in 50 mM HEPES, 150 mM NaCl, 10% glycerol at pH 7.4. Hydrated sulfo-SBED was added to frataxin in a 5-fold excess of label to protein and was incubated at room temperature for 30 min. Labeled frataxin was then dialyzed in the glovebox overnight at 4 °C to remove excess label and the concentration of the labeled frataxin after dialysis was determined prior to crosslinking. Once the concentrations of labeled "bait" (frataxin) and "pray" (Isu2) had been determined, the two proteins were mixed in the presence of ferrous ammonium sulfate in a 1:1 and a 2:1 ratio (frataxin:Isu2) and incubated in the dark for 30–60 min. After the incubation, the sample was placed in a 4 °C water bath and exposed to UV light (365 nm) in 1 minute on/off cycles for 15 min. Between each cycle of light, the protein was mixed. The reaction was then analyzed for crosslinked bands via SDS–PAGE and western blotting with steptavidin.

4.2.9 Western-Blotting for Sulfo-SBED Crosslinking

Under low lighting, the samples were diluted 1:100 and 10 μL was added to 10 μL of 2 × SDS loading dye, with a final concentration of 60 mM Tris-HCl, pH 6.8, 10% glycerol, 2% SDS and 0.003% bromophenol blue with and without 5% β-ME. A 15% SDS–PAGE was run in the dark for 1 hr at 150 volts. The gel was transferred to a PVDF membrane for 1 hr at 100 V at 4

°C. The membrane was blocked with 3% bovine serum albumin (BSA) fraction V in TBS buffer (20 mM Tris, 140 mM NaCl, pH 7.5) for 2 hr and then washed 3 times with TBSTT buffer (0.1 % Tween-20 and 0.2 % Triton X-100 in TBS buffer) with gentle agitation. The membrane was then incubated with a 1:2000 dilution of steptavidin–alkaline phosphatase in TBSTT buffer containing 1% BSA (6 μL of streptavidin-AP in 30 mL buffer) for 2–3 hr with gentle agitation. The membrane was then washed 4 times with TBSTT buffer for 10 min each and then transferred to staining solution (100 mM Tris-HCl, 100 mM NaCl, 5 mM $MgCl_2$) containing 0.33 mg/mL NBT (nitrobluetetrazolium) and 0.166 mg/mL BCIP (5-bromo-4-chloro-3'-indolyphosphate p-toluidine) until purple colored bands developed. The staining process was stopped by rinsing the membrane twice in water.

4.2.10 In-Gel Trypsin Digest and Peptide Analysis by Mass Spectrometry

All materials and reagents were prepared and kept keratin-free. A 15% SDS–PAGE, containing 19 μL of the SBED-frataxin Isu2 crosslinking reaction in SDS loading dye without β-ME was run and stained with coomassie. After destaining, the ~29 kDa band corresponding to a potential crosslink between frataxin and Isu2 was excised from the gel. The gel slice was further destained in 50% methanol/5% acetic acid overnight. Destain was subsequently removed and the gel slice dehydrated in acetonitrile and then evaporated to dryness using an Eppendorf SpeedVac (Hamburg, Germany). Fresh 10 mM DTT was added to the gel slices and incubated at room temperature for 30 min and then decanted. The DTT also served to promote the biotin transfer in the crosslinker to Isu2 by reduction of the disulfide bond that linked the two proteins. Reduced thiols were then derivatized with 50 mM iodoacetamide for 30 min in the dark and then washed with 100 mM ammonium bicarbonate. The gel slices were dehydrated with acetonitrile and evaporated to dryness. The gel slices were then incubated with 30 μL of 20 ng/μL trypsin

for 10 min and then 20 μL of 50 mM ammonium bicarbonate was added. The slices were incubated at 37 °C overnight. Any unincorporated liquid was removed and the peptides extracted with 30 μL of 5% formic acid in 50% acetonitrile two times. The extractions were combined and evaporated to a final volume of 10–20 μL. The samples were desalted with Millipore C18 ZipTips (Billerica, MA) and eluted in 50% acetonitrile with 0.1% formic acid in water. Dihydroxybenzoic acid matrix (DHB, 5 mg/mL) was made in 50% acetonitrile with 0.1% trifluoracetic acid in water. The sample was mixed at a 1:5 (peptide:DHB) ratio and spotted onto a stainless steel target. A Brüker Ultraflex MALDI–ToF mass spectrometer was externally calibrated with a standard peptide mix. Spectra were collected and averaged at 67% laser power. The spectra were analyzed using flexAnalysis v3.3 (Brüker Daltonics, Billerica, MA).

4.2.11 EDC/NHS Chemical Crosslinking

All samples were prepared under strict anaerobic conditions in a Vacuum Atmospheres anaerobic glovebox. Frataxin and Isu2 were buffer exchanged into buffer M (100 mM MES, 500 mM NaCl at pH 6.0), diluted to 10 mg/mL and incubated together at a 1:1 ratio (frataxin:Isu2) with 1.4 mM iron ammonium sulfate for 30 min at room temperature. EDC (1-(3-dimethylaminopropyl)-3-ethylcarbodiimide HCl) and sulfo-NHS (N-hydroxysulfosuccinimide) were prepared fresh in buffer M and added to the frataxin–Isu2 complex to a final concentration of 4 mM and 10 mM respectively and incubated for 2–3 hrs at room temperature. A 15% polyacrylamide gel containing 20 μL of the crosslinking reactions in 5 μL of 6×–SDS loading dye without β-ME was run and stained with coomassie. After destaining, the ~29 kDa band representing a potential crosslink between frataxin and Isu2 was excised from the gel. The in–gel trypsin digest and mass spectrometry was performed as described for sulfo-SBED crosslinking in **Section 4.2.10**.

4.2.12 Hydrogen–Deuterium Exchange Mass Spectrometry Deuterium Trapping

Stock solutions of 600 μM frataxin incubated with 1.8 mM ferric chloride and 600 μM Isu2 were prepared in 25 mM HEPES, 150 mM NaCl at pH 7.4. To determine the amount of deuterium incorporated into frataxin after a 10 min incubation in D_2O at 25 °C, 2 μL of 600 μM frataxin was incubated with 23 μL of D_2O for 8 min followed by a second addition of 25 μL of D_2O and incubated for an additional 2 min (simulates mixing the deuterated proteins for the complex). The deuteration was quenched by adding 125 μL of 0.15% formic acid and immediately placed on ice. The quenched protein was digested for 5 min on ice with 5 μL of 5 mg/mL pepsin. The amount of deuterium that remains after back-exchanging deuterated frataxin with water was also determined. Two microliters of 600 μM frataxin was incubated with D_2O for 8 min at 25 °C. Twenty five μL of D_2O was added and incubated for an additional 2 min at 25 °C. One hundred twenty five microliters of water was added and incubated at 25 °C for 2 min and immediately quenched with 3 μL of 7.5% formic acid on ice. The quenched protein was digested for 5 min on ice with 5 μL of 5 mg/mL pepsin. For the frataxin–Isu2 complex trapping experiments, 2 μL of each 600 μM protein stock were separately incubated with 23 μL of D_2O for 8 min at 25 °C. The deuterated proteins were mixed and incubated for 2 min at 25 °C. The reaction was then diluted with 125 μL of water at 25 °C for 2 min and immediately quenched with 3 μL of 7.5% formic acid on ice. The complex mixture was digested for 5 min on ice with 5 μL of 5 mg/mL pepsin. Varying off-exchange times were run in order to determine the optimal deuterium retention times. The off-exchange time points for the complex included 30 sec, 1 min and 2 min. HDX–MS control samples corresponding to the natural isotope distribution pattern ($m_{0\%}$) and deuterium back-exchange ($m_{100\%}$) were run with each experiment. For the 0% control, protein stock (2 μL of 125 μM frataxin) was incubated with 23 μL of water at 25 °C, followed by

quenching with 25 μL of quench buffer (0.1 M KH_2PO_4, pH 2.3) and digested on ice for 5 min with 2 μL of 5 mg/mL pepsin stock. For all reactions described, the digested peptides were separated over 15 min at 0.1 mL/min using a 0–50% acetonitrile gradient. The mass spectrometer collected spectra in positive ion mode with a scan range from 300–1550 m/z. The nebulizer gas pressure was maintained at 28 psi with the dry gas flow rate and temperature at 7 L/min and 250 °C, respectively.

4.3 RESULTS

4.3.1 $^{1}H–^{15}N$ HSQC NMR of Wild-Type Isu2-His_6 and N88A Isu2–His_6

The human [Fe–S] cluster scaffold protein Isu2 should be classified as an intrinsically dynamic protein (IDP) [23]. Isu2 exists in an equilibrium between the structured (S) and dynamically disordered (D) states and is reported to be less than 30% structured as an apo-protein [25]. It is unique that the partially disordered/dynamic (D) conformation is proposed to be the functional form for [Fe–S] assembly. The equilibrium between the structured (S) and dynamic (D) states was identified through a doubled Trp108 $^{1}H–^{15}N$ cross-peak in the ^{1}H dimension in a HSQC NMR spectrum [2]. The downfield ^{1}H resonance (10.2 ppm) represents the (S) state, whereas the upfield resonance (10.1 ppm) represents the (D) state [23].

$^{1}H–^{15}N$ HSQC NMR experiments with Isu2–His_6 were used to interrogate whether interaction with frataxin and [Fe–S] cluster assembly impact the structural state of Isu2. This will give insight into how order/disorder transitions affect Isu2 function. As shown in **Figure 4.2A**, the NMR spectra indicated that Isu2–His_6 was primarily in the (D) state, in agreement with Markley's findings [23]. Addition of holo–frataxin (*i.e.*, $2Fe^{2+}$–frataxin) to wild-type Isu2–His_6 did not significantly change the population of the tryptophan (S) and (D) resonance peaks. Thus

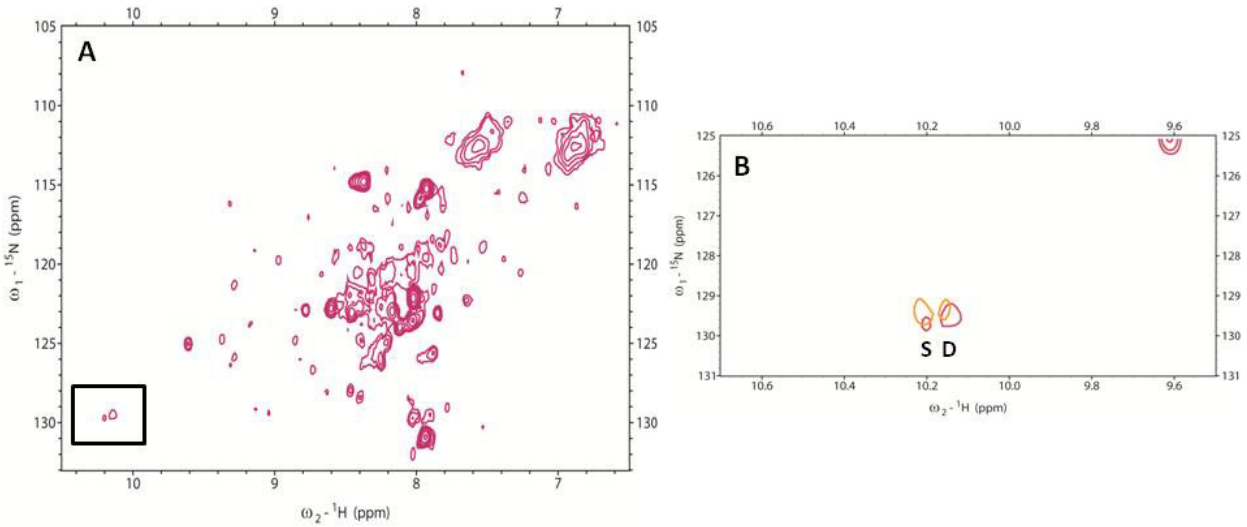

Figure 4.2 HSQC NMR spectrum of wild-type Isu2. (A) Full spectrum of apo wild-type Isu2. The Trp108 cross-peak at ~ 10 ppm represents the equilibrium of both (S) and (D) states of Isu2. (B) Overlay of apo wild-type Isu2 (red) and wild-type Isu2 + holo–frataxin (orange). NMR samples were prepared in 25 mM d_{18}-HEPES with 5% *v*/*v* D_2O.

binding of frataxin, the putative iron donor for [Fe–S] assembly does not alter the structural fold of the Isu2–His_6 scaffold (**Figure 4.2B**).

The Markley group reported that mutation of Asn88 and Asp37 to alanine impacts the structural equilibrium of Isu2. The N88A mutation shifts the structural equilibrium of Isu2 to the structured (S) state, while the D37A mutation shifts the equilibrium to the dynamic (D) state (**Figure 4.3**) [23]. The N88A Isu2–His_6 mutant was subjected to ^{1}H–^{15}N HSQC NMR to determine if the structural fold of Isu2–His_6 was similar to that of Cai *et al*. N88A Isu2–His_6 appeared to be more structured than wild-type Isu2–His_6, as indicated by the large cross-peak for the Trp108 resonance in the mutant NMR spectrum (**Figure 4.4**). In the presence of holo–frataxin, a single tryptophan cross-peak was observed for N88A Isu2–His_6, but at 10.14 ppm, it was between the (S) and (D) state values (**Figure 4.5A**). A single upfield tryptophan resonance could indicate that frataxin converts N88A Isu2–His_6 to a more dynamic state in the holo-frataxin–N88A Isu2 complex and the environment of the tryptophan has been altered. The N88A Isu2–His_6 spectrum with a reconstituted [Fe–S] cluster and frataxin revealed that the resonance for the tryptophan residue was shifted further upfield (10.09 ppm), compared to the holo-frataxin–N88A Isu2–His_6 complex **(Figure 4.5B)**. Thus, it appears that frataxin may bind Isu2 in both the (S) and (D) states, but can also convert structured Isu2 to the dynamic state and that after [Fe–S] cluster assembly, Isu2 becomes more disordered. This could be relevant to the mechanism of cluster transfer to chaperone proteins.

4.3.2 [Fe–S] Cluster Assembly

To determine the effects of frataxin on [Fe–S] cluster assembly rates, an assay monitoring the change in absorbance at 426 nm (the characteristic absorbance of a [2Fe–2S] cluster) was

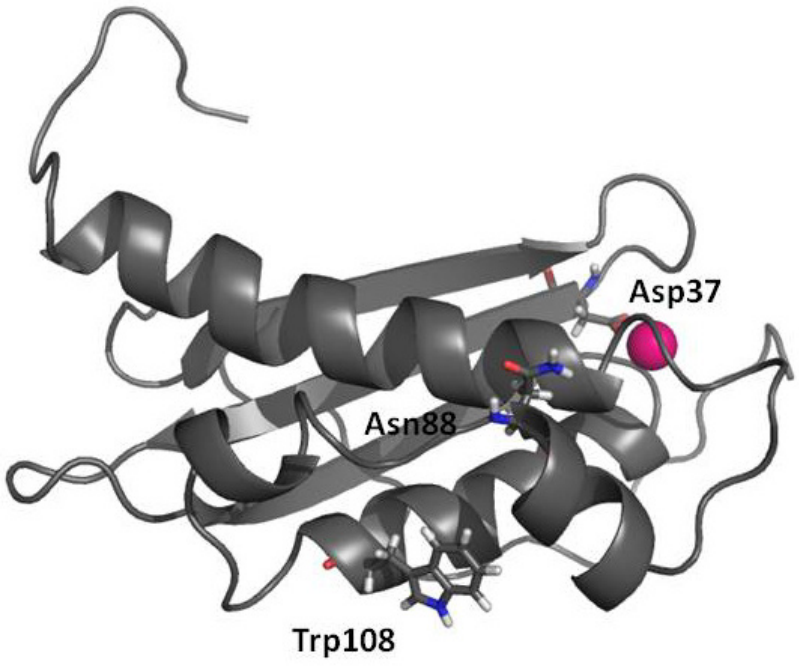

Figure 4.3 NMR structure of murine Isu2. Asp37 and Asn88 impact the structural equilibrium of Isu2. The Trp108 residue aids in identification of the structural state of Isu2 in HSQC NMR spectra (PDB: 1WFZ).

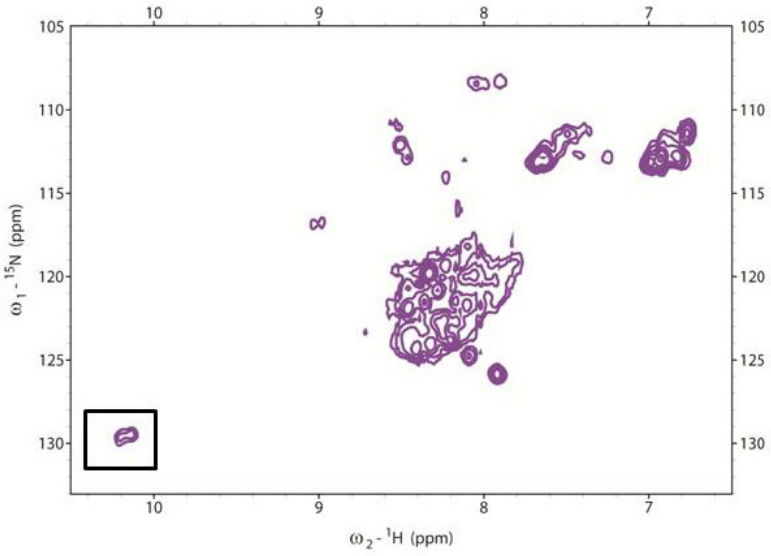

Figure 4.4 HSQC NMR spectrum of apo N88A Isu2. The single cross-peak for the Trp108 resonance indicates that N88A Isu2 is mostly in the (S) state. NMR samples were prepared in 25 mM d_{18}-HEPES with 5% *v*/*v* D_2O.

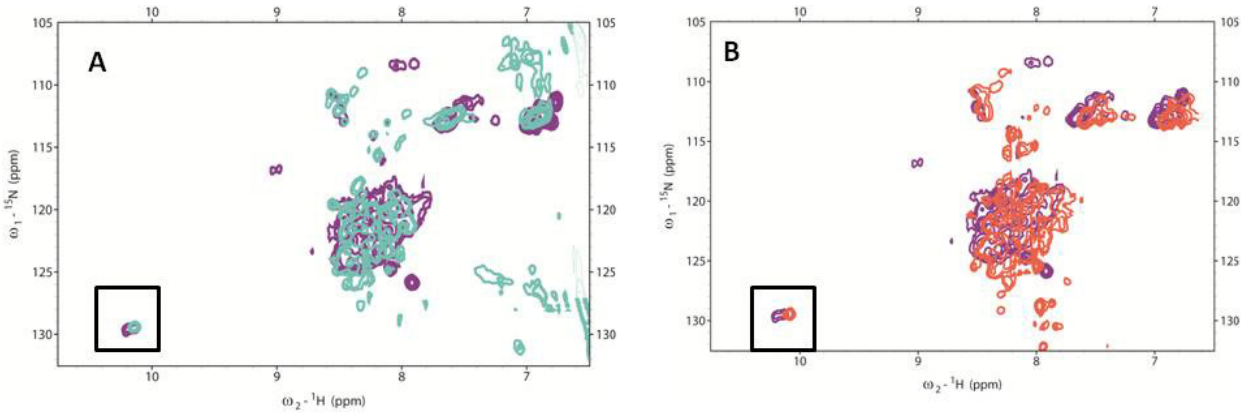

Figure 4.5 HSQC NMR spectrum of N88A Isu2. (A) Overlay of apo N88A Isu2–His_6 (purple) and N88A Isu2–His_6 + holo–frataxin (teal). The single cross-peak for Trp108 resonance at 10.14 ppm (teal) indicates an intermediate state between (S) and (D). (B) Overlay of apo N88A Isu2-His_6 (purple) and N88A Isu2–His_6 + [Fe–S] cluster (peach). The single cross-peak for Trp108 resonance at 10.09 ppm indicates that with a bound [Fe–S] cluster, N88A Isu2–His_6 is exclusively in the (D) state. NMR samples were prepared in 25 mM d_{18}-HEPES with 5% *v*/*v* D_2O.

employed. Assembly assays with wild-type Isu2 were attempted, but a black precipitate (iron sulfide) that hampered curve fitting was formed from released, dissembled [Fe–S] clusters (data not shown). Instead, the D37A Isu2 mutant (without a C-terminal histidine tag) was used for the assembly assays because D37A stabilizes the newly formed cluster, slowing its release and subsequent disassembly in solution [21]. As shown in **Figure 4.6A** with fitted rates in **Table 3**, D37A Isu2 can assemble clusters with only exogenous Fe^{2+} and S^{2-}; this is the basal rate of assembly (k_i = 0.018 s^{-1}). Upon the addition of frataxin pre-incubated with 2 molar equivalents of Fe^{2+} ($2Fe^{2+}$–frataxin) in the presence of S^{2-}, there was a 4-fold increase in the initial rate of cluster formation to 0.074 s^{-1} (**Figure 4.6B**). Iron-loaded bovine serum albumin (BSA) and S^{2-} were used as a negative control, and [Fe–S] clusters were not assembled by D37A Isu2. This demonstrated that the rate of [Fe–S] cluster assembly is not stimulated by iron-release by any metalloprotein and is due to the specific interaction between frataxin and Isu2.

In **Chapter 3**, His86 was identified as a ligand in the high-affinity Fe^{2+} binding site and that mutation of this residue caused altered the stoichiometry from 3 to 2 metal ions per frataxin molecule. The H86A frataxin mutant was tested to determine if the high-affinity Fe^{2+} coordination site was also important for stimulation of [Fe–S] cluster assembly. H86A frataxin pre-incubated with 2 equivalents of Fe^{2+} gave the same assembly rate (k_i = 0.019 s^{-1}) as the basal value of D37A Isu2 in the absence of frataxin (**Figure 4.6C**). H86A frataxin was then pre-equilibrated with up to 4 equivalents of Fe^{2+} to possibly account for non-stoichiometric binding, but the initial rate was not enhanced; therefore, H86A frataxin is unable to stimulate the rate of [Fe–S] cluster assembly *in vitro*. H177A frataxin with 2 equivalents of Fe^{2+} was also able to enhance the [Fe–S] cluster assembly rate, but only 2-fold. This indicates that His177 may also contribute to iron-donation for [Fe–S] assembly *in vitro* **(Table 3)**.

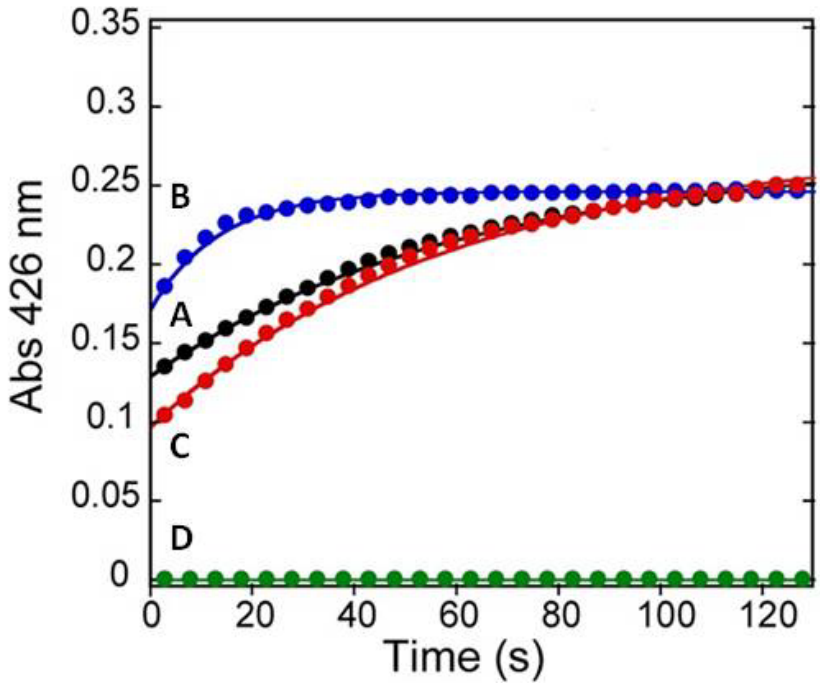

Figure 4.6 [Fe–S] cluster assembly rates. (A) Basal rate of [Fe–S] cluster assembly on 100 μM D37A Isu2 with no frataxin (black circles). (B) Rate of [Fe–S] cluster assembly with 100 μM holo wild-type frataxin (blue circles). (C) Rate of [Fe–S] cluster assembly with 100 μM holo–H86A frataxin (red circles). (D) No cluster was formed with 100 μM bovine serum albumin as the Fe^{2+} donor (green circles). Assembly assays were performed in 25 mM HEPES, 100 mM NaCl, at pH 7.4 and 25 °C.

Table 3. [Fe–S] cluster assembly rates for wild-type frataxin and two histidine mutants.

Fe^{2+}-Frataxin Variant	Rate (s^{-1})	Fold Change
-	0.018 s^{-1} ±0.001	-
Wild-type	0.074 s^{-1} ± 0.002	+ 4-fold
H86A	0.019 s^{-1} ± 0.002	No change
H177A	0.04 s^{-1} ± 0.001	+ 2-fold

4.3.3 Frataxin–Isu2 Binding

By eliminating the high-affinity Fe^{2+} coordination site in H86A frataxin, the stimulatory effects on [Fe–S] cluster assembly had been diminished. To ensure that this was not reflective of a loss of the binding interaction between H86A frataxin and D37A Isu2, intrinsic tryptophan fluorescence spectroscopy titrations were performed. The tryptophan signal for both wild-type frataxin and H86A frataxin were quenched by titration of D37A Isu2 in the presence of ferric iron (**Figure 4.7**). Binding affinities for the frataxin– D37A Isu2 interaction were also determined using a single-site binding model. Wild-type frataxin interacts with D37A Isu2 with a dissociation constant (K_D) of 1.4 μM compared to the slightly diminished dissociation constant for H86A frataxin–D37A Isu2 interaction of 2.9 μM. These results indicate that H86A frataxin is important for Fe^{2+} transfer, but does not have a direct role in Isu2 binding.

4.3.4 Photo-Activated Chemical Crosslinking

To determine the regions involved in the frataxin–Isu2 interaction, the photo-active chemical crosslinker sulfo-SBED was used to covalently trap the complex (**Figure 4.1A**). Sulfo-SBED is a trifunctional crosslinker that has an *N*-hydroxysuccinimide ester group that reacts with the lysine amines from frataxin ("bait") to label them, a photo-reactive phenyl azide that will form covalent crosslinks to Isu2 ("prey"), and a biotin group to aid in detection of the crosslinked complex via interaction with streptavidin. **Figure 4.8**, a representative western blot with streptavidin detection, showed that purified frataxin (~14 kDa) was successfully labeled with sulfo-SBED (lane 2) and that dithiothreitol (DTT) reduction of the disulfide linker effectively removed biotin moiety (lane 3). To determine which lysine residues were successfully labeled, SBED–frataxin was digested with trypsin, the disulfide linker was reduced, and the digest was submitted to MALDI–ToF mass spectrometry. Frataxin has 10 lysine

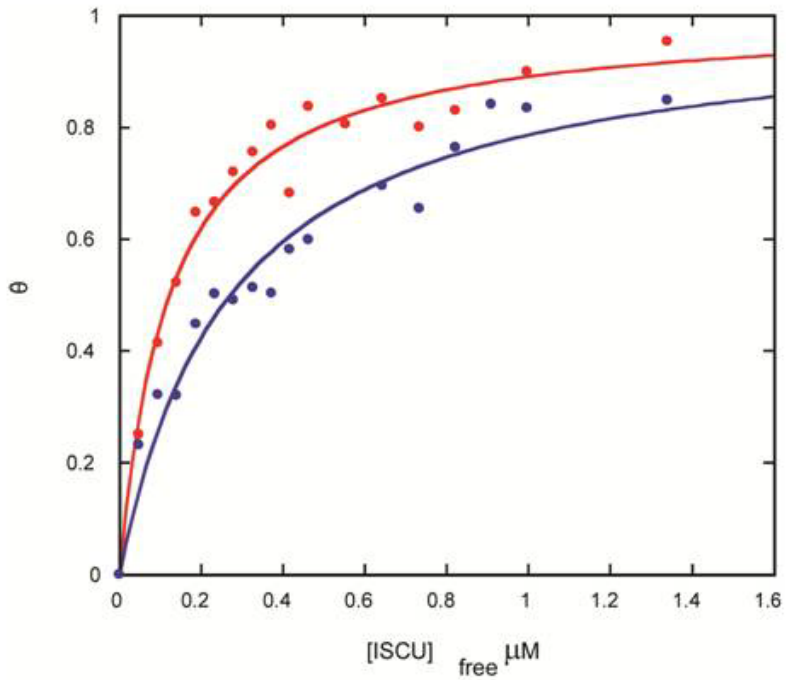

Figure 4.7 Fluorescence binding curve of 0.5 μM wild-type frataxin (red) and 0.5 μM H86A frataxin (blue) titrated with D37A Isu2. Titrations were performed in 50 mM HEPES, 150 mM NaCl, at pH 7.4 and 23 °C.

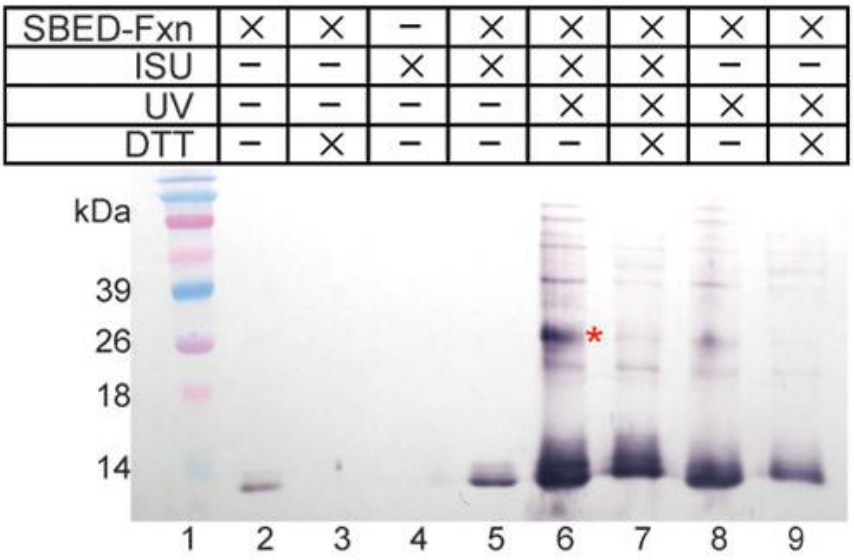

Figure 4.8 Western blot of sulfo-SBED crosslinking reactions. Bands containing the biotin marker were detected by streptavidin-AP, indicated by the purple bands. The asterisk indicates a potential crosslink with a molecular weight of ~27 kDa.

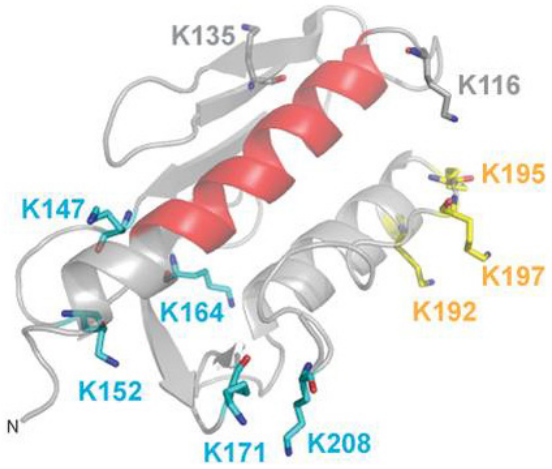

Figure 4.9 Frataxin lysine residues. Lysine residues Lys147, Lys152, Lys164, Lys171 and Lys208 were labeled by sulfo–SBED. Lysine residues Lys192, Lys195 and Lys197 were not labeled but were identified by the trypsin digest. Lysine residues Lys116 and Lys135 were not identified by the trypsin digest (PDB: 1EKG).

residues, but only 5 of them (Lys147, Lys152, Lys164, Lys171 and Lys208) contained the 3-mercaptopropanamido moiety from the residual SBED label after the reduction of the disulfide linker. These SBED-labeled lysine residues cluster around the acidic α1 helix (**Figure 4.9**). Three lysine residues (Lys192, Lys195 and Lys197) were not SBED-labeled, but were identified in the trypsin digest. The remaining two lysine residues were not identified due to a missed trypsin cleavage that gave a peptide above the detectable MS mass range. The missed cleavage is a result of Pro117 following Lys116 (**Figure 4.10**).

SBED–frataxin was mixed with Isu2 in the presence of Fe^{2+} to form a 1:1 complex. The complex was exposed to UV light at 365 nm to activate the azide group of the crosslinker and to covalently crosslink Isu2 and frataxin. No crosslink was observed for SBED–frataxin and Isu2 without UV exposure (lane 5). After SBED–frataxin and Isu2 was irradiated with UV light, a new band was noted at ~29 kDa, indicating potential crosslinks between frataxin (14 kDa) and Isu2 (13 kDa) were formed (lane 6). After the addition of DTT to initiate biotin label transfer from bait to prey, the ~29 kDa band was no longer observed but a smaller protein around 14 kDa was seen, presumably SBED–Isu2 (lane 7). A small amount of photo-activated crosslinking was observed in the control frataxin sample without Isu2 (lane 8). A frataxin–frataxin crosslink was not unexpected since frataxin can aggregate at high concentrations in the presence of iron [17]. A control consisting of bovine serum albumin (BSA) and SBED–frataxin was also performed to determine if there was any non-specific crosslinking. The western blot of the BSA control did not reveal a significant amount of crosslinking between frataxin and BSA (~83 kDa complex) after UV exposure.

To determine which Isu2 peptides were involved in the crosslink with frataxin, an in-gel trypsin digest was performed followed by MALDI–ToF MS. The band corresponding to the ~29

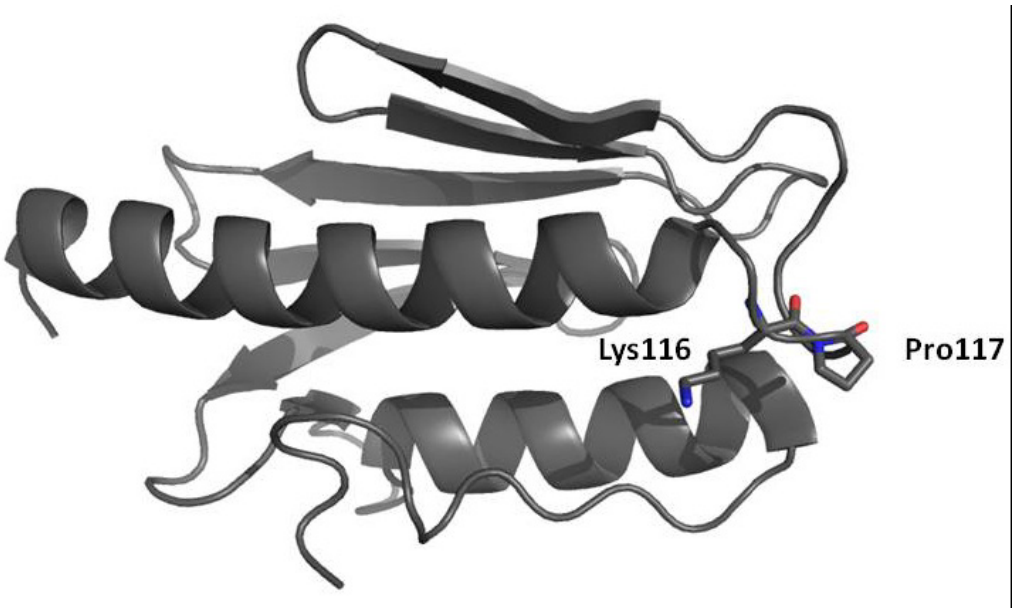

Figure 4.10 Frataxin structure showing missed Lys116. Lys116 was missed by the trypsin cleavage because it neighbors Pro117 (PBD:1EKG).

kDa crosslink was cut from the gel, reduced with DTT to break the disulfide linker, and acetylated before digestion. Given that the disulfide linker between Isu2 and frataxin was reduced during the in-gel digest it cannot be determined which SBED-labeled lysine residues were linked to Isu2. The reduction of the disulfide linkage during the in-gel trypsin digest will transfer the biotin label to Isu2, which would add 548.7 mass units to a peptide involved in a crosslink. Isu2 peptides 35–47, 92–112 and 111–121 were biotin labeled. Each of these peptides flanks the highly conserved region of Isu2 where [Fe–S] clusters are assembled based on the model of Isu2 in the structured state (**Figure 1.12**).

4.3.5 EDC/NHS Crosslinking

EDC (1-ethyl-3-[3-dimethylaminopropyl]carbodiimide) crosslinking in the presence of sulfo-NHS (*N*-hydroxysulfosuccinimide), which increases the efficiency of coupling [26], was used as a complementary technique to sulfo-SBED crosslinking to further clarify the residues involved in the interaction between frataxin and Isu2. EDC is a covalent zero-length crosslinker that labels free carboxylate residues of the "bait" protein and conjugates to free amino groups of the "prey" protein (**Figure 4.1B**). In contrast to the sulfo-SBED crosslinking experiments, frataxin and Isu2 were incubated anaerobically in the presence of Fe^{2+} to form a 1:1 native complex prior to the addition of EDC/NHS. Therefore, both proteins can act as bait or prey. An increase in molecular weight on SDS–PAGE will indicate a covalent crosslink between frataxin and Isu2 occurred.

Each protein was first incubated with EDC/NHS without the partner protein to determine if any crosslinking due to oligomerization was occurring. Isu2 showed some self-crosslinking because there was no reducing agent present to prevent disulfide bonds, but heating the samples with DTT diminished these bands (**Figure 4.11**). (Reducing agents were not used as they

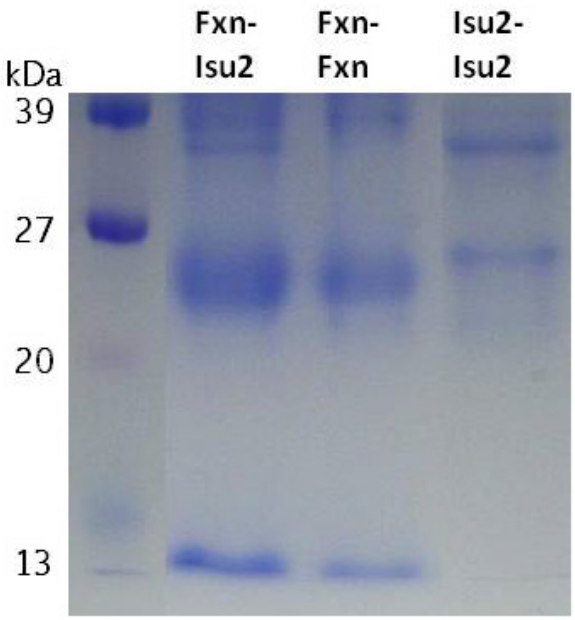

Figure 4.11 SDS–PAGE of EDC/NHS crosslinking reaction with frataxin and Isu2. Bands corresponding to ~26 kDa were excised from the gel and analyzed for potential crosslinks via MALDI-ToF.

interfere with EDC/NHS crosslinking.) Crosslinking with the frataxin–Isu2 complex yielded a band corresponding to ~29 kDa which was excised from the gel. Peptides involved in the crosslink(s) between Isu2 and frataxin were identified by peptide mass fingerprinting of MALDI-ToF data using MS–Bridge. Crosslinks were observed between peptide 105–115 from Isu2 and peptide 197–210 of frataxin and peptide 112–125 from Isu2 with peptide 197–210 from frataxin (**Figure 4.12**). Isu2 peptide 105–115 contains His105 and Cys106 of the [Fe–S] cluster assembly site. Peptide 197–210 of frataxin is the disordered C-terminal tail that has been proposed to stabilize frataxin–protein interactions [27]. Because the complex between frataxin and Isu2 was formed prior to crosslinking, the peptides identified most likely represent the outer surface of the frataxin–Isu2 interaction.

4.3.6 HDX–MS Deuterium Trapping

The HDX–MS deuterium trapping experiments were used to determine the regions of frataxin and Isu2 that are directly involved in the interface of the interaction. In contrast to chemical crosslinking, HDX–MS deuterium trapping does not crosslink the two proteins, but rather identifies the regions between two proteins that are solvent-protected by the interaction [28-30]. In this experiment, holo–frataxin and Isu2 were individually incubated with D_2O and then mixed to form a 1:1 complex. The complex was diluted with H_2O to back-exchange deuterated amides for hydrogen. Amide protons within the interface of the protein–protein interaction are less solvent accessible and therefore trap (*e.g.*, protect) deuterium [30]. After digestion with pepsin, frataxin peptides that retain deuterium in the frataxin–Isu2 complex are most likely involved in the interaction interface. Thus far, only frataxin peptides have been identified because Isu2 is resistant to pepsin cleavage.

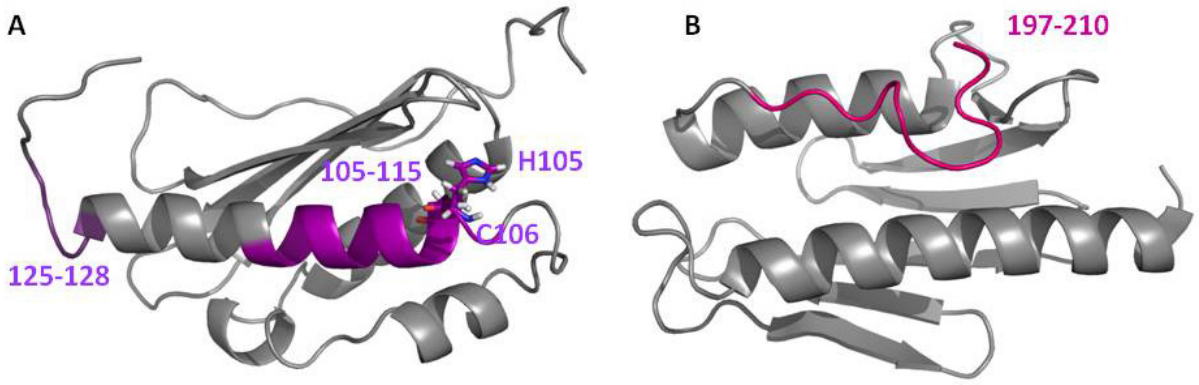

Figure 4.12 Peptides identified by EDC/NHS crosslinking on (A) Isu2 (PDB:1WFZ) and (B) frataxin (PDB:1WFZ). Peptides 105–115 and 125 – 128 of Isu2 were identified in a crosslink with peptide 197–210 of frataxin by MALDI–ToF .

Control experiments determined the extent of deuterium incorporation for holo–frataxin prior to complex formation. This was considered the starting amount of deuterium incorporated. The sample was then diluted in water to determine how much deuterium was retained in the free frataxin. This value was compared to the amount retained in the frataxin–Isu2 complex. Regions with higher deuterium retention in the complex compared to frataxin only are those protected by interaction with Isu2. Frataxin peptides 99–103 and 124–128 showed retention of deuterium after back–exchange with water, indicating protection by Isu2 (**Figure 4.13**). Peptide 99–103 is in the middle of the α1 helix of frataxin, adjacent to the N-terminal tail that contains the high-affinity Fe^{2+} coordination site with His86. It is also adjacent to the many acidic residues implicated in weaker Fe^{2+} coordination sites along the acidic ridge (*e.g.*, Asp112, Asp115). Peptide 124–128 is in the β1 sheet and contains Asp124, whose amide proton resonance was shifted in the HSQC NMR experiments with Fe^{2+} and Co^{2+} in **Chapter 2 Section 2.8.4.** In addition, previous HDX–MS results that indicated these two peptides were protected by Fe^{2+} [31], thus the iron could be important for the interaction with Isu2. Peptide 81–89 was not protected by Isu2 indicating that the N-terminus (which contains Fe^{2+} ligand His86) is not involved in Isu2 binding. Taken together with the crosslinking results, the deuterium trapping results indicate that frataxin and Isu2 interact in the same vicinity as Fe^{2+} coordination.

4.4 DISCUSSION

The interaction between frataxin and Isu2 has been well studied in yeast and bacteria [27, 32]. However, how and where human frataxin interacts with Isu2 is still unclear. The most well studied homolog of Isu2 is from IscU *E. coli* [25]. Although there is 70% sequence identity between IscU and Isu2, the differences in the structural dynamic properties are vastly different. Cai *et al.* determined that human Isu2 is less than 30% structured while *E. coli* IscU is 70% (S)

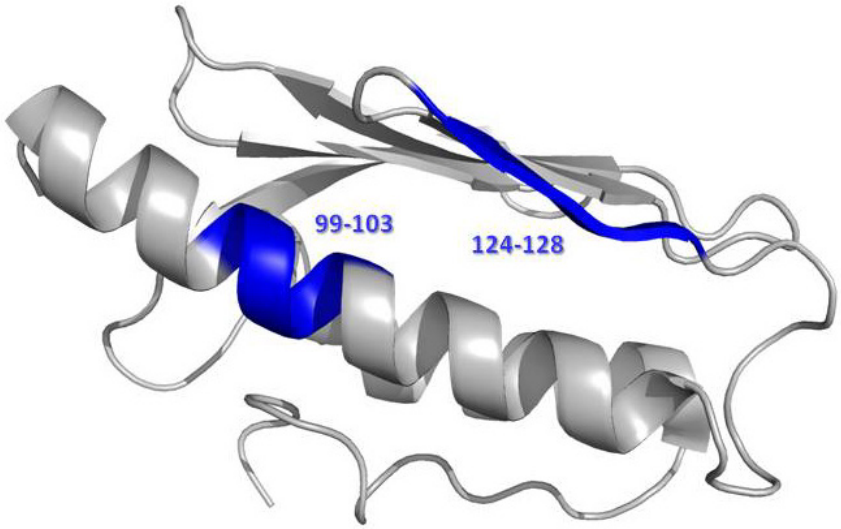

Figure 4.13 Frataxin peptides protected by Isu2 in HDX deuterium trapping assays. Peptides 99–103 and 124–128 showed increased deuterium incorporation in complex with Isu2 (PDB:1EKG).

[23]. For *E. coli* apo–IscU the interconversion between the structured and dynamic states involves the conversion of two peptidyl-prolyl bonds from *trans* in the structured (S) state to *cis* in the dynamic (D) state on a time scale of ~1 s. This means that even though the (D) state of IscU lacks dispersion of chemical shifts characteristic of a fully structured protein, it contains a fold with two high-energy cis peptide bonds. The energy of these bonds explains the slow conversion between the two states in the *E.coli* system [25]. Further, the human cysteine desulfurase (Nfs1) was demonstrated to stabilize the dynamic (D) form of Isu2, but it remains unclear under what structural conditions human Isu2 interacts with frataxin, the putative iron donor [2]. The goal of **Chapter 4** was to determine the effect frataxin has on the structural equilibrium of Isu2, how the interaction between frataxin and Isu2 impacts the rate of [Fe –S] cluster assembly, and what regions of frataxin and Isu2 are important for Fe^{2+} transfer and [Fe–S] cluster assembly.

4.4.1 Effects of Frataxin on Isu2 Structural Equilibrium

HSQC NMR experiments were used to investigate the Isu2 S↔D structural equilibrium in response to frataxin binding and [Fe–S] cluster assembly. In agreement with Markley, apo-Isu2–His_6 was primarily in the dynamic (D) state. Frataxin binding in the presence of iron did not appreciably affect the S↔D equilibrium of the Isu–His_6 [Fe–S] scaffold (**Figure 4.4**). In order to probe whether frataxin has a structural preference for the (S) or (D) state of Isu2, an N88A Isu2–His_6 mutant was constructed. Mutation of Asn88 perturbs the S↔D conformational equilibrium and stabilizes the protein in the (S) state [23]. Our preparation of N88A Isu2 still contained protein in the dynamic (D) state, which was not observed by Cai *et al*. It is still unknown the cause of this discrepancy. Regardless, the conformation in the mutant is predominantly (S) state. Holo–frataxin binding apparently shifted the conformational

equilibrium to an intermediate state between the structured and dynamically disordered (**Figure 4.5A**). However, the shift from primarily (S) to a more dynamic form indicates that holo–frataxin induced a structural change in the [Fe–S] cluster scaffold. This allows us to better understand how frataxin and Isu2 work together to assemble clusters *in vitro*. In the same manner as holo–frataxin, when apo-N88A Isu2–His_6 had an [Fe–S] cluster bound, the equilibrium was shifted to the dynamic (D) state (**Figure 4.5B**). Thus, Isu2–His_6 undergoes a conformational change from the (S) state to the (D) state upon interaction with holo–frataxin or in a complex with frataxin with an assembled [Fe–S] cluster. Markley suggests that Nfs1 also stabilizes the disordered form of Isu2 [23], but the structural changes observed with frataxin would more so indicate a change in the Isu2 conformation *from* structured *to* disordered upon interaction with the iron/sulfur donors.

4.4.2 Frataxin Stimulates [Fe–S] Cluster Assembly

Isu2 can assemble [Fe–S] clusters spontaneously with the addition of free ferrous iron and sulfur, but it is not physiologically relevant as both free iron and sulfide are toxic [3]. Both Fe^{2+} and S^{2-} are provided by proteins to the Isu2 scaffold to prevent oxidation and dangerous side reactions. However, this reaction can be used to probe how mutations in either frataxin or Isu2 affect the rate of cluster assembly on the Isu2 scaffold *in vitro* [33]. From our [Fe–S] cluster assembly assays, we can conclude that the interaction between frataxin and Isu2 is specific and that frataxin stimulates the rate of [Fe–S] cluster biogenesis by providing Fe^{2+} for the reaction (**Table 3**). This particular assay was performed with the D37A Isu2 mutant, which should be predominantly in the (D) state [21], so the stimulation by frataxin agrees with NMR studies that showed frataxin stabilizes the dynamic state of Isu2 (**Figure 4.6B**). It is likely that

frataxin binding influences both conformational dynamics of Isu2, as well as supplying iron. This has not been demonstrated previously in the literature.

By mutating the His86 Fe^{2+} ligand, frataxin could no longer stimulate the rate of [Fe–S] cluster assembly (**Figure 4.6C**). It was unclear if H86A frataxin was not transferring iron to Isu2 because the high-affinity Fe^{2+} site was disrupted or if the interaction with Isu2 was disrupted. However, H86A frataxin still binds Isu2 with only a slightly diminished dissociation constant (**Figure 4.7**). Thus, His86 is a vital ligand for high-affinity Fe^{2+} binding and for iron transfer to Isu2 for [Fe–S] cluster assembly, but it does not have a role in the interaction with Isu2. H177A frataxin had a small increase in the cluster assembly rate when compared to the basal rate, but based on the absence of coordination observed in Fe^{2+} NMR, we conclude that His177 is most likely not involved in direct Fe^{2+} coordination or donation, but that the mutation may affect Isu2 binding (**Table 3**). More investigation into the H177A frataxin mutant is ongoing. In all, these studies support that frataxin plays both an iron-chaperone and structural role in [Fe–S] cluster assembly. Cluster assembly assays in the presence of Nfs1, the sulfur provider, will further clarify the contributions by frataxin to the more physiologically relevant complex.

4.4.3 Frataxin–Isu2 Interaction Surface

To understand the mechanism of Fe^{2+} transfer from frataxin to Isu2 for [Fe–S] cluster assembly, the interaction surface and the amino acid residues involved in the interaction must be known. The interaction between human frataxin and Isu2 has been demonstrated using pull-down assays [10], thermodynamic binding assays [21] and kinetic assays [18], but none have defined the structural state of the proteins or determined a true binding surface. Two different chemical crosslinking techniques were used in combination with HDX–MS deuterium trapping in an attempt to determine an accurate binding surface for both frataxin and Isu2 that will

pinpoint the residues involved at the interface of the interaction, as well as those on the outer surface that are involved in stabilizing the frataxin–Isu2 interaction. Determining the interface of the interaction will build an understanding of how Fe^{2+} is transferred to Isu2 to assemble [Fe–S] clusters.

In the sulfo-SBED crosslinking experiment, the 5 SBED labeled lysine residues on frataxin cluster around the N-terminal tail and the α1 helix, where the high-affinity Fe^{2+} binding site is proposed. Asp122 and Asp124, which are thought to be essential for the interaction with Isu2, are located are located at the opposite end of the α1 helix (**Figure 4.9**) [13]. The Isu2 peptides involved in crosslinks were 35–47, 92–112 and 111–121. Peptide 92–112 contains a cysteine residue (Cys95) that is strictly conserved in all forms of Isu2 and is considered to be part of the [Fe–S] cluster assembly site. Peptide 111–121 is adjacent to the peptide containing the assembly site (**Figure 4.14**) and peptide 33–47 is in the N-terminal region of Isu2, which is intrinsically disordered [34]. Since the crosslinker spacer is about 14 Å, the covalent attachments should not be within the immediate binding site between frataxin and Isu2, but several angstroms away. When plotted onto the Isu2 structure in the (S) state, there is a potential surface identified for frataxin to dock with Isu2. This surface surrounds the three conserved cysteine residues and one conserved histidine residue (Cys69, Cys91, C138 and H137) at which [Fe–S] clusters are proposed to be assembled [35]. It is important to note that although residues from Isu2 can be identified in the interaction, it is not yet possible to map an interaction surface using the current solution structure of Isu2 in the (S) state since we demonstrated that frataxin stabilizes the (D) state if Isu2. The closest approximation of the (D) state comes from ensemble NMR structures of *E. coli* apo–IscU, which is ~80% structured [25]. The dynamic disorder was

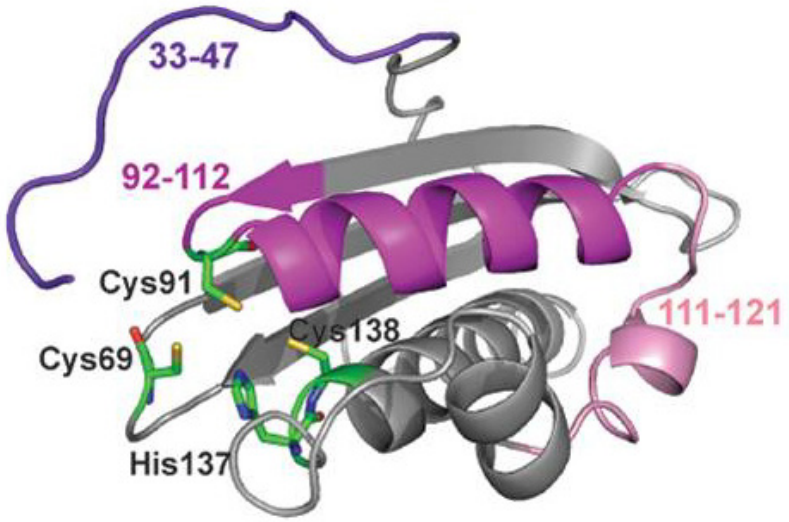

Figure 4.14 Isu2 peptides involved in a crosslink with frataxin mapped to the mouse Isu2 homolog structure (PDB:1WFZ).

noted for the cysteine-containing loops at the [Fe–S] cluster assembly site, but it is known from circular dichroism spectroscopy that IscU lacks significant secondary structure.

The EDC/NHS carbodiimide crosslinking revealed that peptide 105–115 from Isu2 was conjugated to peptide 197–210 of frataxin and peptide 112–125 from Isu2 also with peptide 197–210 from frataxin (**Figure 4.12**). Both of the Isu2 peptides contained residues identified peptides with sulfo-SBED crosslinks and both are adjacent to the cluster assembly site. Peptide 197–210 from frataxin is the C-terminal flexible loop and although it may not seem as though the C-terminus could be useful for the interaction with Isu2, it has been proposed that the C-terminus of proteins can be essential for stabilizing interactions with partner proteins [27]. Since EDC couples carboxyl groups to primary amines via an amide bond (*i.e.*, zero-length) the identified crosslinked peptides should be closer to the primary interaction surface of frataxin and Isu2.

The HDX–MS deuterium trapping further identified two frataxin peptides involved in the interaction with Isu2, peptides 99–103 and 124–128 (**Figure 4.14**). Peptide 99–103 is in the middle of the α1 helix and is adjacent to the high-affinity Fe^{2+} coordination site containing His86 and to many of the carboxylate residues thought to coordinate Fe^{2+} such as Asp112 and Asp115. Peptide 124–128 contains Asp124, which is thought to be directly involved in the interaction with Isu2 since mutation of D124 led to a decreased interaction between frataxin and Isu2 in pull-down assays [13]. Given that D122 and D124 in the β1 strand had changes in chemical shift in the presence of Fe^{2+} (**Chapter 2**) and has some involvement in the interaction with Isu2, it is probable that D124 is a key residue for Fe^{2+}-dependent Isu2 binding. Importantly, the peptide containing His86 (peptide 81–90) did not show HDX protection from the interaction with Isu2, supporting the idea that His86, while vital for high-affinity Fe^{2+} coordination and transfer to Isu2 for [Fe–S] cluster assembly, is not within the binding site for Isu2.

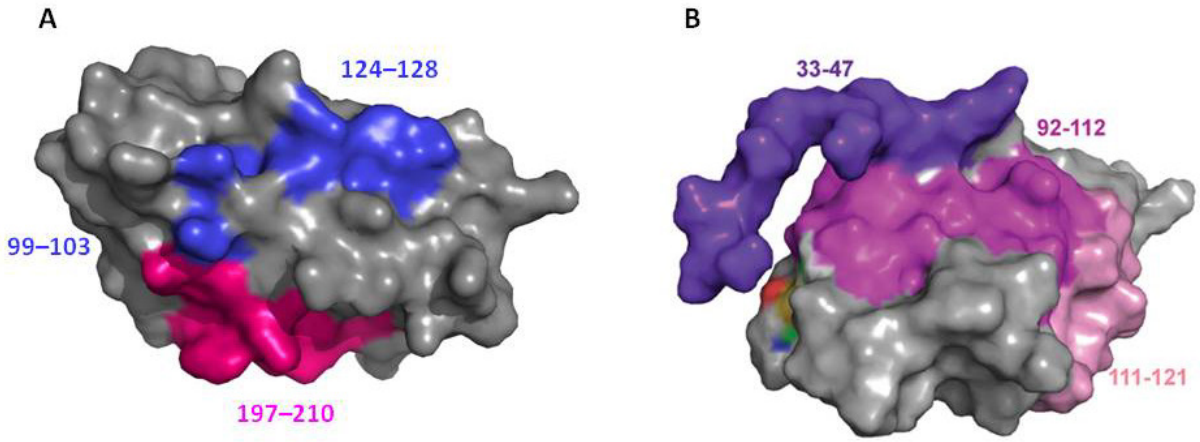

Figure 4.15 (A) Frataxin surface rendering (PDB:1EKG) with peptides from all experiments with Isu2 interaction. The peptides 99–103 and 124–128 from the deuterium trapping experiments (sky blue) and peptide 197–210 from the EDC/NHS crosslinking experiments (magenta) involved in the interaction with Isu2 form a potential interaction surface for docking of Isu2. (B) Isu2 from mouse surface rendering (PDB:1WFZ) with peptides from all experiments with frataxin interaction. The peptides 35–47, 92–112 and 111–121 also appear to form a potential interaction surface for docking of frataxin.

Putting all of the results together, there is an interaction surface on frataxin in the vicinity of Fe^{2+} coordination along the α1 helix/β1 strand that does not cover the Fe^{2+} binding site containing His86, which we propose to be the site of iron donation to Isu2 (**Figure 4.15A**). The interaction surface on Isu2 surrounds the conserved cysteine residues that are in the proposed [Fe–S] cluster assembly site and a peptide flanking this vital region (**Figure 4.15B**). Although an interaction surface for frataxin can be defined, it is problematic for Isu2. The only available solution structure for Isu2 is in the (S) state [34]; Isu2 is most likely in the dynamic state, as demonstrated in this chapter. However, by obtaining more structural information through techniques such NMR, crosslinking, HDX–MS and circular dichroism, strides can be made to obtain a more accurate structure of Isu2 during partner protein interaction and [Fe–S] cluster assembly.

REFERENCES

1. Beinert, H., R.H. Holm, and E. Munck, *Iron-sulfur clusters: nature's modular, multipurpose structures.* Science, 1997. **277**(5326): p. 653-9.

2. Markley, J.L., et al., *Metamorphic protein IscU alternates conformations in the course of its role as the scaffold protein for iron-sulfur cluster biosynthesis and delivery.* FEBS Lett., **587**(8): p. 1172-9.

3. Gerber, J. and R. Lill, *Biogenesis of iron-sulfur proteins in eukaryotes: components, mechanism and pathology.* Mitochondrion, 2002. **2**(1-2): p. 71-86.

4. Raulfs, E.C., et al., *In vivo iron-sulfur cluster formation.* Proc. Natl. Acad. Sci. U S A, 2008. **105**(25): p. 8591-6.

5. Nakamura, M., K. Saeki, and Y. Takahashi, *Hyperproduction of recombinant ferredoxins in escherichia coli by coexpression of the ORF1-ORF2-iscS-iscU-iscA-hscB-hs cA-fdx-ORF3 gene cluster.* J. Biochem., 1999. **126**(1): p. 10-8.

6. Lill, R., et al., *The role of mitochondria in cellular iron-sulfur protein biogenesis and iron metabolism.* Biochim. Biophys. Acta., 2012 **1823**(9): p. 1491-508.

7. Schwartz, C.J., et al., *The cysteine desulfurase, IscS, has a major role in in vivo Fe-S cluster formation in Escherichia coli.* Proc. Natl. Acad. Sci. U S A, 2000. **97**(16): p. 9009-14.

8. Wiedemann, N., et al., *Essential role of Isd11 in mitochondrial iron-sulfur cluster synthesis on Isu scaffold proteins.* EMBO J., 2006. **25**(1): p. 184-95.

9. Adinolfi, S., et al., *A structural approach to understanding the iron-binding properties of phylogenetically different frataxins.* Hum. Mol. Genet., 2002. **11**(16): p. 1865-77.

10. Gerber, J., U. Muhlenhoff, and R. Lill, *An interaction between frataxin and Isu1/Nfs1 that is crucial for Fe/S cluster synthesis on Isu1.* EMBO Rep., 2003. **4**(9): p. 906-11.

11. Ramazzotti, A., V. Vanmansart, and F. Foury, *Mitochondrial functional interactions between frataxin and Isu1p, the iron-sulfur cluster scaffold protein, in Saccharomyces cerevisiae.* FEBS Lett., 2004. **557**(1-3): p. 215-20.

12. Stehling, O., et al., *Iron-sulfur protein maturation in human cells: evidence for a function of frataxin.* Hum. Mol. Genet., 2004. **13**(23): p. 3007-15.

13. Schmucker, S., et al., *Mammalian frataxin: an essential function for cellular viability through an interaction with a preformed ISCU/NFS1/ISD11 iron-sulfur assembly complex.* PLoS One, 2011 **6**(1): p. e16199.

14. Tsai, C.L. and D.P. Barondeau, *Human frataxin is an allosteric switch that activates the Fe-S cluster biosynthetic complex.* Biochemistry. 2010 **49**(43): p. 9132-9.

15. Leidgens, S., S. De Smet, and F. Foury, *Frataxin interacts with Isu1 through a conserved tryptophan in its beta-sheet.* Hum. Mol. Genet., 2009 **19**(2): p. 276-86.

16. Bridwell-Rabb, J., et al., *Effector role reversal during evolution: the case of frataxin in Fe-S cluster biosynthesis.* Biochemistry. 2012 **51**(12): p. 2506-14.

17. Pastore, A. and H. Puccio, *Frataxin: a protein in search for a function.* J. Neurochem., 2013 **126 Suppl 1**: p. 43-52.

18. Huang, J., E. Dizin, and J.A. Cowan, *Mapping iron binding sites on human frataxin: implications for cluster assembly on the ISU Fe-S cluster scaffold protein.* J. Biol. Inorg. Chem., 2008. **13**(5): p. 825-36.

19. Ye, H. and T.A. Rouault, *Human iron-sulfur cluster assembly, cellular iron homeostasis, and disease.* Biochemistry, 2010 **49**(24): p. 4945-56.

20. Gakh, O., et al., *Normal and Friedreich ataxia cells express different isoforms of frataxin with complementary roles in iron-sulfur cluster assembly.* J. Biol. Chem., 2010 **285**(49): p. 38486-501.

21. Yoon, T. and J.A. Cowan, *Iron-sulfur cluster biosynthesis. Characterization of frataxin as an iron donor for assembly of [2Fe-2S] clusters in ISU-type proteins.* J. Am. Chem. Soc., 2003. **125**(20): p. 6078-84.

22. Puccio, H. and M. Koenig, *Friedreich ataxia: a paradigm for mitochondrial diseases.* Curr. Opin. Genet. Dev., 2002. **12**(3): p. 272-7.

23. Cai, K., et al., *Human Mitochondrial Chaperone (mtHSP70) and Cysteine Desulfurase (NFS1) Bind Preferentially to the Disordered Conformation whereas Co-chaperone (HSC20) Binds to the Structured Conformation of the Iron-Sulfur Cluster Scaffold Protein (ISCU).* J. Biol. Chem., 2013 **288**(40): p. 28755-70.

24. Kay L.E., K.P., Saarinen T., *Pure Absorption Gradient Enhanced Heteronuclear Single Quantum Correlation Spectroscopy with Improved Sensitivity* J. Am. Chem. Soc, 1992. **114**: p. 10663-10665.

25. Kim, J.H., M. Tonelli, and J.L. Markley, *Disordered form of the scaffold protein IscU is the substrate for iron-sulfur cluster assembly on cysteine desulfurase.* Proc. Natl. Acad. Sci. U S A. 2012 **109**(2): p. 454-9.

26. Staros, J.V., R.W. Wright, and D.M. Swingle, *Enhancement by N-hydroxysulfosuccinimide of water-soluble carbodiimide-mediated coupling reactions.* Anal. Biochem., 1986. **156**(1): p. 220-2.

27. Prischi, F., et al., *The N-terminus of mature human frataxin is intrinsically unfolded.* FEBS J., 2009. **276**(22): p. 6669-76.

28. Ehring, H., *Hydrogen exchange/electrospray ionization mass spectrometry studies of structural features of proteins and protein/protein interactions.* Anal. Biochem., 1999. **267**(2): p. 252-9.

29. Busenlehner, L.S., et al., *Location of substrate binding sites within the integral membrane protein microsomal glutathione transferase-1.* Biochemistry, 2007. **46**(10): p. 2812-22.

30. Singh, H., et al., *Escherichia coli SufE sulfur transfer protein modulates the SufS cysteine desulfurase through allosteric conformational dynamics.* J. Biol. Chem., 2013 **288**(51): p. 36189-200.

31. Gentry, L.E., et al., *His86 from the N-terminus of frataxin coordinates iron and is required for FeS cluster synthesis.* Biochemistry, 2013 **52**(35): p.

32. Adinolfi, S., et al., *Bacterial frataxin CyaY is the gatekeeper of iron-sulfur cluster formation catalyzed by IscS.* Nat. Struct. Mol. Biol., 2009. **16**(4): p. 390-6.

33. Yoon, T., E. Dizin, and J.A. Cowan, *N-terminal iron-mediated self-cleavage of human frataxin: regulation of iron binding and complex formation with target proteins.* J. Biol. Inorg. Chem., 2007. **12**(4): p. 535-42.

34. Ramelot, T.A., et al., *Solution NMR structure of the iron-sulfur cluster assembly protein U (IscU) with zinc bound at the active site.* J. Mol. Biol., 2004. **344**(2): p. 567-83.

35. Wu, G. and L. Li, *Biochemical characterization of iron-sulfur cluster assembly in the scaffold IscU of Escherichia coli.* Biochemistry, (Mosc). 2012 **77**(2): p. 135-42.

CHAPTER 5

OVERALL CONCLUSIONS AND FUTURE WORK

5.1 Summary

The stoichiometry and location of Fe^{2+} coordination by frataxin has remained unclear for many years [1-4]. In Chapter 2, we demonstrated that human frataxin binds 3 Fe^{2+} ions along the α1 helix with residues Asp112/Asp115, the β1 sheet with residues Asp122/Asp124, and a previously unidentified coordination site in the N-terminal tail. In contrast to previous reports indicating that human frataxin binds Fe^{2+} in a non-specific manner [5], we determined that frataxin contains one high-affinity Fe^{2+} coordination site.

In Chapter 3, we determined that His86 was a ligand in the high-affinity Fe^{2+} coordination site [6]. We also determined that while His177 could potentially coordinate Fe^{2+}, the binding was most likely based on the solvent accessibility of the imidazole side chain than specific binding. The validity of His177 as a legitimate, functional iron coordination site is still in question and will require further investigation. However, we also ruled out His183 as a possible metal coordinating ligand.

In Chapter 4, we determined that the dynamic nature of Isu2 structure is influenced by the presence of holo–frataxin, inducing a structural change that converts the structured state to an intermediate state between structured and dynamic. Upon assembly of an [Fe–S] cluster, Isu2 converted completely to the dynamic state. It was also determined that the specific interaction between holo–frataxin and Isu2 stimulates the assembly of [Fe–S] clusters. His86 was shown to

be vital for Fe^{2+} transfer to Isu2, as H86A could not stimulate cluster assembly [6]. Finally, we determined a potential interaction surface for the frataxin–Isu2 interaction that is in the same vicinity of Fe^{2+} coordination. The interaction surface for Isu2, however, is difficult since the only available structure is in the (S) state. However, the residues involved in the interaction with Isu2 are in the vicinity of the [Fe–S] cluster assembly site and even involve residues responsible for coordinating [Fe–S] clusters [7].

5.2 Biological Impact

The interaction between frataxin and Isu2 is vital for the efficient assembly of [Fe–S] clusters. Without frataxin to deliver Fe^{2+} for [Fe–S] cluster biogenesis, mitochondrial processes such as the TCA cycle are inhibited and have detrimental effects on the mitochondria and eventually the entire cell [8]. From the research presented in this dissertation, we have identified key amino acid residues involved in Fe^{2+} coordination and how those residues impact the frataxin–Isu2 interaction. In addition, we have identified potential interaction surfaces for frataxin and Isu2 for efficient iron transfer. Although the representation of the Isu2 surface is not entirely representative of the dynamic state of Isu2, the regions we observed are likely to be involved in the interaction with frataxin *in vivo*.

With our work, we have begun to shed light on the native interactions occurring during [Fe–S] cluster assembly. One of the main issues with treating Friedreich's ataxia is finding a way to maintain the vital functions required of the mitochondria without the presence of frataxin. If there was a way to bypass frataxin and assemble [Fe–S] clusters with similar rate stimulation, steps could begin for effective FA treatments [9]. While this research does not directly lead to a

cure for Friedreich's ataxia, a better understanding of frataxin–protein interactions will help move research forward.

5.3 Future Work

To determine the residues that may be involved in the coordination sphere with His86, residues in the N-terminus that are likely to coordinate metals should be mutated to alanine and characterized as H86A frataxin was characterized in this dissertation. Asp91 in the N-terminus showed shifting of the amide proton cross-peak in Fe^{2+} HSQC NMR and would be a likely candidate to coordinate Fe^{2+} with His86. Asp112 and Asp115 were also shown to bind Fe^{2+} and should be mutated to determine if those residues are important for [Fe–S] cluster assembly or interaction with Isu2. Asp122 and Asp124 should be mutated and their interaction with Isu2 characterized by EDC/NHS crosslinking and HDX–MS deuterium trapping.

To learn more about the structural changes occurring with Isu2 during interaction with frataxin, D37A Isu2 should be characterized by HSQC NMR to compare with the more structured N88A mutant of Isu2 and wild-type Isu2. Each Isu2 sample with holo–frataxin and a bound [Fe–S] cluster can be compared to determine the structural state of Isu2 during the interaction. The N88A Isu2 mutant should be constructed without the histidine tag to determine if the histidine tag is affecting the structural equilibrium between (S) and (D).

To gain a better understanding of the entire [Fe–S] cluster assembly complex, the interaction between wild-type frataxin and Nfs1–Isd11 should be characterized first. It should be determined if frataxin stimulates the cysteine desulfurase activity of Nfs1–Isd11. Sulfo-SBED photo-activated crosslinking can identify peptides involved in these interactions to gain a better understanding of the complex architecture. Once the interaction between frataxin and NFS1 has

been characterized, the entire complex can be characterized with HDX–MS deuterium trapping experiments in order to determine an interaction interface for the complex. Currently, it is not known how each protein in the [Fe–S] assembly complex interacts with the others, and deuterium trapping can identify peptides of the "bait" protein (such as frataxin) that are protected by the interaction with the other proteins in the complex.

REFERENCES

1. Yoon, T. and J.A. Cowan, *Iron-sulfur cluster biosynthesis. Characterization of frataxin as an iron donor for assembly of [2Fe-2S] clusters in ISU-type proteins.* J Am Chem Soc, 2003. **125**(20): p. 6078-84.

2. Yoon, T. and J.A. Cowan, *Frataxin-mediated iron delivery to ferrochelatase in the final step of heme biosynthesis.* J Biol Chem, 2004. **279**(25): p. 25943-6.

3. Bencze, K.Z., et al., *Human frataxin: iron and ferrochelatase binding surface.* Chem Commun (Camb), 2007(18): p. 1798-800.

4. Prischi, F., et al., *The N-terminus of mature human frataxin is intrinsically unfolded.* FEBS J, 2009. **276**(22): p. 6669-76.

5. Pastore, A. and H. Puccio, *Frataxin: a protein in search for a function.* J Neurochem. 2013 **126 Suppl 1**: p. 43-52.

6. Gentry, L.E., et al., *His86 from the N-terminus of frataxin coordinates iron and is required for FeS cluster synthesis.* Biochemistry, 2013 52(35): p. 6085-96.

7. Watson, H.M., et al., *Heterotrifunctional chemical cross-linking mass spectrometry confirms physical interaction between human frataxin and ISU.* Biochemistry. **51**(35): p. 6889-91.

8. Bencze, K.Z., et al., *The structure and function of frataxin.* Crit Rev Biochem Mol Biol, 2006. **41**(5): p. 269-91.

9. Anzovino, L., Huang, Richardson, *Fixing Frataxin: "Ironing Out" the Metabolic Defect in Friedreich's Ataxia.* J. Pharmacology, 2006.